

SSC-170

MTRB LIBRARY

**Studies of  
Some Brittle Fracture Concepts**

by

**R. N. WRIGHT**

**W. J. HALL**

**S. W. TERRY**

**W. J. NORDELL**

and

**G. R. ERHARD**

**SHIP STRUCTURE COMMITTEE**

Copies available from Secretary, Ship Structure Committee,  
U. S. Coast Guard Headquarters, Washington, D. C. 20226

## SHIP STRUCTURE COMMITTEE

*MEMBER AGENCIES:*

BUREAU OF SHIPS, DEPT. OF NAVY  
MILITARY SEA TRANSPORTATION SERVICE, DEPT. OF NAVY  
UNITED STATES COAST GUARD, TREASURY DEPT.  
MARITIME ADMINISTRATION, DEPT. OF COMMERCE  
AMERICAN BUREAU OF SHIPPING

*ADDRESS CORRESPONDENCE TO:*

SECRETARY  
SHIP STRUCTURE COMMITTEE  
U. S. COAST GUARD HEADQUARTERS  
WASHINGTON, D. C. 20226

September 1965

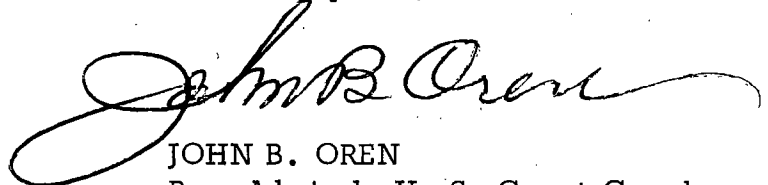
Dear Sir:

For many years the Ship Structure Committee, among other groups, has been sponsoring studies in the brittle-fracture field of materials. Many of these investigations and resulting data indicated that there might be an underlying principle that would explain the behavior of welded assemblies and thus permit their rational interpretation. In an attempt to find such a rationale and provide improved understanding of existing procedures for the evaluation of the fracture toughness of welded structures, the accompanying analytical study was undertaken by the University of Illinois.

In sponsoring this research project, the Ship Structure Committee received guidance and review from the National Academy of Sciences through its Ship Hull Research Committee, and a project advisory committee (SR-163, "Fracture Concepts") established specifically for liaison with the principal investigator. The Academy undertakes this research advisory service to the Ship Structure Committee through a contract arrangement.

Comments on this report would be welcomed and should be addressed to the Secretary, Ship Structure Committee.

Sincerely yours,



JOHN B. OREN  
Rear Admiral, U. S. Coast Guard  
Chairman, Ship Structure  
Committee

SSC - 170

Final Report  
of  
Project SR-163  
"Fracture Concepts"  
to the  
Ship Structure Committee

STUDIES OF SOME BRITTLE FRACTURE CONCEPTS

by

R. N. Wright, W. J. Hall, S. W. Terry, W. J. Nordell and G. R. Erhard

University of Illinois  
Urbana, Illinois

under

Department of the Navy  
Bureau of Ships Contract NObs-86688

Washington, D. C.  
National Academy of Sciences-National Research Council  
September 1965

---

## ABSTRACT

Interpretive studies based on available information on the low-stress brittle-fracture behavior of mild steel are made to suggest additional guides for the evaluation of the fracture resistance of fabricated steel structures.

Linear elastic fracture mechanics is used in evaluation of the fracture toughness disclosed by the arrest of cleavage fractures in notched and welded wide plate specimens. Fracture toughness values also are obtained from strain field measurements in the vicinity of propagating cracks on the verge of arrest in 6-ft-wide plates. The results clearly show the trend towards "toughening" at higher temperatures and the major role residual stress fields can play in driving fractures.

An experimental investigation was conducted to investigate the influence of welding on the yield behavior of metal from the thermally affected zone in the vicinity of a weld. The rate-temperature dependent component of the yield stress appears to be the same for base metal and metal from the thermally affected zone, but the yield stress of the thermally affected zone metal shows a substantially increased rate-temperature independent component.

A critical stress model for the prediction of brittle cleavage fracture is developed and applied to cleavage initiation, propagation, and arrest. The model approximately accounts for inelastic behavior near a flaw by truncating the elastic stress distribution. Effects of rate, temperature, notch acuity, local strain hardening, residual stress, and propagation velocity are considered; the model demonstrates good qualitative representation of the effects of these parameters on the susceptibility to cleavage. Correlations with experimental results show the model is capable of quantitative representation of the effects of rate and temperature on the applied stress required for the initiation of brittle cleavage fracture and the stress required for continued cleavage propagation. The study suggests that low-stress cleavage initiation at service temperatures can be associated with a marked local reduction of critical fracture stress, that residual stresses can be responsible for the propagation through sound metal of fractures initiated in damaged material, and that the critical fracture stress and fracture mechanics approaches are equivalent when applied to cleavage propagation and arrest.

## CONTENTS

	<u>Page</u>
INTRODUCTION . . . . .	1
PART I. Studies of Fracture Toughness . . . . .	2
PART II. Time-Temperature Effects on Yield Stress . . . . .	15
PART III. Critical Stress Model for Cleavage Fracture . . . . .	27
PART IV. Summary . . . . .	64
ACKNOWLEDGMENT . . . . .	67
REFERENCES . . . . .	68
APPENDIX A . . . . .	72
Residual Stress Measurements	
APPENDIX B . . . . .	76
Linear Elastic Fracture Analysis Expressions and Sample Computations	
APPENDIX C . . . . .	81
Notch Stress Distributions	

## INTRODUCTION

In recent years a large amount of information on the low-stress brittle fracture of mild steel has been obtained experimentally. Concomitant advances have been made in the development of fracture analysis procedures and engineering fracture criteria as well as in the understanding of the micromechanism of cleavage fracture. A need existed to compare brittle fracture criteria with experimental observations in order to obtain additional insight into the factors responsible for the occurrence of low-stress brittle fracture. The objective of the program was to consider available information on the fracture behavior of steel, and through certain interpretive studies to suggest additional guides for the evaluation of the fracture toughness in fabricated structures. The studies were restricted to mild steels, and to investigation of those parameters known to affect the fracture behavior.

Part I of the report is concerned with studies of fracture toughness evaluated by the linear elastic fracture mechanics approach. Considerable data exist for two-stage fracturing in welded and notched mild steel plates. These data include statically initiated low- and high-stress cleavage fractures of both through and arrested types, as well as measurements of the residual stress fields for plates of various thickness, width, and treatments, namely, preheated, mechanically stress relieved, and as-welded. A measure of the fracture toughness of the material may be obtained by determining the stress intensity factor  $K$  at arrest considering the crack-driving effect of the residual stress as well as the applied stress. The linear fracture mechanics approach is considered applicable because fracture occurred at low applied stress, and a small amount of plastic deformation is associated with fracture propagation. Computations also are made for certain tests in 6-ft-wide plates in which fracture propagation took place under low applied stress, and the fractures were on the verge of arrest.

The influence of stress rate (or strain rate) and temperature on the brittle behavior of low-carbon steels is directly associated with the effects of these factors on the resistance to inelastic deformation. Part II of this report gives quantitative expressions for the effects of time and temperature on the yield stress level. Results are presented for a limited experimental program conducted to study the effects of welding on the yield behavior of the material in the thermally affected zone near the weld.

Part III considers a critical fracture stress concept of cleavage fracture. The effects of stress rate or strain rate, temperature, residual stress, notch acuity, and strain hardening in the vicinity of a flaw on low-stress brittle cleavage fracture initiation and propagation are formulated in the light of a critical fracture stress. Correlations with laboratory tests are employed to study the validity of the concept and potential design applications.

Detailed developments of the concepts explored are presented in Parts I, II, and III. A unified summary of the findings is presented in Part IV.

Part I

STUDIES OF FRACTURE TOUGHNESS

1. Background and Objectives

One of the techniques employed in design against brittle fracture, especially at the present time for high strength steels, is the fracture mechanics approach. Early on this particular program the investigators (1)\* undertook a study of two-stage fracturing in welded and notched mild steel plates. Such fractures had been observed in the tests conducted as a part of the Welding Procedures Program (2,3). It was believed that the existing data would permit a comprehensive study of the fracture toughness of the base material, which at the same time would fulfill one of the objectives of this program, i.e. to examine the fracture mechanics approach as applicable to mild steels. The early studies (1) on fracture toughness are carried further to include later data from welded and notched plate tests of the Welding Procedures Program and the SSC Low-Cycle Fatigue Program (Subproject No. SR-149). Also, additional fracture toughness computations of the same type are made for a number of the 6-ft-wide plate tests using the strain data recorded during fracture propagation.

The profuse number of articles on fracture mechanics and the specialized nature of many of the contributions quite often promote confusion as to what is the objective of work in this field; in simple terms, the approach is directed toward determination of fracture toughness which may be interpreted as a property of the structure. The fracture toughness is evaluated by the stress intensity factor which is a function of stress and crack length. As might be expected, and particularly for low-carbon structural steels, the evaluation of fracture toughness is more complicated than just implied, and involves consideration of such factors as temperature, stress distribution, time effects, plate thickness, prestraining, aging, etc. In terms of application, from an engineering point of view it appears that the major use of the fracture toughness approach will be in the rating of different steels against one another; other possible uses include providing a basis for evaluation of resistance to crack propagation, and guidance as to critical flaw sizes in certain applications.

There is no one reference which presents a comprehensive picture of the fracture mechanics approach at the present time; however, many excellent progress summaries exist, among which for example are References 4 through 8. No attempt is made herein to present a comprehensive background summary.

Although it might still be classified as being in the developmental stage, there is no doubt that the linear elastic fracture mechanics approach has direct application in the field of high strength steels, and in fact has been used in an engineering capacity in this area. The recent summary articles by the ASTM Special Committee (8) constitute an outstanding contribution in terms of promoting the application of this technique. Other countries, such as Japan, are employing the same general type of technique for high strength steels.

For mild steels or metals whose properties are affected by loading rate and temperature, the problem becomes more difficult; only recently has

---

\* Numbers in parentheses refer to references

interest really been revived in applications of fracture mechanics to these materials. One of the first outstanding contributions in terms of mild steels was that of Wells (9) in which he studied the effect of residual stress on the propagation of low-stress fractures in welded steel plates, and noted that cracks, which occurred at low stress in as-welded plates, arrested in the region of the minimum value of G, the crack extension force or strain energy release rate. The study noted was concerned only with the behavior of as-welded specimens and clearly pointed the way to future work of this type.

Later work by Barton, Hall and Videon (10,11) showed that residual stress fields in 6-ft-wide plates could significantly alter the fracture characteristics, particularly the speed of the brittle fractures; in many of these tests measurements of speed and strain distribution were made during crack propagation. These results are of interest in terms of examining fracture toughness values because in many cases there was evidence that the fractures were nearing an arrest condition, and in many cases indeed did arrest.

The observations that led to making these calculations were that in the tests of the welded and centrally notched wide plates, conducted over a range of temperatures, thicknesses, and notch types, some specimens had a tendency to undergo single-stage fracture, while other specimens exhibited two-stage fracturing. The term two-stage fracturing refers to the case where upon application of external machine load (and sometimes spontaneously without external load) a short crack occurs and arrests (hereafter referred to as the primary crack), generally at a low applied average stress level, followed by complete fracture (secondary fracture) at a stress level normally (but not always!) at or above general yield on the remaining net section. The fracture stress versus temperature data indicated a rather narrow threshold of stress level in which the primary fractures occurred, as may be noted in Fig. 1. Although the low-stress

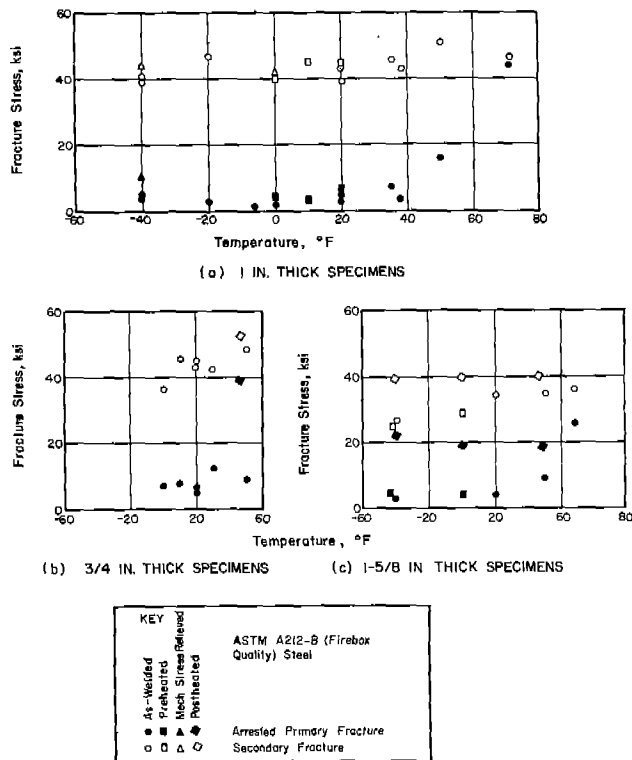


Fig. 1. Two-Stage Fracture Data.

threshold has been interpreted as a minimum critical stress level for propagation, the situation is clouded by residual stress and size effects.

Some studies (10,11) of speed and strain distribution of such fractures have been made, and it was found that the fractures picked up some speed quite quickly in the vicinity of the notch but thereafter slowed down again as the crack propagated into the compressive zone. The studies in narrow and wide plates showed that with these varying speeds there could be a significant redistribution of strain. This of course could complicate the picture even more so far as a critical stress level is concerned.

It has been observed by many investigators that the band of average applied stress separating single-stage and two-stage fracture is rather narrow; i.e., if the average stress can be increased slightly single-stage fracture will occur. In other words the go versus no-go situation for primary crack arrest would provide a measure of the fracture toughness,  $K_{IC}$ , for the base material. As such the approach involved is the inverse of the normal procedure, where a crack is started from a flaw and is propagated to a point where it becomes unstable. In the present case, a knowledge of the residual stress and applied stress system is employed to compute the driving force that is active at the propagation-arrest condition.

While this work was going on, Wells has issued another report (12) describing work of this same general type carried out on notched and welded plates employing his crack opening displacement (C.O.D.) concept which leads to essentially the same results as the method employed herein for the K value.

## 2. Fracture Toughness of Wide Plates With Central Notches and Longitudinal Welds

The analysis approach employed is the linear elastic fracture analysis procedure for plane stress conditions. There is reason to believe, as noted later, that plane strain computations might be more applicable for some of the thicker plates at lower temperatures. Obviously plastic deformation plays some role in the process. The present ASTM procedures (8) illustrate some approximate methods of handling plastic zone corrections for high strength materials; suggestions for handling lower strength materials also are available (13). However, the noted techniques do not appear compatible with the inverse procedure employed in evaluating K, and no plastic zone size correction was employed in the calculations made herein. Recent studies of the inelastic behavior in the vicinity of a flaw, such as that reported by Hahn and Rosenfeld (14), should provide a basis for improved plastic zone corrections.

The residual stress field, used in calculating the driving force, comes from both measured values and estimated fields derived therefrom. The residual stress systems used in these calculations were measured by a relaxation technique (15) summarized briefly in Appendix A. It is to be noted that the residual stress systems were measured in plates containing no notches, and it has been assumed that the small notches that were either present or inserted for the purpose of starting the fractures did not influence significantly the residual stress fields at some distance from the notch. There is evidence in terms of measurements to support this thesis in general.

The calculations have been made for specimens fracturing at low applied stress levels. At high applied stress levels one would expect yielding in the vicinity of the welds where high residual tensile stresses exist initially, which influences the stress distribution and thus the K computation. Some calculations

were made considering the effect of yielding of the weld (1); they suggested that ignoring this localized behavior does not influence the driving force significantly for the low applied stresses considered herein.

The modified Griffith expression for plane stress is commonly expressed as

$$GE = \pi a \sigma^2 \quad (1)$$

where G is the crack extension force, E is Young's Modulus, "a" is the half crack length, and  $\sigma$  is the applied stress on a plane normal to expected crack extension. The term on the right of Eq. (1) is defined as the square of the stress intensity factor, or

$$K^2 = \pi a \sigma^2 \quad (2)$$

Then, the relationship between K and G is

$$K^2 = GE \quad (3)$$

At the onset of unstable fracture, as commonly measured in crack extension tests, the term K becomes  $K_c$  where the subscript c refers to the critical value.

Westergaard's linear elastic analysis (16) is commonly employed for computing the stress intensity factor. For the case of a crack on the x-axis, the y-direction stress on the x-axis at a distance r ahead of the crack tip for small values of r may be expressed approximately in terms of K as follows:

$$\sigma_y = \frac{K}{\sqrt{2\pi r}} \quad (4)$$

The solution may be obtained using Westergaard's stress function procedure and the semi-inverse method which is presented in Appendix B. The equations, from Appendix B, utilized for the computation of the fracture toughness values made herein, are

$$K_r = 2\sqrt{\frac{a}{\pi}} \sum_{i=1}^u \sigma(x_i) \left[ \sin^{-1}\left(\frac{x_i}{a}\right) - \sin^{-1}\left(\frac{x_{i-1}}{a}\right) \right] \quad (5)$$

where  $K_r$  is the stress intensity factor value when the stress in the plate varies across the plate width (i.e., for this case the residual stress), "a" is the half crack length,  $x_i$  is the distance from the centerline of the weld, and  $\sigma(x_i)$  is the active residual stress over the interval  $x_i$ . In a flawed plate the residual stress distribution at a distance from the crack is assumed to be the same as that measured in an unflawed plate.

For a uniformly distributed stress Eq. (5) yields

$$K_r = K_a = \sigma \sqrt{\pi a} \quad (6)$$

where  $K_a$  is the stress intensity value corresponding to a uniform stress distribution across the plate (i.e., for this case the external applied stress) and  $\sigma$  is the external applied stress. Equations (5) and (6) are for a plate of infinite effective length (12). A sample computation is presented in Appendix B.

TABLE 1. SUMMARY OF MATERIAL PROPERTIES.

(a) ASTM A212-B (Firebox Quality) Steel<sup>(1)</sup>

(1) Tensile Test Data (Standard ASTM 0.505 in. Diameter)

Plate	Plate Thickness, in.	Longitudinal*				Transverse*			
		Yield Stress, ksi	Max. Stress, ksi	Elong. (2 in.), percent	Red. in Area, percent	Yield Stress, ksi	Max. Stress, ksi	Elong. (2 in.), percent	Red. in Area, percent
A	1	38.7	76.2	33	57	38.4	75.7	30	49
B	1	34.1	67.1	33	64	34.7	67.5	34	57
B	3/4	39.8	72.2	36	62	39.2	73.0	31	58
C	1-5/8	33.4	72.4	34	59	33.0	73.3	26	53

(2) Check Chemical Analysis -- percent

Plate	Plate Thickness, in.	C	Mn	Si	P	S	Al
A	1	0.29	0.92	0.29	0.010	0.029	0.014
B	1	0.24	0.86	0.18	0.006	0.031	0.008
B	3/4	0.28	0.86	0.20	0.006	0.032	0.010
C	1-5/8	0.26	0.82	0.14	0.020	0.036	0.006

(b) ABS Class C Ship Steel<sup>(19)</sup>

(1) Tensile Test Data (Standard ASTM 0.505 in. Diameter) -- Longitudinal Only\*

Temperature, deg. F	Lower Yield Stress, ksi	Upper Yield Stress, ksi	Ultimate Strength, ksi	Elongation in 2-in., percent	Reduction of Area, percent
+78	39.4	41.6	70.6	35.2	60.0
-40	43.5	46.1	76.0	35.0	60.0

(2) Check Chemical Analysis -- percent

C	Mn	P	S	Si	Cu	Cr	Ni	Al
0.24	0.69	0.022	0.030	0.20	0.22	0.08	0.15	0.034

\* Average of two specimens taken parallel to direction of loading (longitudinal) or perpendicular to direction of loading (transverse).

(c) Semi-Killed Mild Steel<sup>(10)</sup>

(1) Tensile Test Data (Standard ASTM 0.505 in. Diameter)

Yield Stress		Maximum Stress		Percent Elongation		Percent Reduction	
Long.	Tran.	Long.	Tran.	Long.	Tran.	Long.	Tran.
33.8	34.0	61.8	61.8	40.7	39.1	66.9	61.0

(2) Check Chemical Analysis -- percent

C	Mn	P	S	Si	Cu	Ni	Al
0.19	0.74	0.019	0.028	0.055	0.02	Trace	0.03

Analysis of the ASTM A212-B (Firebox Quality) Steel

The fracture toughness was evaluated for wide plates of ASTM A212-B (firebox quality) steel (1,2,3) with the mechanical and chemical properties presented in Table 1(a). The specimen is depicted in Fig. 2; the specimen width and thickness are identified in Table 2. The specimens contained a longitudinal butt weld with a central notch (Fig. 3) sawed in the weld metal and plate material; the plane of the notch is normal to the axis of the weld and the direction of maximum principal applied stress.

The stress intensity factors arising from the residual stress ( $K_r$ ) and the applied stress ( $K_a$ ) are linear functions of the stress; therefore  $K_r$  and  $K_a$  can be added together algebraically to obtain the critical value of  $K_c$  at the time of arrest, or

$$K_c = K_r + K_a \quad (7)$$

The values of  $K_r$  and  $K_a$  were computed using Eqs. (5) and (6).

In making the computations for  $K_r$  the gross longitudinal residual stress distribution was represented as a step function as shown in Fig. 4 for a typical as-welded situation with 1-in.-thick plate. For very short cracks ( $2a < 6$  in.) it was found necessary to use the closely spaced steps shown by curve A. For longer cracks, it was found that the stress distribution could be represented more approximately by curve B. The computation of  $K_r$  was made by use of Eq. (5) for various crack lengths, and a typical  $K_r$  versus crack length distribution is shown in Fig. 4.

Space limitations preclude the presentation of all the residual stress step distribution and  $K_r$  curves for the different plate thickness and heat treatments. Typical  $K_r$  curves for the mechanically stress relieved and postheated cases are shown in Fig. 5. The curves for the preheated specimens were nearly identical to the as-welded case. In some cases it was necessary to estimate the

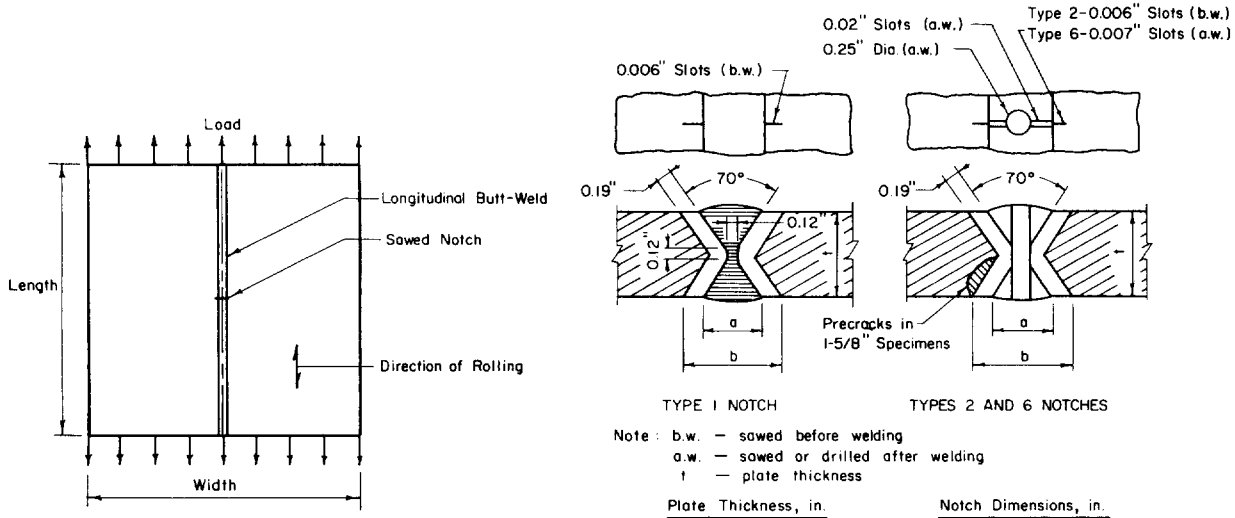


Fig. 2. Longitudinally Welded Wide-Plate Specimen with Sawed Notch.

TYPE 1 NOTCH                      TYPES 2 AND 6 NOTCHES

Note: b.w. - sawed before welding  
a.w. - sawed or drilled after welding  
t - plate thickness

Plate Thickness, in.	Notch Dimensions, in.	
	a	b
3/4	0.56	1.02
1	0.74	1.20
1-5/8	1.17	1.63

Fig. 3. Notch Details.

TABLE 2. WELDED PLATE TEST DATA AND COMPUTED  $K_c$  AT ARREST ASTM A212-B (FIREBOX QUALITY).

Spec. No.	Specimen Thickness, in.	Length of Arrested Crack(2a), in.	Primary Fracture Stress, ksi	Applied $K_a$ , ksi $\sqrt{\text{in.}}$	Residual $K_r$ , ksi $\sqrt{\text{in.}}$	Total $K_c$ , ksi $\sqrt{\text{in.}}$	Temp. °F
Type 1 Notch (3-ft wide)							
1-1	1	9.5	6.4	24.7	39	64	-30
Type 2 Notch (3-ft wide unless noted otherwise)							
2-1	1	3.5	1.4	3.4	53	56	-6
2-5	1	3.8	3.4	8.3	52	60	0
2-6	1	4.0	4.6	11.5	51	63	20
2-7	1	2.5	4.0	8.0	60	68	38
2-9	1	4.5	16.2	43.0	59	93	50
2-18	1	4.8	3.6	9.9	48	58	-20
2-21 *	1	4.5	4.1	11.0	46	57	-40
2-22 *	1	3.5	4.2	9.9	52	62	20
2-13 **	1	5.8	4.5	13.7	55	69	0
2-19 **	1	4.0	3.5	8.9	64	73	10
2-20 **	1	9.0	6.5	24.5	44	69	20
2-17 ***	1	4.2	10.4	26.8	9	36	-40
Type 5 Notch (3-ft wide)							
5-1	1	7.0	3.5	11.7	43	55	-40
Type 6 Notch (2-ft wide)							
6-19	3/4	11.4	8.2	34.7	22	57	10
6-20	3/4	6.5	12.8	41.0	37	78	30
6-21	3/4	4.9	9.4	26.1	44	70	50
6-41	3/4	8.0	7.9	28.0	32	60	0
6-42	3/4	3.7	6.7	16.1	50	66	20
6-43	3/4	3.5	7.1	16.7	52	69	20
6-22	1-5/8	6.8	9.6	30.5	49	80	50
6-23	1-5/8	2.4	25.6	49.6	77	127	68
6-28	1-5/8	7.0	3.6	11.9	48	60	-40
6-44	1-5/8	6.2	4.6	14.4	52	66	20
6-33 **	1-5/8	13.0	4.5	20.4	31	51	-42
6-34 **	1-5/8	11.5	4.1	17.4	35	52	0
6-37 ****	1-5/8	2.9	22.2	47.3	11	58	-40
6-38 ****	1-5/8	2.2	19.5	36.6	12	49	0
6-39 ****	1-5/8	2.5	19.0	37.8	11.5	49	48

\* 2-ft-wide plate  
 \*\* Preheated (400 F) specimen  
 \*\*\* Prestrained approximately 0.6%. Weld was cut through after prestraining  
 \*\*\*\* Postheated (1150 F) specimen

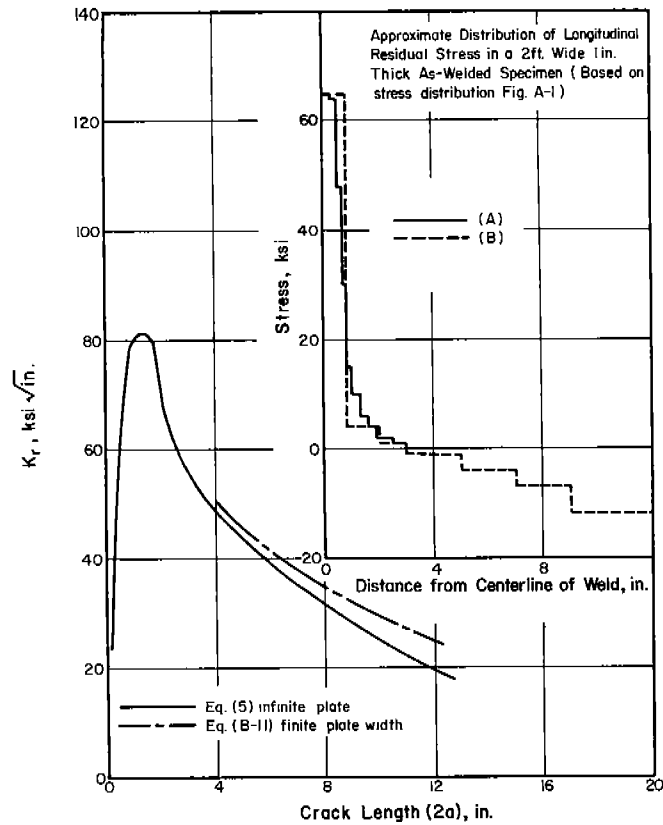


Fig. 4.  $K_I$  Versus Crack Length for 2-ft-wide 1 in. Thick As-Welded Specimen.

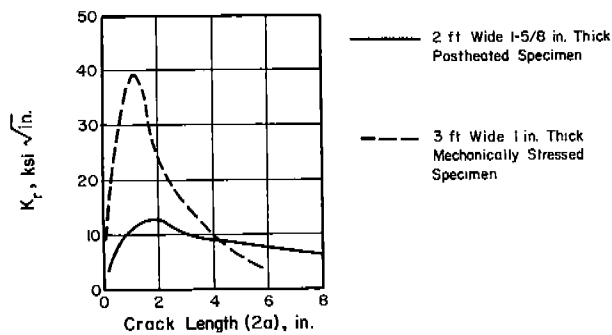


Fig. 5.  $K_I$  Versus Crack Length for 3-ft-wide by 1-in. Thick Mechanically Stress Relieved Specimen and 2-ft-wide by 1-5/8 in. Thick Postheated Specimen.

residual stress distribution, as noted in Appendix A. The  $K_I$  values for the various specimens (representing the appropriate crack length) are tabulated in Table 2. The value of  $K_a$  was computed by Eq. (6) and the value for each specimen is tabulated in Table 2.

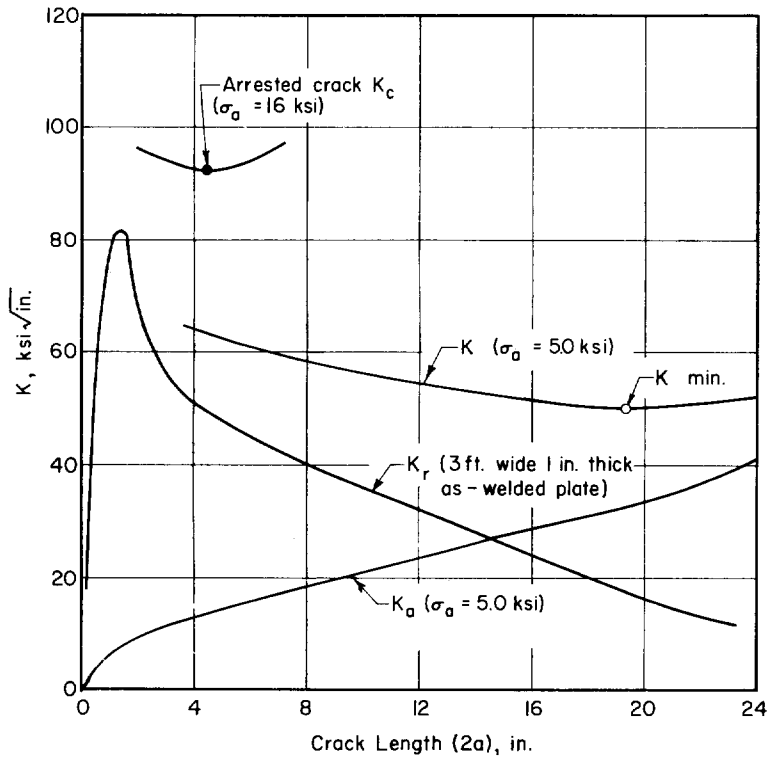


Fig. 6.  $K$  Versus Crack Length-- 3-ft-wide As-Welded Specimen-- 1 in. Thick.

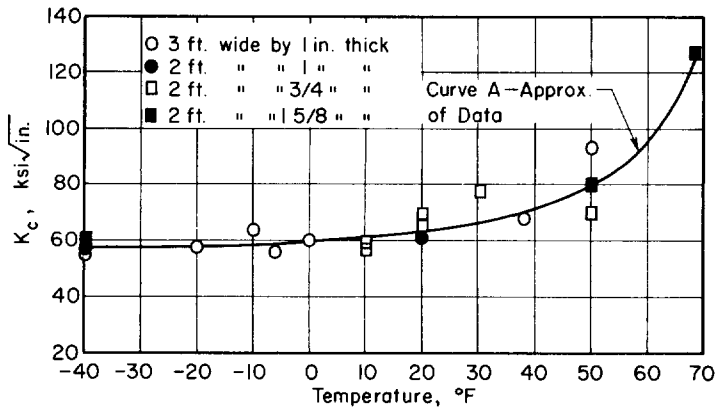


Fig. 7.  $K_c$  at Arrest Versus Temperature-- As-Welded Specimen.

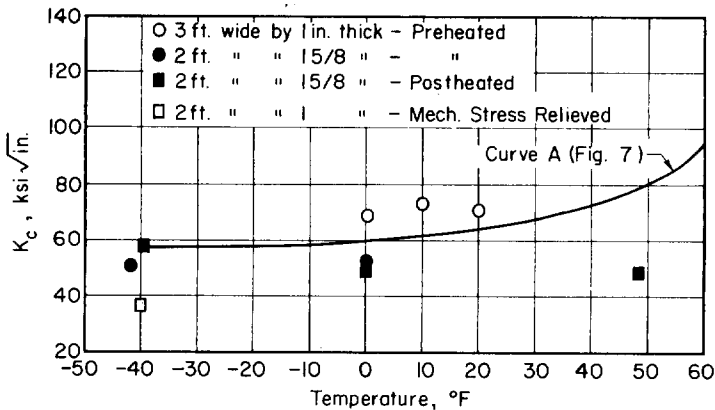


Fig. 8.  $K_c$  at Arrest Versus Temperature-- Preheated, Postheated and Mechanically Stressed Specimens.

For as-welded specimens 3 ft wide and 1 in. thick, a  $K$  versus "a" curve was computed for different values of applied load and results are presented in Fig. 6. The value of  $K$  near the weld-plate junction is large as a result of the large magnitude of the residual stress. As the crack length increases beyond the weld-plate junction the value of  $K$  decreases because the external stress is not of sufficient magnitude to compensate for the rapid decrease in the effect of the residual stress. As the crack length continues to increase, the value of  $K$  increases as a result of  $K_a$  which increases steadily with crack length. The  $K$  versus "a" curve shown in Fig. 6 for an applied stress of 5 ksi is typical for the 2-ft and 3-ft specimens discussed herein. The shift in the minimum point of  $K$  is illustrated in Fig. 6 by short portions of  $K$  versus "a" curves computed for an applied stress of 16 ksi; the computations were made to check that the crack length at arrest corresponded roughly to the minimum  $K$ . The comparison shows the primary crack to have arrested at or prior to reaching the minimum. It should be noted that the values of  $K_a$  (Fig. 6) for the 5-ksi case were computed using Eq. (B-12), of Appendix B, which accounts for the effect of width on the value of  $K$  for long crack lengths.

The values of  $K_C$  at arrest for the as-welded specimens are presented in Fig. 7. Based on the foregoing results, crack arrest at low stress may be attributed to the decreasing support by the high tensile residual stress in the weld of crack propagation as the crack lengthens. Arrest apparently occurs when the value of  $K$  falls below a minimum value  $K_C$  necessary to maintain crack propagation in the plate material. As shown in Fig. 7, the values of  $K_C$  at arrest appeared to increase gradually in the temperature range between  $-40^\circ$  and  $+40^\circ\text{F}$ , and an apparent "fracture toughness transition" occurs at about  $40^\circ$  to  $60^\circ\text{F}$ . At these higher temperatures the ductility becomes more pronounced and manifests itself in terms of a major change in fracture mode (tunneling with increased shear lip). The actual values of  $K_C$  at the high temperatures may be greater than those computed herein because the higher primary fracture stress increases the amount of yielding in

the vicinity of the weld. Curve A in Fig. 7 is an approximation of the computed  $K_C$  values and is presented only for comparison with the data for preheated, postheated, and mechanically stress relieved specimens discussed later.

Thus far, only the values of  $K_C$  at arrest for as-welded specimens have been presented. Additional information on the apparent fracture toughness values were obtained from preheated, postheated, and mechanically stress relieved specimens that failed in two stages. The value of  $K_C$  at arrest was computed in the same manner as for the as-welded specimens. For the 3-ft-wide 1-in.-thick preheated specimens the  $K_C$  values (presented in Fig. 8) were slightly greater than for the as-welded case which is represented by curve A. For the 2-ft-wide by 1 5/8-in.-thick preheated specimens the  $K_C$  values were slightly less than the as-welded case. The computed fracture toughness at arrest for the mechanically stress relieved specimen is not as large as in the case of the as-welded, preheated, and postheated specimens; this may result from the computational scheme, strain aging or some other phenomenon. In the postheated specimens a small crack occurred after welding while the notch was being sawed, creating a severe crack in thermally affected material near the weld. This severe precracking is perhaps responsible for the low  $K_C$  values in the three postheated specimens. All other postheated specimens tested (data not reported herein) reached or exceeded general yield before fracturing.

For the as-welded specimens there does not appear to be a thickness effect on the fracture toughness within the thicknesses studied.

Analysis of ABS Class C Ship Steel (19)

The fracture toughness values were computed in the same manner as for the ASTM A212-B steel assuming the as-welded residual stress distribution presented in Appendix A to be representative of the specimens from the ABS Class C ship steel. Table 3 gives test results and computed  $K$  values at fracture arrest. The  $K_C$  values presented in Fig. 9 for the ABS Class C appear similar to the fracture toughness values for the as-welded ASTM A212-B steel discussed earlier. The two steels have approximately the same material properties (Table 1). Two of the ABS Class C specimens were 1 ft wide and were tested at  $-80^\circ\text{F}$ . Because of the low temperature ( $-80^\circ\text{F}$ ) these two tests were of interest. The  $K_I$  values were assumed to be approximately the same as the 2-ft-wide as-welded specimens (Fig. 4); this assumption probably is incorrect, for other work in Japan has shown that the residual stress near the weld does not attain as high a value for narrow plates as for the wider plates. The noted observation would tend to lower the two  $K_C$  values at  $-80^\circ\text{F}$ , bringing them more in line with the other data.

3. Fracture Toughness of 6-ft-Wide Prestressed Steel Plates

As a part of SSC Subproject SR-155, a number of tests of 6-ft-wide prestressed steel plates were conducted (10). By welding two slots on each edge of the 3/4-in.-thick specimens, it was possible to create a high tensile residual strain field at each edge of the plate and a compressive strain field in the central portion of the plate. The compressive strain amounted to as much as 400 to 500 microin./in. in the longitudinal direction (perpendicular to the normal crack paths) and existed over a central region of 2 to 3 ft of the plate. Some plates had fractures initiated with no external applied load, while others had 3000 psi average net stress applied to hold the specimen taut in the machine. Some fractures propagated completely across the plate, and others arrested, indicating that the fracture conditions were on the verge of a go or no-go situation. The plates were instrumented to record the absolute level of strain in the plate during fracture propagation. These tests were of great interest to many investigators because they permitted calculation of the stress intensity factor for a crack on the verge of arrest, again the reverse situation of a growing crack which suddenly becomes unstable.

Krafft and Eftis (20) recently made similar computations for the stress intensity factor,  $K$ , for a propagating crack, using the data noted above.

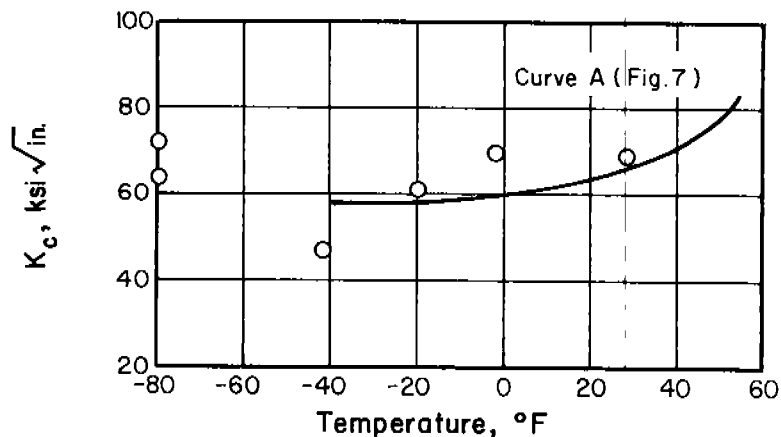


Fig. 9.  $K_C$  Versus Temperature Low-Cycle Fatigue Program, ABS Class C Steel.

TABLE 3. WELDED PLATE TEST DATA AND COMPUTED  $K_C$  AT ARREST\* ABS CLASS C SHIP STEEL.

Spec. No.	Specimen Thickness, in.	Length of Arrested Crack (2a), in.	Primary Fracture Stress, ksi	Applied $K_a$ , ksi $\sqrt{\text{in.}}$	Residual $K_r$ , ksi $\sqrt{\text{in.}}$	Total $K_c$ , ksi $\sqrt{\text{in.}}$	Temp., °F	Remarks
WP-19	3/4	10.6	4.6	19.0	28	47	-42	2-ft-wide non-cycled specimen
WP-20	3/4	4.1	8.8	22.3	50	72	-80	1-ft-wide welded after flexural cycling (2.3 percent strain for 41 cycles)
WP-22	3/4	4.0	5.8	14.3	50	64	-80	1-ft-wide welded after cycling ( $\pm 22$ ksi for 38,000 cycles)
WP-25	3/4	2.6	4.0	8.1	62	70	-2	2-ft-wide non-cycled specimen
WP-26	3/4	7.2	5.0	16.8	42	61	-20	3-ft-wide non-cycled specimen
WP-27	3/4	2.7	5.4	11.2	58	69	+28	3-ft-wide non-cycled specimen

\* Data from Reference (19)

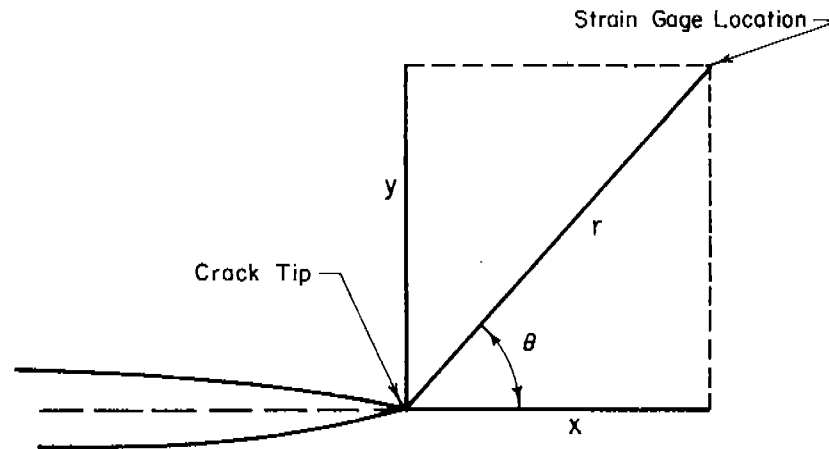


Fig. 10. Coordinates for Crack Tip.

For the stress intensity analysis for the wide plates the linear-elastic analysis of the crack-tip stress field for an infinite plate (17), is given by

$$\sigma_y = \frac{K}{\sqrt{2\pi r}} \cos \frac{\theta}{2} \left( 1 + \sin \frac{\theta}{2} \sin \frac{3\theta}{2} \right) \quad (8)$$

where  $r$  and  $\theta$  are polar coordinates with the origin at the crack tip (Fig. 10). On the assumption that plane-stress conditions hold for the surface measurements made on the 3/4-in.-thick plates, the stress may be computed by

$$\sigma_y = \frac{E}{(1-\nu^2)} (\epsilon_y + \nu\epsilon_x) \quad (9)$$

where  $\nu$  is Poisson's Ratio,  $\epsilon_y$  is the strain measured in the y direction,  $\epsilon_x$  is the strain measured in the x direction,  $\sigma_y$  is the stress in the y direction, and E is Young's Modulus. Combining Eqs. (8) and (9), the stress intensity factor, K, can be expressed as

$$K = \frac{\sqrt{2\pi r} E (\epsilon_y + \nu\epsilon_x)}{(1-\nu^2) \cos \frac{\theta}{2} (1 + \sin \frac{\theta}{2} \sin \frac{3\theta}{2})} \quad (10)$$

Studies (17) have shown that the maximum tensile stress,  $\sigma_y$ , occurs for  $\theta$  values of  $60^\circ$  to  $70^\circ$  in the vicinity of a stationary crack tip. The same analysis was used for the slow propagating cracks encountered herein. It was assumed that the crack tip made an angle of  $60^\circ$  with the gage at the time that maximum value of  $\epsilon_y$  was achieved; the corresponding value of  $\epsilon_x$  was used in the calculations. With the gage location and strain values it was possible to approximate the stress intensity value. The measured and computed data are presented in Table 4. It is reasonable to assume that the computed stress intensity factor constitutes an upper bound to the fracture toughness value for the plate material; it appears to be approximately 30 ksi  $\sqrt{\text{in.}}$ , significantly less than the values for the A212-B and ABS Class C material previously discussed.

TABLE 4. SIX-FOOT-WIDE PRESTRESSED PLATE DATA AND COMPUTED K VALUES.

Test No.	Strain Gage No.	Gage Location From Init. Edge, in.**	Perp. Dist. Gage Center-line Crack, in.**	r for $\theta = 60^\circ$ , in.*	Crack Length, in.*	$\epsilon_y$ **, microinches/inch	$\epsilon_x$ **, microinches/inch	K, ksi $\sqrt{\text{in.}}$ *	Crack Speed, fps*	Temp., $^\circ\text{F}$ **
49	1	18	0.80	0.92	17.5	1270	1050	100	2250	-10
49	2	24	2.25	2.59	22.7	410	640	63	500	-10
49	3	30	2.65	3.05	28.5	240	240	36	200	-10
49	4	36	1.80	2.07	35.0	500	200	52	150	-10
50	5	36	0.10	0.12	35.9	1670	190	38	650	-10
50	6	42	0.20	0.23	41.9	1340	640	47	150	-10
50	7	48	0.47	0.54	47.7	1120	450	59	500	-10
46	5	18	2.50	2.88	16.6	1750	-300	178	2800	0
46	10	42	0.40	0.46	41.8	790	300	38	150	0
46	12	54	2.26	2.61	52.7	660	-300	57	600	0
46	14	66	0.38	0.44	65.8	610	300	30	100	0
47	1	18	0.55	0.63	17.7	1250	410	70	250	-8
47	2	18	2.45	2.83	16.6	330	590	56	250	-8

\*\* Measured data

\* Computed data; crack speeds were rounded to nearest 50 fps

## Part II

### TIME-TEMPERATURE EFFECTS ON YIELD STRESS

#### 4. Introduction

It is generally recognized that the influences of stress rate (or strain rate) and temperature on the resistance of steel to inelastic deformation are largely responsible for the effects of these factors on the tendency to brittle fracture. Yield criteria giving quantitative expression to the influence of stress rate and temperature on the upper yield point of body centered cubic iron alloys are presented below. Similar criterion forms also can be used to express the influence of strain rate and temperature on the lower yield and post-yield flow stresses; examples of such criteria are given elsewhere (22).

An investigation was conducted as part of this program to study the influence of welding on the upper yield stress in the thermally affected zone adjacent to a weld. It is shown in Part III that the embrittling effect of welding may be due in part to the influence of thermal and deformation cycling on the yield level of the metal in the zone adjacent to the weld. The test program is described below and the differences in the yield criteria for base metal and thermally affected zone metal are evaluated.

Yield criterion parameters are given for a number of low-carbon steels used in various investigations. These data provide a measure of the range of validity of the yield criterion, show the apparent ranges of yield criterion parameters, and are used in Part III of this report in applications of the critical stress model for cleavage fracture.

#### 5. Upper Yield Point Criteria

Upper yield point criteria give quantitative representation of the effects of (1) time, often expressed as a stress rate, strain rate, or delay time, (2) temperature, and (3) stress state on the yield stress of steel. The criteria presented here apply to the conventional low-carbon steels used in ship and structural applications. Similar criterion forms are likely to be applicable to other body centered cubic iron alloys that show an upper yield point in the standard tensile coupon test.

The upper yield stress is here defined as the stress level required to establish a deformation or Luder's band across the gage section of a uniaxially stressed coupon. The stress decreases following the establishment of a Luder's band if constant deformation rate is maintained. If stress is held constant or increased, a marked jump in the rate of deformation accompanies the formation of a deformation band in the coupon. In either event the upper yield stress is well defined.

The yield criterion forms used herein are rate-process expressions. The parameters of a yield criterion are evaluated empirically for particular steels. Conrad (23) and other investigators have shown that the parameters can be interpreted in the light of dislocation mechanisms for plastic flow. These interpretations are not explored herein; the yield criterion parameters for a particular steel are considered to be material properties.

Most of the available data on rate and temperature effects on the yield level of low-carbon steel were obtained from testing of uniaxially stressed coupons. The yield criteria are developed herein in terms of uniaxial stress for convenience in evaluating the criteria. Criteria developed for uniaxial stress are converted into terms of octahedral shearing stress for application to an arbitrary state of stress.

The General Form of the Upper Yield Point Criterion is intended to define the effects of time or rate, and temperature on the stress required for the initiation of gross plastic deformation by slip. As rate of stress or strain increases and temperature decreases, resistance to slip increases until plastic deformation occurs by twinning rather than slip. Sleeswyk and Helle (24) suggest that twinning occurs at a critical stress level which is relatively independent of rate and temperature. As temperature increases and rate decreases, aging during the stressing can become significant prior to gross yielding. The yield criterion does not account for twinning or aging; it is applicable only in the ranges of time and temperature for which aging is ineffective and the critical stress for slip is less than that for twinning. The effect of twinning can be included as an upper limit on the yield stress if Sleeswyk's hypothesis is valid. The effect of aging is more difficult to formulate; Campbell and Duby (25) have suggested a procedure. For the low-carbon steels considered herein at the stress rates of interest in the study of the brittle fracture, aging during stressing prior to yield does not appear to be significant at temperatures below 200°F.

The yield criterion considers the upper yield point to be made up of two components:

$$\sigma_y = \sigma_{ym} + \sigma_y^i \quad (11)$$

where  $\sigma_y$  denotes the axial upper yield stress,  $\sigma_{ym}$  represents the rate-temperature independent component of the upper yield stress, and  $\sigma_y^i$  represents the rate-temperature dependent component of the upper yield stress. The rate-temperature independent component,  $\sigma_{ym}$ , is considered to have defined physical significance; it is the minimum value of yield stress that will be observed in a very long duration test and is constant within the temperature range for which the yield mechanism is unchanged.

The rate-temperature dependent component,  $\sigma_y^i$ , is related to the time rate and temperature of testing by the expression:

$$A = \int_{t_1}^{t_y} \exp\left(-\frac{U}{RT}\right) dt \quad (12)$$

$t_1$	time at which stress exceeds $\sigma_{ym}$ , seconds
$t_y$	time of yield, seconds
$U$	activation energy, cal/mol
$R$	gas constant, (1.986 cal/mol-K)
$T$	absolute temperature, K
$A$	constant, seconds

The activation energy,  $U$ , is a function of the rate-temperature dependent component of the stress; often it can be represented reasonably by the Yokobori (26) form.

$$U = B \ln \left( \frac{\sigma_o}{\sigma^i} \right) \quad (13)$$

$B$  constant, cal/mol

$\sigma_o$  constant, ksi

$\sigma^i$  rate-temperature dependent component of stress, ksi

$\sigma^i = \sigma_y^i = \sigma_y - \sigma_{ym}$  for yield stress

Substituting from the activation energy expression of Eq. (13) into Eq. (12) yields.

$$A = \int_{t_1}^{t_y} \left( \frac{\sigma_y^i}{\sigma_o} \right)^{B/RT} dt \quad (14)$$

For constant stress testing, that is, for stress constant at  $\sigma_y$  for a duration  $t_d = t_y - t_1$ , where  $t_d$  is ordinarily called the delay time, the criterion becomes:

$$t_d = A \sigma_o^{B/RT} \sigma_y^{-B/RT} \quad (15)$$

For constant stress rate testing, that is for the stress rate constant at  $\dot{\sigma}$  for  $\sigma$  approaching  $\sigma_y$ , the yield criterion takes the form:

$$\dot{\sigma} = \frac{1}{A} \frac{\sigma_o^{-(B/RT)} \left( \frac{B}{RT} + 1 \right) \sigma_y^{B/RT}}{\frac{B}{RT} + 1} \quad (16)$$

For the yield criterion of Eq. (14), the material properties involved in yield behavior are represented by four parameters: the rate-temperature independent component of the upper yield stress  $\sigma_{ym}$ , the constant frequency factor  $A$ , and the constants  $B$  and  $\sigma_o$  from the activation energy expression. This criterion, and its more general form given by Eq. (12), can be adapted by direct or numerical integration to any form of variation of the stress with time prior to yielding.

The Simplified Form of Yield Criterion applies for loading conditions limited to reasonably constant stress rate prior to yield. The yield stress remains defined by Eq. (11), but the yield criterion of Eq. (12) is replaced by the expression:

$$C = \frac{1}{\dot{\sigma}} \exp \left( - \frac{U}{RT} \right) \quad (17)$$

where C has units of seconds/ksi. Again, using the activation energy form of Eq. (13), Eq. (17) becomes

$$\dot{\sigma} = \frac{1}{C} \sigma_o^{-\frac{(B/RT)}{B}} \sigma_y^{\frac{(B/RT)}{B}} \quad (18)$$

The total upper yield stress may be expressed by substituting in Eq. (11) as:

$$\sigma_y = \sigma_{ym} + \sigma_o \exp \left[ \frac{2.3 RT}{B} (\log C + \log \dot{\sigma}) \right] \quad (19)$$

Again, the material properties are represented by four parameters in the yield criterion:  $\sigma_{ym}$ ,  $\sigma_o$ , B, and C.

In considering the effect of state of stress on the yield stress, the von Mises-Hencky or critical octahedral shearing stress criterion is employed. The expressions of the yield criteria given above may be converted from simple tension or axial stress to octahedral shearing stress by replacing each uniaxial stress term by 2.12 times a corresponding octahedral shear term. Equation (11) becomes

$$\tau_y = \tau_{ym} + \tau_y' \quad (20)$$

and Eq. (19) becomes

$$\tau_y = \tau_{ym} + \tau_o \exp \left[ \frac{2.3 RT}{B} (\log C + .33 + \log \dot{\tau}) \right] \quad (21)$$

The simplified criterion can be expressed in terms of a rate-temperature parameter:

$$\beta = T(-\log C - 0.33 - \log \dot{\tau}) = T(-\log C_o - \log \dot{\tau}) \quad (22)$$

Introducing  $\beta$  in Eq. (21), the upper yield point criterion becomes

$$\tau_y = \tau_{ym} + \tau_o \exp \left( -\frac{\beta}{K} \right) \quad (23)$$

where  $K = B/2.3R$  and has units of temperature.

Procedures for the Evaluation of the Yield Criterion of Eq. (12) for an arbitrary form of the activation energy function are given elsewhere (22). The following more direct procedure may be used for evaluation of the simplified criterion of Eq. (17) with the activation energy form of Eq. (13). The rate-temperature independent component  $\sigma_{ym}$  can be estimated closely from the trend of the data at very low rates of stress. With  $\sigma_{ym}$  known the test data can be plotted as  $\log \sigma_y'$  vs  $\log \dot{\sigma}$ . From Eq. (19) (illustrated in Fig. 11) it will be observed that theoretically straight lines connecting data points for the same temperature should intersect at a common point of coordinates  $(-\log C, \log \sigma_o)$ . The slope of a ray from this point through data points for one common temperature is  $RT/B$ .

$$\sigma'_y = \sigma_0 \exp \left[ \frac{2.3 RT}{B} (\log C + \log \dot{\sigma}) \right]$$

$$\log \sigma'_y = \log \sigma_0 + \frac{RT}{B} (\log C + \log \dot{\sigma})$$

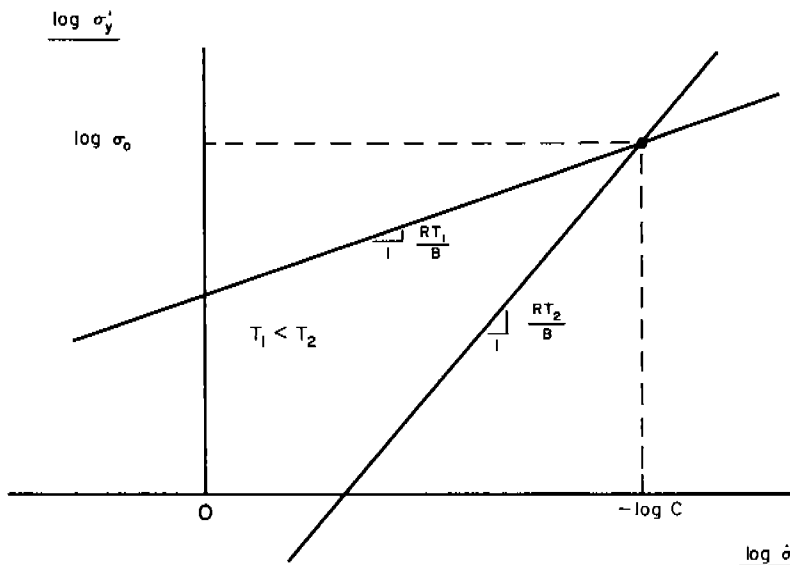


Fig. 11. Plot of Rate-Temperature Dependent Component for Simplified Yield Criterion.

A simple semi-graphical procedure gives quick convergence to the yield criterion parameters:

(1) A ray is drawn through the data points for each particular temperature to give best fit to data at that temperature.

(2) A point of average intersection of the rays is selected. This defines a trial value of  $\sigma_0$  and  $\log C$ .

(3) Rays giving best fit to the data at each temperature are drawn through the selected intersection point. Their slopes are measured and  $B$  computed for each ray from  $B = RT/\text{slope}$ . An average value of  $B$  is selected.

(4) Another cycle to improve convergence may be carried out by using the average  $B$  computed above in step (3).

If good fit cannot be obtained another value of  $\sigma_{ym}$  can be tried. A poor value of  $\sigma_{ym}$  is indicated if consistently curved lines are required to connect data points at the same temperature. A systematic lack of fit of the criterion indicates that it is not appropriate to the material. The possibility that a form of activation energy other than that of Eq. (13) is required can be investigated using procedures described elsewhere (22).

## 6. The Influence of Welding on Yield Behavior in Thermally Affected Zone

Test Material was taken from half of a 2-ft by 3-ft by 1-5/8-in. ASTM A212-B (firebox quality) plate that had been fractured at an applied stress near yield in an investigation reported by Nordell and Hall (1). The material is referred to hereafter as WN steel. This plate contained a central butt weld parallel to the applied tensile stress and the rolling direction.

The results of standard static tensile tests on the as-received material are tabulated in Table 1. The results of Charpy tests run on another 1-5/8-in. plate from the same heat are shown in Fig. 26. Residual stresses were determined by a relaxation technique in a plate from the same heat fabricated similarly to the one from which the tensile specimens were taken. The observed residual stress was approximately 60 ksi longitudinal (parallel to the weld) and 25 ksi transverse (in the width direction of the plate) at the location of the thermally affected zone specimens of this investigation. A check chemical analysis of the steel is shown in Table 1. The analysis is an average of values taken from the surface, one-quarter thickness, and mid-thickness. The carbon content was 0.04 percent higher near the plate surface than at mid-thickness.

The original 2-ft by 3-ft plate was made by joining plates flame-cut from a 6-ft by 12-ft plate. The edges were beveled by machining in preparation for welding. The weld was a double-vee butt weld, parallel to the direction of tensile loading and rolling. The electrodes used for welding conformed to A.W.S. Class E7018. The interpass temperature was 100°F for the thirty (30) passes used for the butt weld. The residual stress field introduced by the welding was not relieved. The plate was tested as an as-welded plate and is identified as specimen 6-44 in Table 2.

The plate was welded and tested in April, 1963. After the test it was stored until specimens for the present investigation were machined in November, 1963. The temperature during the period was approximately 75°F.

The Specimens used in this investigation were taken from half of the fractured plate described above. On the basis of their location in the plate, Fig. 12, the specimens are denoted as thermally affected zone (TAZ) or unaffected base metal (base). The specimen axes were oriented parallel to the rolling direction and parallel to the axis of the plate weld. The TAZ specimens contained no weld metal and were not in the discolored heat affected zone immediately adjacent to the weld; they were located in the region of the first stage of two-stage fracture, and in the region of cracking of some plates during sawing of notches. The edge of the TAZ specimen was at roughly the same distance from the weld as the edge of the sawed notch. Photomicrographs of the metal near the axes of the specimens were prepared as part of this investigation. No significant difference between the TAZ and base material were observed. The ferrite grain size was ASTM 5.

The dimensions of the tensile coupons appear in Fig. 13. The individual specimens were sawed from the plate, machined to 3/8-in. diameter in a lathe, threaded, and machined to a gage diameter of 0.200 in. Cuts were 0.005 in. in depth with final cuts of 0.001 in. The specimens were hand polished using emery cloth. The specimens were not heated beyond a temperature comfortable to the touch at any stage. The final diameter was  $0.200 \pm 0.002$  in.

The Testing Machine used in this study was a 20-kip capacity, gas operated, slow- or rapid-loading device. Stress rates were varied from  $10^{-2}$  ksi/sec to  $10^5$  ksi/sec by methods described elsewhere (22).

#### Instrumentation

Budd metal film strain gages were used to measure strain. Two types were used, C6-144B and C6-141B. Both types are temperature-compensating with 1/4-in. gage length. The 144 series was used for the extreme temperatures (+250°F and -109°F) and the 141 series for the moderate temperature (+32°F). For high temperature (+250°F) tests C-2 epoxy cement was used. In low temperature (-109°F)

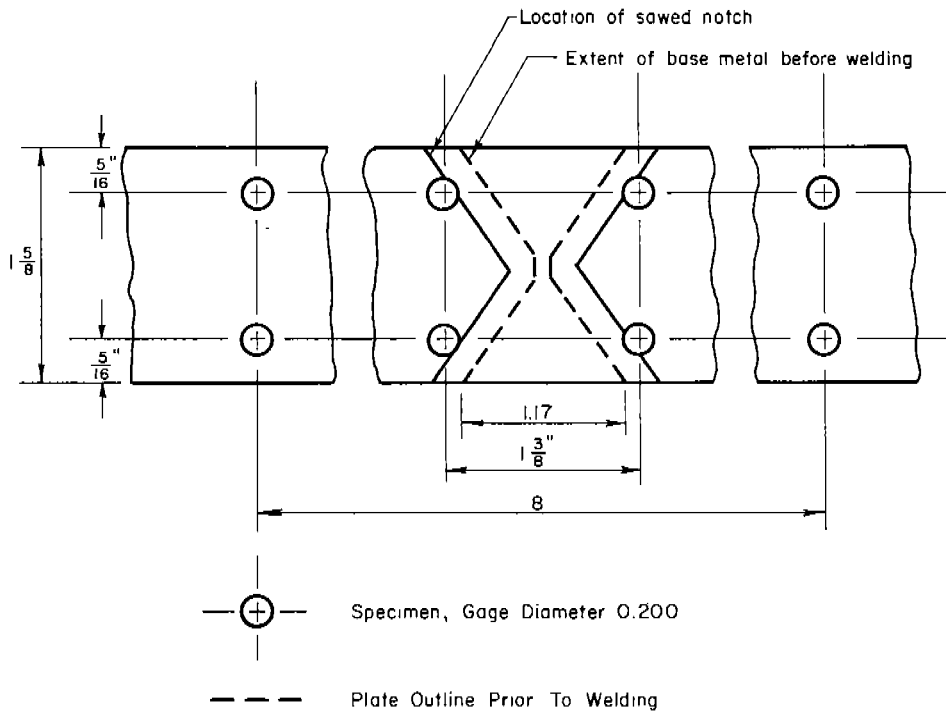


Fig. 12. Specimen Location in Welded Plate.

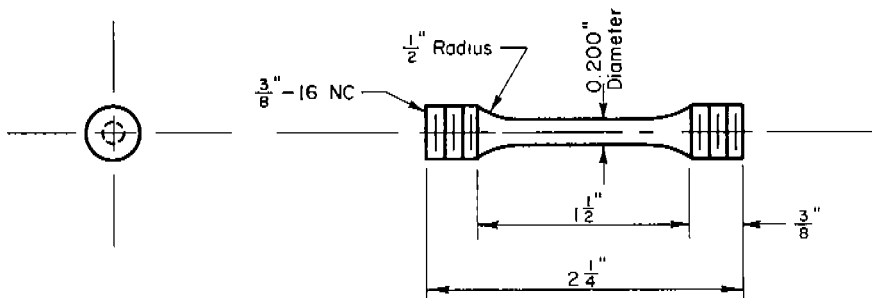


Fig. 13. Tensile Specimen.

and moderate temperature (32°F) tests GA-5 epoxy cement was used. Two gages were applied diametrically opposite one another on the specimen gage section. In curing the strain gage cement, specimens to be tested at 250°F were heated to 200°F for 140 minutes; the other specimens were heated to 175°F for 260 minutes.

The strain measuring gages were connected independently into four-arm (one active arm) bridges. Tensile strain calibrations were placed on the record by introducing known resistances in series with the active gage. The load was measured by a dynamometer employing a four-arm strain gage bridge placed to average out bending and provide self-temperature compensation.

The test data were recorded simultaneously on a Honeywell 8100 tape system and on a Consolidated Electrodynamics Corporation Type 5-124 oscillograph. Time traces were obtained from the tapes from a playback system. Data from the oscillograph records were reduced manually.

The temperatures were determined by the use of thermocouples connected to a Type H, Leeds and Northrup, Speed-0-Max. The temperature of the specimen was measured at the top and bottom shoulders. For temperature control the speci-

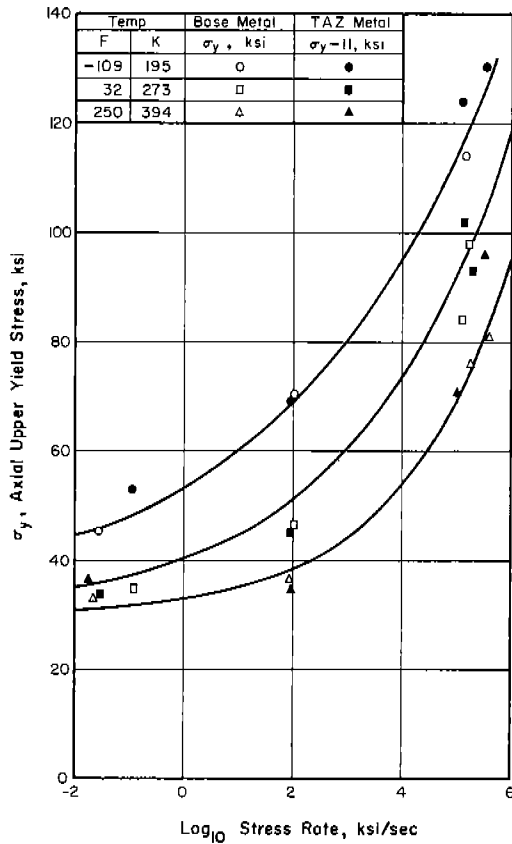


Fig. 14. Upper Yield Point for WN Steel and Computed Curves for Simplified Form of Yield Criterion.

men was placed in a bath. The bath fluids were dry ice and alcohol (-109°F), ice and water (+32°F), and heated transformer oil (+250°F). The oil was circulated by pumping from a larger reservoir. In cooling, the ice was packed in the bath around the specimen to pre-cool bath material and specimen. The fluid (alcohol or water) was added to the bath to get uniform temperature. Cooling time after introduction of the fluid was 10 to 20 minutes.

Test Data are plotted in Fig. 14 as the axial upper yield stress versus the logarithm of the stress rate in ksi/sec. Open data points apply to the base metal specimens, while closed points give the upper yield stress with 11 ksi subtracted for the specimens from the thermally affected zone adjacent to the welds. The curves appearing on these figures correspond to yield criterion parameters discussed below. The variation of the yield stress with stress rate and temperature is nearly identical for the material from the two regions. The only apparent systematic difference is that the yield stress appears to be some 11 ksi higher for the specimens from the thermally affected zone. The test data for the two materials at one temperature appear to fall on a single curve within the scatter inherent in the data.

The slow test data at 250°F appear nearly coincident with the slow test data at 32°F. This may be a result of aging prior to yield. The somewhat greater scatter in the TAZ data may be attributed to greater potential variation in the properties of specimens from a zone of gradient microstructure.

TABLE 5. STEEL GRAIN SIZE AND COMPOSITION.

Steel	Parent Stock	ASTM Grain Size	Check Analysis, percent								
			C	Mn	Si	P	S	Al	Cu	Ni	N
WN	1-5/8 in. plate A212-B	5	.26	.82	.14	.02	.036	.006	-	-	-
WHH	3/4-in. plate A7 Killed	6	.17	.89	.18	.02	.034	.06	.08	.025	-
CW	5/8-in. diam. hot rolled	7	.17	.39	-	.017	.04	-	-	-	-
KC	1-in. plate hot rolled	4	.04	.28	.01	.05	.045	-	-	-	.024

TABLE 6. PARAMETERS OF GENERAL YIELD CRITERION.

$$\sigma_y = \sigma_{ym} + \sigma_y'$$

$$A = \int_{t_1}^{t_y} \left[ \frac{\sigma_y'}{\sigma_o} \right]^{B/RT} dt$$

Steel	$\sigma_{ym}$ , ksi	A, sec	$\sigma_o$ , ksi	B, cal/mol
WN, Base	28	$1.0 \times 10^{-7}$	214	3000
WN, TAZ	39	$1.0 \times 10^{-7}$	214	3000
WHH	38	$1.0 \times 10^{-7}$	220	2350
CW	32	$4.0 \times 10^{-9}$	214	3750

### 7. Yield Criterion Parameters

The data obtained in the study described above were used to evaluate the parameters of the general yield criterion of Eq. (14) and the simplified yield criterion of Eq. (19). The results are given in Tables 6 and 7 respectively, for the material identified as WN steel. The curves shown in Fig. 14 correspond to the simplified form of the yield criterion. The agreement between the data points and curves is fair. In the evaluation of the yield criterion it appeared that the activation energy form of Eq. (13) fits the data very well at any one temperature. However, there appears to be some effect of temperature on the activation energy; such influence is not considered in Eq. (13).

TABLE 7. PARAMETERS OF SIMPLIFIED YIELD CRITERION.

$$\sigma_y = \sigma_{ym} + \sigma'_y \quad \sigma'_y = \sigma_o \exp \left[ -\frac{\beta}{K} \right]$$

$$\tau_y = \tau_{ym} + \tau'_y \quad \tau'_y = \tau_o \exp \left[ -\frac{\beta}{K} \right]$$

Steel	K, °K	$\sigma_{ym}$ , ksi	$\sigma_o$ , ksi	$\beta$ (for $\dot{\sigma}$ and $\dot{\tau}$ in ksi/sec), °K	$\tau_{ym}$ , ksi	$\tau_o$ , ksi
WN, Base	780	30	178	$T(8.00 - \log \dot{\sigma}) = T(7.67 - \log \dot{\tau})$	14	84
WN, TAZ	780	41	178	$T(8.00 - \log \dot{\sigma}) = T(7.67 - \log \dot{\tau})$	19	84
WHH	670	38	234	$T(9.05 - \log \dot{\sigma}) = T(8.72 - \log \dot{\tau})$	18	110
CW	953	32	190	$T(9.50 - \log \dot{\sigma}) = T(9.17 - \log \dot{\tau})$	15	90
KC	766	31	250	$T(8.00 - \log \dot{\sigma}) = T(7.67 - \log \dot{\tau})$	15	118

Data giving the upper yield point for wide ranges of both temperature and a time parameter such as stress rate or delay time are available for a steel termed CW used in a number of investigations reported by the Clark-Wood group (27,28,29,30) as well as Krafft and Sullivan (31) and a steel termed WHH tested by Wright, Hall and Hamada (22). The properties of these steels are given in Table 5, the parameters determined for the general yield criteria of Eq. (14) are given in Table 6, and parameters for the simplified constant stress rate criterion of Eq. (19) appear in Table 7. The parameters of the simplified constant stress rate criterion also are shown in Table 7 for a steel, termed KC, studied by Knott and Cottrell (32). The data for the latter steel were too limited to warrant evaluation of the general yield criterion; the evaluation for the simplified criterion is not well defined and must be used with caution.

The fit of the simplified yield criterion to the experimental data for the CW and WHH steels is shown in Figs. 15 and 16. The plotted data points have an abscissa  $\beta = T(-\log C - \log \dot{\sigma})$  and an ordinate  $\sigma'_y = \sigma_y - \sigma_{ym}$ . In computation for the plotting, measured values of T,  $\dot{\sigma}$ , and  $\sigma_y$  were used in conjunction with the appropriate criterion parameters log C and  $\sigma_{ym}$ . Much of the CW data was obtained in constant stress tests providing data on the variation of delay time with stress. In order to show these data in Fig. 15 the general yield criterion was used to compute an equivalent stress rate giving the same upper yield stress at the same temperature

$$\dot{\sigma} = \frac{\sigma'_y}{t_d \left( \frac{B}{RT} + 1 \right)} \quad (24)$$

where B has the value appropriate to the general yield criterion of Eq. (14).

The WN steel tested as part of this program exhibited the same rate-temperature dependent component of the yield stress in both the base metal and

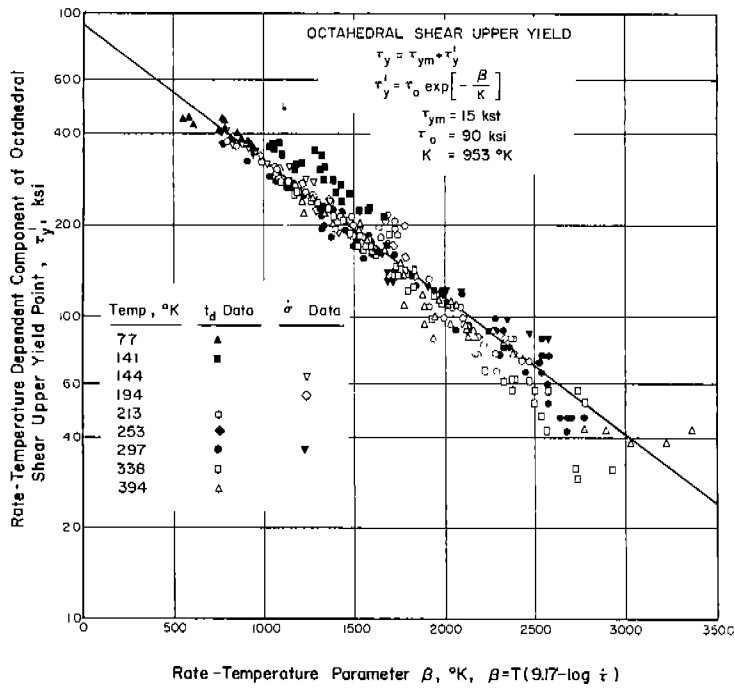


Fig. 15. Rate-Temperature Dependent Component of Upper Yield Stress for CW Steel.

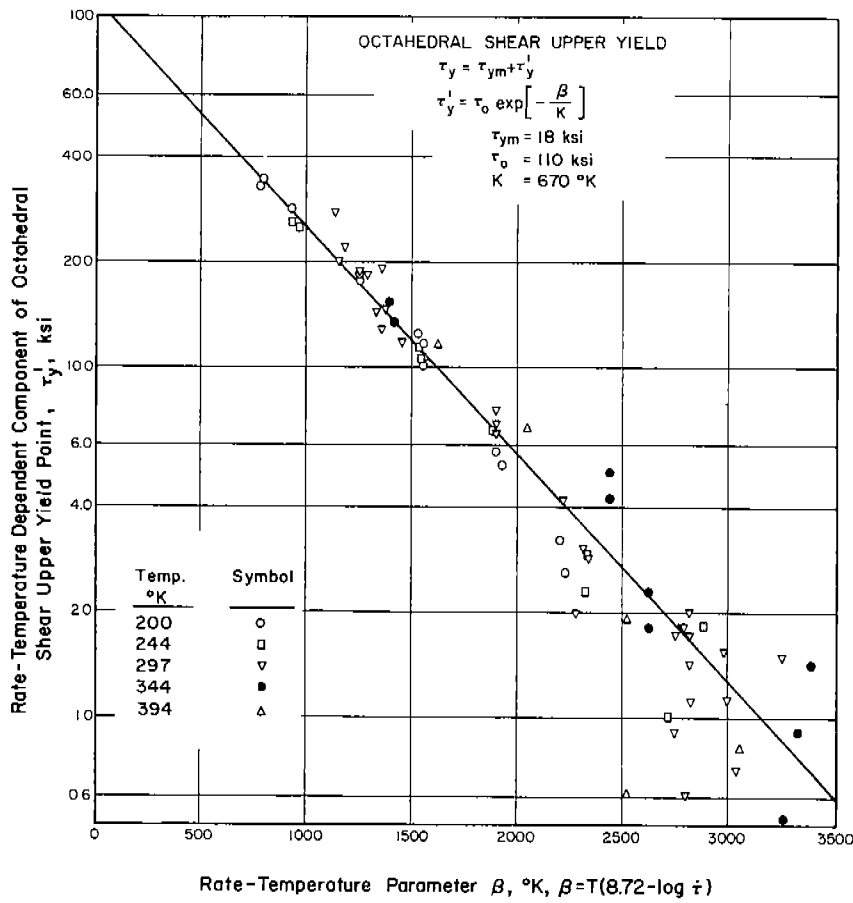


Fig. 16. Rate-Temperature Dependent Component of Upper Yield Stress for WHH Steel.

the thermally affected zone. The influence of the thermal and deformation history associated with the welding appeared entirely in the rate-temperature independent component of the yield stress. If the rate-temperature dependent component is unaffected by prior heating, cooling, and deformation that do not change the basic structure of the alloy, the effects on yield behavior of welding operations and procedures intended to reduce the embrittling effects of welding can readily be studied. The effects on the rate-temperature independent component  $\sigma_{ym}$  can be determined by static tensile coupon testing at a known strain rate and temperature if the unaffected rate-temperature dependent component  $\sigma'_y$  is known for these conditions.

The scope of this investigation was inadequate to define the range of thermal and deformation history that can be imposed without affecting  $\sigma'_y$ , the rate-temperature dependent component. However, a goodly amount of evidence suggests that the rate-temperature dependent component of the yield stress is insensitive to the deformation and thermal history. Wright, Hall and Hamada (22) were able to use the same values of the parameters B and  $\sigma_o$  of Eq. (19) in applications to upper yield stress and flow stress at plastic strains up to 0.06. The parameter C changed markedly between the upper yield stress and flow stress at 0.02 plastic strain and more gradually thereafter. Bennett (33) and Conrad (23) have shown that steels having a wide variety of composition and grain size have similar rate-temperature dependent components of upper yield, lower yield and flow stresses. These observations tend to confirm the hypothesis that the effects of deformation and thermal history appear in the rate-temperature independent component of the yield or flow stress. The grain size dependent component of yield or flow stresses reported by Heslop and Petch (34) and Petch (35) also appears to belong to this term.

#### 8. Yield Criterion Application

The upper yield point criterion of Eq. (19) is used in Part III of this report for estimation of plastic zone size in the vicinity of a stress raiser and for prediction of the initiation of gross yielding in a structural element or test specimen. Neither application coincides exactly to the condition for which the criterion was evaluated -- the initiation of gross plastic deformation in a smooth uniaxial coupon.

The type of uniaxial coupon used to obtain most of the test data is unlikely to provide a uniform uniaxial stress state. Stress concentrations result from fillets on the specimen and stress gradients also result from minor eccentricities of loading. Hutchison (36) used center annealed long wires to achieve near-ideal stress conditions and much larger yield drops than were observed in the testing considered herein. The upper yield point criterion as developed herein applies more to the stress-time-temperature conditions required to make a plastic zone, initiated under higher than average stress, grow across a coupon on the order of 1/2 in. in diameter than to the conditions required for the local initiation of yielding as a function of local stress.

The time required for a yielded region to grow large enough to permit gross plastic deformation probably is size dependent. This size effect is expected to influence the parameter C of the yield criterion. Size effect is not considered herein in applications of the yield criterion because its quantitative formulation is unknown. Studies leading to a size dependent formulation of the yield criterion would be valuable.

Part III

CRITICAL STRESS MODEL FOR CLEAVAGE FRACTURE

9. Background

The low nominal stress fracture of steel structures undoubtedly involves very high stresses in the local region of separation of the material. In the sub-microscopic sized region where interatomic bonds are breaking normal stresses must be of the order of the theoretical cleavage strength of about  $E/10$ . Such stress magnitudes can occur in the vicinity of a microcrack located in a region of microscopic dimension which is subjected to stresses of the order of  $E/100$ . The highly triaxial stress distribution and steep strain gradient in the vicinity of macroscopic flaws permit stresses of the order of  $E/100$  to occur in an element subjected to average stresses of the order of  $E/1000$ . The multiplication process noted suggests why brittle behavior of a structure is possible under normal design loading.

In an early study of the conditions for brittle structural behavior Ludwik (37) suggested that cleavage fracture follows when the stress required for additional inelastic deformation rises to a critical stress level required for cleavage. This concept has been generally validated by experiments, but for low-carbon steel specimens free of severe stress raisers and gross material damage, very low temperatures or very large inelastic deformations are required to raise the resistance to inelastic deformation to a level permitting cleavage fracture. Elements of real structures have fractured in a brittle manner at normal environmental temperatures and low nominal stresses with a negligible amount of associated gross inelastic deformation. Mylonas (38) and others have shown that the initiation of such brittle behavior may be associated with severely damaged material, i.e. the physical properties of the metal in the vicinity of the cleavage initiation have been altered by the local thermal and deformation history. Flaws or stress raisers contribute to the damage of the material and produce severe stress conditions in the damaged material.

Because cleavage fracture occurs very locally in an element, the Ludwik critical fracture stress concept has not provided a useful fracture criterion when expressed in terms of nominal stress computed by ordinary engineering formulas. If attention is directed to a small region in the vicinity of a flaw that may or may not give rise to a cleavage fracture, more success is obtained with the concept of a critical fracture stress criterion for cleavage. Hendrickson, Wood and Clark (39) have taken the maximum principal normal stress occurring in the plastic zone surrounding a notch in an otherwise elastic specimen to be the critical stress in the sense of the Ludwik fracture criterion. If strain hardening is negligible this maximum stress acts at the elastic-plastic interface. Their results indicate that brittle cleavage follows when temperatures are low enough, stress (or strain) rates are high enough, and the triaxial stress state in the region of the notch is sufficiently severe to so limit the size of the plastic zone that the principal normal stress at its boundary reaches a critical level. This critical fracture stress, of the order  $E/100$ , appears to be relatively insensitive to temperature and stress (or strain) rate.

Energy and strain criteria also have been suggested for prediction of susceptibility to cleavage fracture. Orowan (40) has shown that a critical fracture stress criterion is equivalent to a Griffith-Irwin type of energy criterion. A critical fracture stress criterion appears to permit a more direct consideration of rate and temperature effects upon material properties. Criti-

cal strain and critical stress are definitely equivalent with respect to atomic bonds being severed in cleavage. A principal normal critical fracture stress in the vicinity of a cleavage crack may be more or less directly related to the normal strain, and the resistance to additional inelastic deformation and the amount and size of microflaws may be related to the shearing strain history. No generally applicable criterion for cleavage can be developed without consideration of the deformation state and its influence on the material properties. However, it appears that a strain criterion for cleavage would be expressed in terms of normal strain and, therefore, be equivalent to a critical stress criterion.

The application of the concept of critical fracture stress to the evaluation of brittle cleavage resistance of structures fabricated with usual low-carbon ship steel alloys is considered herein. The engineering problem of major concern is low stress cleavage. Thus, by definition, most of a structural element of concern is stressed at working stress levels and the element is essentially elastic. The plastic zones are confined to the immediate vicinity of flaws, and the principal normal stress at the elastic-plastic interface can be a meaningful measure of the tendency to cleavage. As noted recently (38) this general type of approach has yet to be applied with rigorous stress-deformation relations and, as such, has recognized shortcomings. None the less the writers feel that the critical stress concept expressed in terms of the maximum principal normal stress at a pseudo elastic-plastic interface can provide a measure of susceptibility to cleavage fracture for defined ranges of conditions.

#### 10. Critical Stress Model for Cleavage

The critical fracture stress criterion considers that cleavage fracture results when the maximum principal normal stress in a region of plastically deformed material reaches a critical level. A mechanism for cleavage consistent with the existence of a critical fracture stress is discussed below; following that an approximate analytical model is developed for the application of the critical stress concept to conditions of cleavage initiation, propagation, and arrest.

The influence of factors known to affect the tendency to cleavage (such as flaw acuity, stress or strain rate, temperature, prior inelastic deformation, and residual stress) are studied herein in the light of the critical fracture stress criterion. Successful representation of observed behavior would justify studies intended to obtain empirical correlations permitting engineering applications of the critical stress model, as well as theoretical studies aimed at an improved critical stress model.

#### Micromechanism of Cleavage

The writers are not aware of a generally accepted micromechanism for the growth of a cleavage fracture. The following general discussion of cleavage fracture in body centered cubic iron alloys is advanced to point out the physical significance of the critical fracture stress criterion and show how various material properties may influence the critical fracture stress.

Much evidence exists to associate cleavage fracture with the growth of microcracks as has been described by Hahn, et al (41) and McMahon (42). A microcrack can grow because the strain or stress concentration at its boundary is adequate to break interatomic bonds. The growth of a microcrack also can be visualized in terms of dislocation climb as shown by Friedel (43). Friedel's analysis and experimental observations by others show that only very sharp

microcracks are susceptible to growth as cleavage cracks. A sharp microcrack is likely to be unstable; it either grows in cleavage or is blunted by plastic deformation. A variety of mechanisms for the formation of microcracks have been advanced (41,42,44); most such mechanisms require inelastic deformation for the formation of microcracks and are therefore consistent with the experimentally observed requirement that local plastic flow precede cleavage.

The tendency for a roughly penny-shaped microcrack to grow by cleavage fracture would appear to be related to the magnitude of the normal stress acting perpendicular to the plane of the crack. Friedel (43) relates the microcrack to an array of climbing dislocations and expresses the equilibrium stress  $\sigma_e$  normal to the crack as

$$\sigma_e = \frac{G}{(1-\nu)} \frac{h}{L} \quad (25)$$

with  $G$  the shear modulus,  $\nu$  Poisson's ratio,  $h$  the microcrack height, and  $L$  the microcrack length. The tendency to cleavage growth would depend upon the crystallographic plane occupied by the microcrack and its orientation with respect to the principal normal stress. The concern is with the type of microcracks that lead to cleavage and it may be assumed that the volume of highly stressed material, or macroflaw length, is large enough compared to grain size so that favorably oriented microcracks can appear. A size effect must occur, but the following development assumes all cases of interest are associated with a high probability of the presence of a critically oriented microcrack.

The critical fracture stress is here associated with the effective principal stress normal to a microcrack which causes it to grow as a cleavage crack. Microcracks leading to cleavage fracture appear to be one or two grain diameters in length. Therefore the critical fracture stress is a local stress, effective over areas of the order of the grain area, but this area is large enough to suggest that continuum mechanics principles may be employed for computation of the critical fracture stress. As a matter of interest, Drucker (46), among others, is studying the application of continuum mechanics principles to real materials behavior. Observations of microcracks leading to cleavage fracture suggest that the ratio  $h/L$  in Eq. (25) may be of the order of 1/100. With  $G = 12 \times 10^3$  ksi,  $\nu = 1/3$ , and  $h/L = 0.01$ ,  $\sigma_e$  is 180 ksi which is of the order of critical fracture stresses determined by Hendrickson, Wood and Clark (39), Barton and Hall (45) and others. They used elasto-plastic analyses to determine the plastic zone size and the principal normal stress at the elastic-plastic interface in notched specimens at the time of observed cleavage initiation. Using this principal normal stress as a measure of the critical fracture stresses, values of 210 ksi and 246 ksi were obtained for low-carbon steel alloys comparable to those employed in ship structures. These can be considered representative figures and are of the order reported by other investigators.

The critical fracture stress may be a material property defined by the sharpest microcrack which tends to form in the metal. It is logical for the microcrack acuity to reach its critical value (minimum  $h/L$ ) for a microcrack about one grain diameter long. For a microcrack to exist the height  $h$  must be one lattice spacing. For the shortest microcrack -- a vacancy --  $h/L$  is one;  $h$  would tend to increase more slowly than  $L$  if the microcrack can grow fairly easily in an individual grain. The mismatch of cleavage planes in adjacent grains would provide a tendency for the microcrack to blunt at a grain boundary. It can be hypothesized that for the critical  $h/L$ ,  $L$  is of the order of the grain diameter. If  $h$  is nearly independent of  $L$  for a sharp microcrack extending over only one grain, a critical fracture stress defined by  $\sigma_e$  of

Eq. (25) would be inversely proportional to grain diameter. With  $\sigma_{1c}$  representing critical fracture stress and  $d$  the grain diameter

$$\sigma_{1c} \propto \sigma_e \propto \frac{h}{L} \propto \frac{1}{d} \quad (26)$$

As shown later, the inverse proportionality of critical fracture stress to grain diameter of Eq. (26) leads to a  $d^{-1/2}$  variation of nominal stress for cleavage in sharply flawed structural elements.

If the critical fracture stress is of the order of  $E/100$ , in low-carbon steels such stresses can occur at normal temperatures only in the vicinity of gross stress raisers which induce the hydrostatic type stress distribution required for high principal normal stresses without overall inelastic deformation of the structural element. Cleavage would begin at the point in the plastic zone at the root of a stress raiser where a sufficiently sharp microcrack is first associated with a sufficiently high local principal normal stress. For an elastoplastic material the maximum principal normal stress occurs at the elastic plastic interface; because this is a surface of blocked plastic flow it also may be a favorable site for microcrack formation. In real strain hardening materials the maximum principal normal stress can occur within the plastic zone; the larger plastic strains occurring within the plastic zone may be conducive to microcrack formation there. The critical stress model for cleavage used herein is consistent with cleavage beginning either well within the plastic zone or near the elastic-plastic interface. The resulting cleavage fracture is not continuous in a microscopic sense; the growing cleavage crack will encounter zones of material poorly oriented for cleavage and momentarily arrest locally; but stress-time conditions ordinarily are adequate to permit immediate reinitiation of the cleavage process in favorably oriented material and ductile tearing of unfavorably oriented material. In the following development the process of cleavage is considered to be essentially continuous in the macroscopic sense.

It may not be necessary to formulate the mechanics of microcrack growth, if for a particular microstructure a particular form of microcrack results from plastic flow, and if the principal normal stress in the vicinity of the microcrack exceeds a critical value, the microcrack grows as a cleavage crack. Under such conditions the critical fracture stress becomes identified with the microstructure.

Hereafter the critical stress for fracture is considered in the above sense. A region of material that has undergone inelastic deformation is assumed to contain critical microcracks. If the principal normal stress in the region exceeds the critical fracture stress, cleavage fracture is predicted. The critical fracture stress is assumed to have the limited rate and temperature sensitivity of the elastic constants although this point merits further study. The critical fracture stress is considered to depend upon the local thermal and deformation history since these factors can affect the microstructure and consequently the size and proportions of microcracks.

#### Approximate Critical Stress Model

An approximate critical stress model is obtained by defining the extent of the plastic zone in the vicinity of a gross stress raiser by the elastic stress field and using the maximum elastic principal normal stress at the elastic-plastic interface as a measure of the critical fracture stress in the plastic zone. The yield criterion discussed in Part II is used to determine the extent of the plastic zone as a function of stress rate and temperature with the three dimensional stress state accounted for by the critical octahedral shearing stress

or von Mises yield condition. For the consideration of very sharp flaws it also is necessary to define, as a material property, a minimum plastic zone size.

Detailed descriptions of the application of the model to conditions of cleavage initiation and propagation are given later. The basic procedure for a given structural element or specimen containing a gross stress raiser is as follows. For a given loading condition, temperature, and rate of increase of stress (or velocity of crack propagation), (1) the elastic stress field in the vicinity of the flaw is evaluated, (2) the distance from the flaw at which the yield criterion (considering local stress rate, stress state, and temperature) is satisfied determines the extent of the plastic zone, and (3) the value of the maximum principal normal stress at the elastic-plastic interface is compared to the critical fracture stress to determine whether the condition for cleavage is satisfied. Brittle or low stress cleavage fracture is predicted when the nominal or average stress in the element is less than that required to produce general yielding for the conditions of nominal stress rate and temperature, while at the same time the critical fracture stress is attained in the plastic zone in the vicinity of the stress raiser.

This application of the model will not produce a dependable quantitative measure of conditions for brittle cleavage when plastic zones are large. The location of the elastic-plastic interface is guided only by the elastic stress distribution and can be expected to deviate more from the true location as plastic zone size increases. In addition, the maximum principal normal stress at the elastic-plastic interface becomes a progressively poorer measure of the maximum principal normal stress within the plastic zone as the zone becomes larger and strain hardening effects increase. However, it is felt that the simplified application provides a measure of the influence of variations in factors such as notch acuity, rate of loading, temperature, residual stress, and prior inelastic deformation on the cleavage fracture susceptibility of fabricated steel structures. It has the advantage that it may readily be applied for evaluation of susceptibility to cleavage fracture. By means of judicious experimental correlations to define ranges of applicability it appears possible to employ this application of the critical stress model for predictions of resistance to fracture.

Based as it is on the elastic stress field, this application of the critical stress model for cleavage cannot be applied to the prediction of cleavage following gross plastic deformation. The basic critical stress model for cleavage should be equally applicable to ductile cleavage, but it will be necessary to determine the influence of inelastic deformation on the critical fracture stress and to develop procedures for defining the maximum principal normal stress in a yielded region.

The Yield Criterion discussed in Section 8 is used to define the extent of inelastic deformation in the vicinity of a macroscopic flaw and the gross yielding of a structural element as a function of temperature and the rate of increase of stress. Except for unknown size effects, this criterion relates quite closely to the conditions for growth of a plastic zone at a macroscopic flaw. The upper yield stress criterion provides a fair measure of the conditions for general yielding under a uniform state of stress -- that is when general yielding can occur in an unflawed portion of the structural element. It is recognized that a lower yield point criterion might be more appropriate for identifying conditions for general yielding, but only limited data are available on the lower yield point as a function of strain rate and temperature. Also, in practical situations it is difficult to determine the strain rate that should be used in such a criterion.

The Stress Field is defined by the elastic stress distribution corresponding to the flaw geometry and applied load at the point on the axis of the flaw where the yield criterion of Eq. (19) is satisfied. In general, no correction to the level of average applied stress is made to account for the difference between the inelastic and elastic stress distributions in the plastic zone. The maximum principal normal stress on the axis of the flaw at the elastic-plastic boundary is used as a measure of the peak principal normal stress in the plastic zone. Appendix C gives a number of solutions for elastic stress fields in the vicinity of various idealized flaws in tensile and flexural nominal stress fields for both static and propagating flaws.

Criterion for Minimum Extent of Plastic Zone -- For sharp flaws the plastic zone, determined as described above, may be less than the grain diameter of the steel. It is difficult to visualize a partially yielded grain because the resistance to movement of dislocations within a grain is small compared to the yield stress of polycrystalline steel. For this reason, the extent of the plastic zone is not permitted to be less than the grain diameter if yielding at the geometrical root of the flaw is indicated by the yield criterion.

The grain diameter is expected to define the particle size criterion for minimum extent of plastic zone, but the one-to-one correspondence suggested above may not be the optimal definition. The geometrical root of the flaw need not correspond exactly to a grain boundary, and the effective particle size may depend on grain size distribution and grain shape as well as the equivalent spherical grain diameter used herein. The truncation of the elastic stress field for a sharp notch also could be accomplished using the Neuber (48) elementary particle concept. The latter procedure has the advantage of maintaining equilibrium of stresses summed over a finite notched element, however, this refinement would not significantly influence the trend of results and the size of the elementary particle still would have to be assumed.

#### Application to Cleavage Initiation

The application of the model to cleavage initiation from a static flaw is demonstrated below. The material properties: critical fracture stress, yield criterion, and minimum plastic zone size, are assumed to be known. The structural element considered is a wide plate containing a small central flaw that may be treated as an elliptical notch in an infinitely wide plate. The applied stress field in the plate is a nominally uniform tensile stress perpendicular to the long axis of the flaw. The influence of temperature and rate of increase of the applied stress on the mode of behavior, pre-yield brittle cleavage or gross yielding, is determined in the development below. The effects of variations in the material properties, residual stress in the vicinity of the flaw, and flaw acuity also are considered.

Conditions for cleavage or yield are explored by assuming that the plastic zone extends to a particular distance from the notch root. The principal normal stress at this point is set equal to the critical fracture stress; the corresponding value of the applied stress is determined from the appropriate notch stress field expression. Then, using the yield criterion, for a given rate of increase of the applied stress, the temperature is determined: (1) for the condition that the plastic zone at the notch root will extend just to the point in question, and (2) for the applied stress to be a gross yield stress for the structural element. If the temperature from (1) exceeds that from (2) brittle cleavage initiation at this extent of plastic zone is impossible. If the same yield criterion is used for the definition of the extent of the plastic

zone and the appearance of gross yield, the relative magnitude of temperature from (1) and (2) remain unchanged for a particular point of initiation as applied stress rate is changed. The process is repeated for other distances from the notch root until the brittle behavior temperature regime is defined for the range of applied stress rates of interest.

For example, consider the following assumed material properties.

Poisson's Ratio:	$\nu = 0.3$
Critical Fracture Stress:	$\sigma_{1c} = 220 \text{ ksi}$
Yield Criterion:	WN Steel, Table 7
Minimum Extent of Plastic Zone (Grain Diameter)	$d = 0.003 \text{ in.}$

The cleavage fracture model is first applied to a wide plate containing an elliptical notch of half length divided by root radius,  $a/\rho$ , equal to 100. The elastic stress field expressions given by Eq. (C-3) of Appendix C are used to define the stress field in the vicinity of the flaw.

Considering conditions for cleavage fracture at a distance  $ka \geq d$  from the notch root:

(1) The ratios  $\sigma_\ell/\sigma_n$  and  $\sigma_t/\sigma_n$  are computed for a particular value of  $k$  using Eq. (C-3) of Appendix C.

(2) Stress  $\sigma_\ell$  is taken equal to  $\sigma_{1c}$ ; corresponding values for  $\sigma_t$  and the applied stress for fracture,  $\sigma_{nf}$  are determined.

$$\sigma_{nf} = \sigma_{1c} \frac{\sigma_n}{\sigma_\ell} \quad (27)$$

(3) Using plane strain conditions for the vicinity of the notch root, because the root radius normally will be small compared to plate thickness and a plastic zone of an extent of the order of the root radius will be confined by adjacent elastic material,

$$\begin{aligned} \sigma_1 &= \sigma_\ell \\ \sigma_2 &= \sigma_t \\ \sigma_3 &= \nu (\sigma_1 + \sigma_2) \end{aligned} \quad (28)$$

$$\tau_k = \frac{1}{3} \sqrt{(\sigma_1 - \sigma_2)^2 + (\sigma_2 - \sigma_3)^2 + (\sigma_3 - \sigma_1)^2},$$

octahedral shear at distance  $ka$  from the notch root

(4) The stress state for cleavage in a plastic zone extending a distance  $ka$  from the notch root is defined. The next step requires the determination of the temperature and rate of application of the applied nominal stress that correspond to this extent of plastic zone.

$$\tau_y = \tau_k \text{ computed above}$$

$$\tau'_y = \tau_y - \tau_{ym}$$

Using the yield criterion

$$\tau'_y = \tau_o \exp \left( - \frac{\beta}{K} \right) \tag{29}$$

$$\beta = T(-\log C_o - \log \dot{\tau}_k) = 2.3 K(\log \tau_o - \log \tau'_y)$$

For a particular value of  $\dot{\tau}_k$ , one may solve directly for the corresponding temperature T. It is meaningful to relate  $\dot{\tau}_k$  to the rate of application of the nominal stress  $\dot{\sigma}_n$

$$\dot{\tau}_k = \frac{\tau_k}{\sigma_n} \dot{\sigma}_n \tag{30}$$

so

$$\beta = T(-\log C_o - \log \frac{\tau_k}{\sigma_n} - \log \dot{\sigma}_n) \tag{31}$$

The resulting nominal fracture stress-temperature curve is shown in Fig. 17 for applied stress rates  $\dot{\sigma}_n$  of 1 ksi/sec and 100 ksi/sec and crack half lengths of 0.1 and 1 in. The ordinate is given in terms of nominal stress  $\sigma_n$  rather than k; a one-to-one correspondence between  $\sigma_n$  and k exists with  $\sigma_n$  increasing with k. At low temperatures  $\sigma_n$  for fracture is constant and corresponds to fracture initiating at the minimum extent of plastic zone ( $k = d/a$ ). For a given temperature fracture is predicted to occur at the stress level given by the curve appropriate to the stress rate and crack length. At temperatures higher than that corresponding to a vertical tangent to the fracture stress curve, cleavage fracture cannot initiate according to the model, the ratio  $\tau/\sigma$  is increasing as k increases, and the critical fracture stress cannot be attained. For the notch geometry considered and the material employed the transition temperature between brittle and ductile behavior is defined by the vertical tangent to the fracture curve.

Another limit to the appearance of brittle cleavage occurs if the nominal stress becomes great enough to produce gross yield of the plate before the critical fracture stress is attained in the vicinity of the notch root. This limit can be shown on the same plot as the nominal fracture stress. The stress state controlling gross yielding of the plate in an unflawed region corresponds to a state of plane stress.

For a yield stress  $\sigma_{ny}$

$$\tau_y = \sigma_{ny} \frac{\sqrt{2}}{3}$$

$$\dot{\tau} = \dot{\sigma}_n \frac{\sqrt{2}}{3} \tag{32}$$

$$\tau'_y = \tau_y - \tau_{ym}$$

Corresponding stress rates  $\dot{\sigma}_n$  and temperature are found using the yield criterion as before with

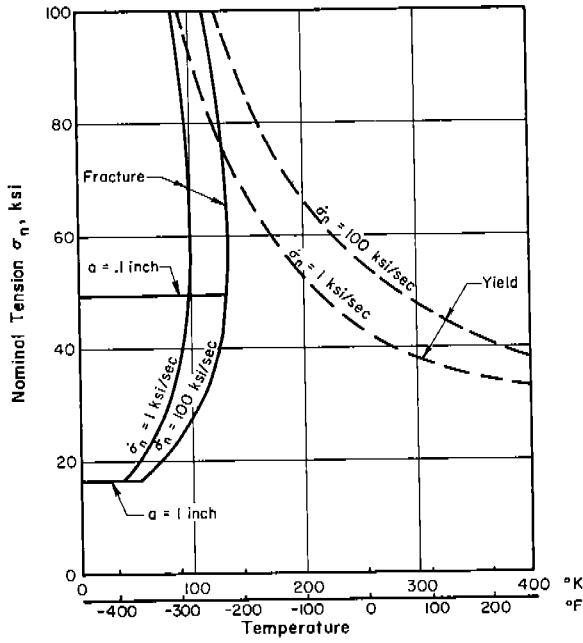
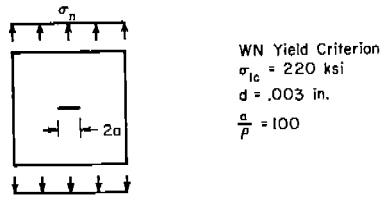


Fig. 17. Fracture and Yield Stress Curves for an Elliptical Notch.

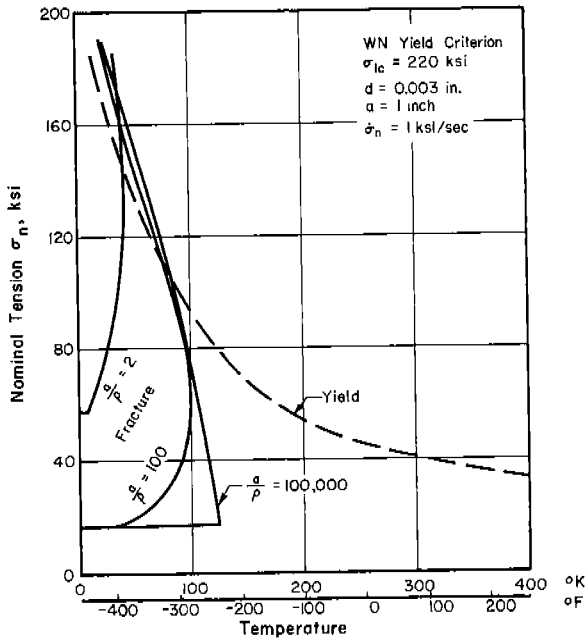


Fig. 18. Fracture Stress Curves for Various Elliptical Notch Acuties.

$$\beta = T(-\log C_o - \log \frac{\sqrt{2}}{3} - \log \dot{\sigma}_n) \quad (33)$$

Nominal stress yield curves are shown in Fig. 17 for  $\dot{\sigma} = 1$  and 100 ksi/sec.

The influence of notch acuity on the transition behavior is shown in Fig. 18. The same material parameters are used, but three notch acuities are considered

Blunt	$a/\rho = 2$
Moderate	$a/\rho = 100$
Sharp	$a/\rho = 100,000$

All curves consider a notch half length "a" of 1 in. and an applied stress rate of 1 ksi/sec. A single yield curve is required since conditions for gross yield of the plate are assumed to be independent of the flaw.

For the blunt notch the transition temperature corresponds to an intersection of the fracture and yield curves, for the moderate notch it corresponds to the vertical tangent to the fracture curve, and for the sharp notch the transition temperature is defined by the minimum extent of plastic zone d. The lower limit on fracture stress in any event corresponds to a plastic zone of minimum extent (here assumed to be one grain diameter).

The coordinates used in Figs. 17 and 18 provide a convenient representation of the fracture or yield level of nominal stress versus the temperature for particular values of notch geometry and nominal stress rate. A plot showing only whether cleavage can be expected to initiate prior to gross yielding for various conditions of stress rate and temperature can be obtained by plotting transition temperatures versus applied stress rate. Such a plot appears in Fig. 19 with curves shown for various notch acuities. Stress rate-temperature conditions plotting above a particular curve are predicted to result in cleavage fracture prior to gross yielding.

The stress field expressions given by Eq. (C-1) of Appendix C may be used for the sharp flaw or crack. In the range  $10\rho < ka < a/100$  these equations give results very similar to those obtained from elliptical notch expressions. The initiation transition temperature for the sharp flaw is a function of the ratio of minimum extent of plastic zone d to half crack length "a". The sharp flaw curve in Fig. 19 corresponds to  $d/a = 10^{-5}$ ; the curve shifts to the left as d/a increases.

The influence of variations in material properties are shown in Fig. 20. Curve (a) provides a reference curve, it corresponds to the material properties used above and  $\dot{\sigma} = 1$  ksi/sec,  $a/\rho = 100$ , and "a" = 1 in. Curve (b) shows the effect of an increase of  $\sigma_{ym}$  at the notch root to 24 ksi. Such local hardening of the material could result from prior plastic strain and aging. Curve (c) shows the influence of a decrease in critical fracture stress to 180 ksi. A reduction in critical fracture stress might result from the presence of unusually severe microcracks. Curve (d) shows the effect of a residual tensile stress in the vicinity of the notch root. This residual stress field has principal components of 60 ksi in the crack opening direction, and 30 ksi in the width and thickness directions. It is representative of the residual stress field in the vicinity of a longitudinal butt weld measured by Norde11 and Hall (1). In computation of the fracture stress-temperature curve the residual stress field magnitude was assumed to be independent of distance from the notch root.

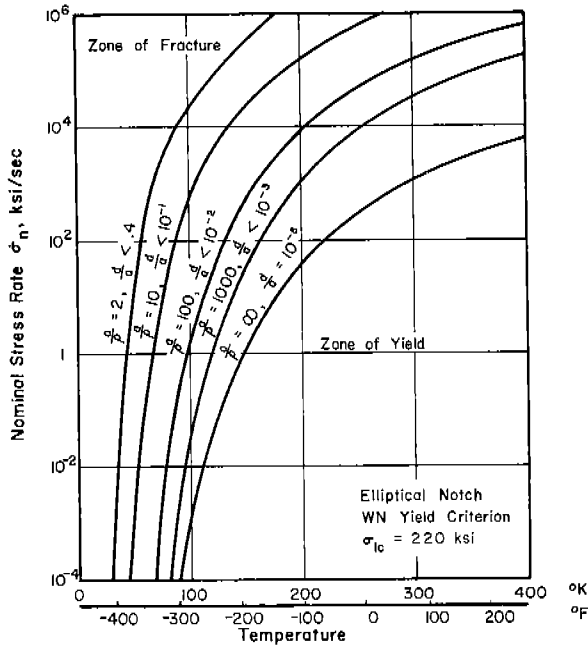


Fig. 19. Rate-Temperature for Ductile-Brittle Transition.

Curve	$\sigma_{1c}$	$\tau_{ym}$ at notch	Residual Stress ksi
(a)	220	14	0-0-0
(b)	220	24	0-0-0
(c)	180	14	0-0-0
(d)	220	14	60-30-30

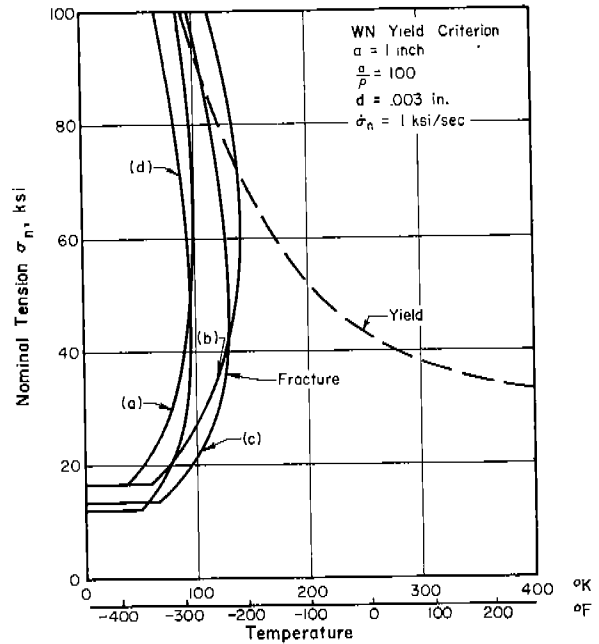


Fig. 20. Influence of Material Parameters and Residual Stress on Fracture Stress and Transition Temperature.

An increase in the rate-temperature independent component  $\tau_{ym}$  of the yield stress at the notch root, or a decrease in the critical fracture stress, causes a reduction in the applied stress for fracture and an increase in the transition temperature. The residual stress field reduces applied stress for fracture but the transition temperature also is reduced because the high shearing component of the residual stress field makes growth of the plastic zone easier.

Because residual stresses near welds and flaws result from inelastic deformation of the material, it appears reasonable to require that a high intensity residual stress field be a yield point field, that is,

$$\tau_{ym} = \frac{1}{3} \sqrt{(\sigma_{1r} - \sigma_{2r})^2 + (\sigma_{2r} - \sigma_{3r})^2 + (\sigma_{3r} - \sigma_{1r})^2} \quad (34)$$

where  $\sigma_{1r}$ , etc., are the principal residual stresses. Certainly, the shearing component of the residual stress field can be no greater than that given by Eq. (34); it is of great interest to question whether, for  $\sigma_{1r}$  greater than the uniaxial yield stress, the shearing component can be less. In the vicinity of sharp flaws plastic flow will occur under both loading and unloading to zero

applied stress. It therefore appears reasonable to require that at the notch root the rate-temperature independent component of the yield stress and the residual stress field be related by Eq. (34).

The pronounced embrittling effect of strain hardening at the notch root, demonstrated by curve (b) of Fig. 20 is greatly moderated by an associated yield condition residual stress field. A plane stress residual stress field of 60 ksi, 30 ksi, 0 ksi would correspond by Eq. (34) to  $\tau_{ym} = 24$  ksi. The fracture stress curve for such combined conditions has about the same transition temperature as curve (a) for no residual stress or strain hardening, but the applied stress for fracture at transition is reduced.

Thus, in the light of this critical stress model applied to cleavage initiation, residual stress and strain hardening in the vicinity of a flaw have a limited embrittling effect. The brittle-ductile transition temperature for a given notch acuity and rate of stress application is almost unaffected. The stress required for initiation of cleavage at subtransition temperature is markedly reduced by the residual stress.

A reduction in the critical fracture stress as a result of damage to the material in the vicinity of a flaw has a pronounced embrittling effect. The embrittlement appears both in an increase of the ductile-brittle transition temperature, and in a reduction of the applied stress required for initiation in the temperature range of brittle behavior. The type of damage resulting in reduction of the critical fracture stress might involve the creation of unusually large, sharp microcracks, or the providing of conditions conducive to their creation. Perhaps the expression of the embrittling influence of large prestrains and associated thermal histories in terms of their influence on the critical fracture stress will provide a useful quantitative expression of the phenomenon of exhaustion of ductility observed by Mylonas and others.

#### Application to Cleavage Propagation

In this section the critical stress model for brittle cleavage fracture is applied to the determination of the stress and velocity at which a cleavage fracture will propagate. The stress field at the crack tip is taken from the solution by Yoffe (47) for a slit of length  $2a$  moving at constant velocity in an infinitely wide plate under plane strain deformation conditions. The material parameters used for illustration are the same as those used in the previous section in the discussion of cleavage fracture initiation.

The stress field at the crack tip is given by Eq. (C-2) of Appendix C. The parameter  $H$  expresses the influence of crack velocity,  $v_c$ , and has a minimum value of 1 for  $v_c = 0$ .  $H$  becomes infinite at the Rayleigh surface wave velocity. For finite crack velocity,  $H > 1$ , the transverse stress  $\sigma_t$  will exceed the crack opening stress  $\sigma$  for all  $k$  smaller than  $k_H$  at which  $\sigma_t = \sigma_l$ . If  $\sigma_t$  exceeds  $\sigma_l$  the crack will not proceed smoothly but will bifurcate or fracture irregularly

with an accompanying high dissipation of energy. Therefore, it is assumed that steady cleavage crack propagation at velocity  $v_c$  requires that the critical fracture stress be attained at a distance at least  $k_H a$  from the crack root. Introducing the concept of minimum plastic zone size,  $d$ , the critical fracture stress must be attained at a distance  $ka \geq d$  from the notch root. Thus, there are two limits on the value of nominal stress required to permit a cleavage crack to continue to propagate at velocity  $v_c$ :

(1)  $\sigma_n$  must be great enough to make  $\sigma_l \geq \sigma_{lc}$  at the distance  $k_H a$  from the crack tip.

WN Yield Criterion  
 $\sigma_{1c} = 220 \text{ ksi}$   $\nu = 0.3$   
 $d = 0.003 \text{ in.}$   $E = 30 \times 10^3 \text{ ksi}$

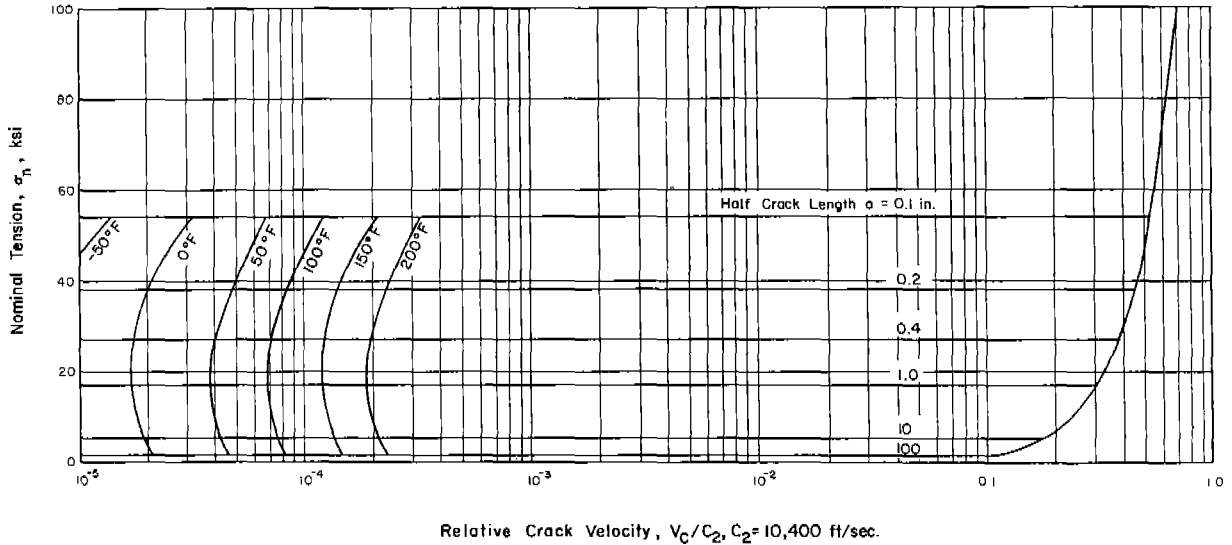


Fig. 21. Stress Required for Cleavage Propagation at Velocity  $V_c$  with Temperature Limits.

(2)  $\sigma_n$  must be great enough to make  $\sigma_\ell \geq \sigma_{1c}$  at the distance  $d$  from the crack tip.

Both criteria must be met.

The parameter  $k_H$  is obtained by solving for  $H$  in Eq. (C-2) of Appendix C;  $H$  is a function of the crack velocity  $v_c$  and the elastic constants. Then by equating  $\sigma_\ell$  and  $\sigma_t$

$$k_H = \frac{1}{2} \left( 1 - \left( \frac{1}{H} \right) \right)^2 \quad (35)$$

The value of  $k$  corresponding to the plastic zone size  $d$  is given by

$$k_d = \frac{d}{a} \quad (36)$$

The larger of these defines the distance from the crack tip at which the critical fracture stress must be attained for propagation to continue. Taking  $\sigma_\ell = \sigma_{1c}$  and  $k = \max(k_H, k_d)$ , the required level of average applied stress is given by

$$\sigma_n = \sqrt{2k} \sigma_{1c} \quad (37)$$

The result of this approach is shown in Fig. 21 for  $\sigma_{1c} = 220 \text{ ksi}$  and  $d = .003 \text{ in.}$  Crack velocity is plotted relative to the shear wave velocity; half crack lengths, "a", of 0.1, 0.2, 0.4, 1.0, 10 and 100 in. are considered.

The yield criterion has not yet been introduced. The following requirements for brittle cleavage propagation are based on the yield criterion:

(1) The applied stress required for brittle fracture propagation may not exceed the nominal stress for gross yield. This limit on the applied stress

may be obtained using the yield criterion with the temperature and the duration, or rate of increase, of the nominal stress.

(2) If  $\sigma_{1c}$  is to be attained for the value of  $\sigma_n$  given by Eq. (37), the plastic zone at the crack tip may not extend beyond the distance  $ka$  from the crack tip. Stress rates associated with cleavage fracture propagation

$$\frac{d\tau}{dt} = - \frac{d\tau}{dk} \frac{v_c}{a} \quad (38)$$

are so high for propagating cracks that this requirement limits propagation only at very low velocities if plane strain deformation conditions apply at the crack tip and the yield criterion of Eq. (19) is applicable when extrapolated to these high stress rates. The temperature contours at which this limit is reached are shown in Fig. 21. Brittle cleavage for a particular temperature and crack length is impossible for velocities less than that of the intersection of the temperature and stress curves.

(3) The plastic zone at the crack tip must extend to the distance  $ka$  since the critical fracture stress applies to metal that has undergone plastic deformation. The horizontal portions of the fracture stress curves in Fig. 21 meet this criterion since they correspond to  $k = k_d$  and the first grain has most certainly been plastically deformed by the intense shear at the geometrical crack tip. The rapidly rising fracture stress curve at high velocities corresponds to  $k = k_H$  where the above criterion has not been met. The requirement of corresponding plastic zone size would result in a more rapid rise of stress versus velocity, since one would require that  $\tau = \tau_y$  at  $k = k_H$ , giving  $\sigma_\ell > \sigma_{1c}$ . However, behavior in this region is not of great engineering interest.

Of the material parameters, the critical fracture stress and the minimum extent of plastic zone appear to be of primary importance in propagation. The yield criterion seems to have significant effect only in its definition of the yielding limit on the applied stress. Considering the horizontal portions of the curves of Fig. 21, which define the minimum stress at which a particular flaw can propagate, the effects of the parameters  $\sigma_{1c}$ , "a", and d on the nominal stress for fracture  $\sigma_{nf}$  are given by a simple relation derived as follows

$$\begin{aligned} \sigma_{nf} &= \sqrt{2k} \sigma_{1c} \\ k &= d/a \\ \sigma_{nf} &= \sigma_{1c} \sqrt{\frac{2d}{a}} \end{aligned} \quad (39)$$

If the applied stress  $\sigma_n$  is less than  $\sigma_{nf}$  required for cleavage propagation by the above equation, a cleavage crack of length "a" will not propagate -- even if cleavage is initiated by impact or local defective material. For the overall effect of grain size, if  $\sigma_{1c}$  is proportional to  $d^{-1}$ ,  $\sigma_{nf}$  will be proportional to  $d^{-1/2}$ .

Shear lip effects are not considered in the above development. The amount of shear lip is likely to depend upon the temperature and velocity of crack propagation. The presence of shear lip and the resulting curved fracture front will affect the stress distribution and therefore the conditions for cleavage propagation. As a result, a temperature effect may be observed on stress required for cleavage propagation that is not considered above.

The similarity between the critical fracture stress concept and fracture mechanics concepts should be emphasized here. In elementary fracture mechanics terms the crack opening stress at the distance  $d$  from the geometrical root of the crack is

$$\sigma_{\ell} = \frac{K}{\sqrt{2\pi d}} \quad (40)$$

For  $\sigma_{\ell} = \sigma_{1c}$  and  $K = K_c = \sigma_{nf} \sqrt{\pi a}$

$$\sigma_{1c} = \frac{\sigma_{nf} \sqrt{\pi a}}{\sqrt{2\pi d}} = \frac{\sigma_{nf}}{\sqrt{\frac{2d}{a}}} \quad (41)$$

Equation (41) is identical to Eq. (39). Therefore, the critical fracture stress and the fracture toughness  $K_c$  are related as follows

$$K_c = \sigma_{1c} \sqrt{2\pi d} \quad (42)$$

Residual stress effects may be handled as shown for the fracture mechanics approach in Part I. If the local residual stress at the distance  $d$  from the notch is known, its magnitude may be subtracted from  $\sigma_{1c}$  in Eq. (39) to determine the  $\sigma_{nf}$  required to maintain propagation. A long range, uniform residual stress field may be added to the applied  $\sigma_n$  to arrive at an effective value. The damaging influence of residual stress is clear. It permits a short cleavage crack to grow long enough to propagate under the influence of a low applied stress.

The foregoing development considers plane strain deformation conditions to exist in the vicinity of the crack tip over a distance of the order of the particle size criterion  $d$ . The assumption of plane strain should be reasonable except for very thin elements. If plane stress conditions are considered the picture changes markedly. Shear stresses at the vicinity of the crack tip must approach half the critical fracture stress if cleavage is to occur; as a result the fracture model does not predict cleavage propagation at velocities less than  $0.1 c_2$ . Above this velocity the stress analysis is not reliable since inertial forces in the thickness direction are not considered in its derivation. As shown by Frankland (49), for small plastic zones and high crack velocities, inertial forces result in high thickness direction tensile stress and an approach to plane strain conditions. High velocity cleavage propagation in thin plates probably is possible.

## 11. Correlation With Test Results

The application of the critical stress model for cleavage, described in the previous section, to situations of brittle cleavage initiation and propagation shows excellent qualitative representation of the effects of parameters known to influence brittle behavior. In this section the model is applied to test results to determine whether it can provide quantitative results of engineering value.

Data on cleavage initiation obtained by Hendrickson, Wood and Clark (39) and Barton and Hall (45), and used by them for evaluation of the critical fracture stress with an elasto-plastic solution for the notch root stress field, are fitted to determine the apparent critical fracture stress corresponding to the model developed above. A variety of notch bend tests are studied in the light

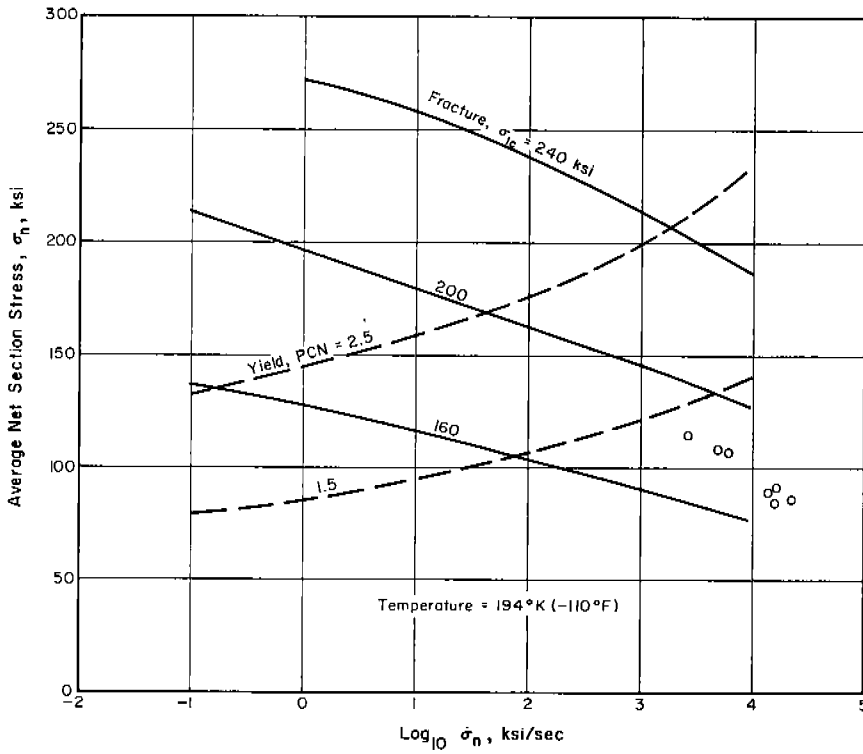


Fig. 22(a). Hendrickson, Wood, and Clark Notched Axial Specimens.

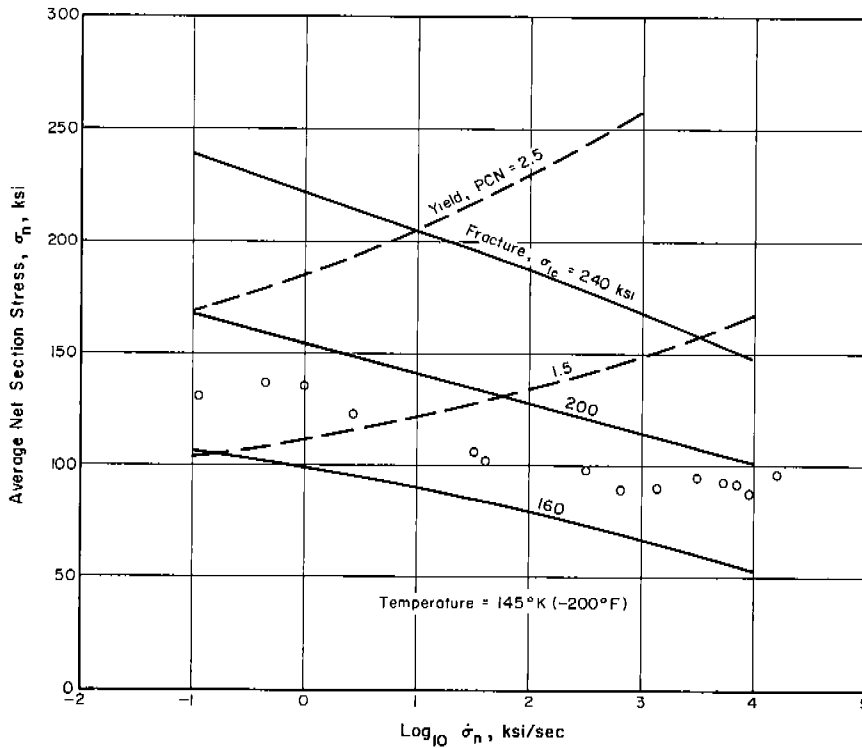


Fig. 22(b). Hendrickson, Wood, and Clark Notched Axial Specimens.

of the critical stress model. Low applied stress fracture initiations in welded plates are reviewed to identify the changes in material properties responsible for the extremely brittle behavior observed.

The critical stress model requirements for cleavage propagation are compared to results obtained from investigations of the behavior of wide plates subjected to notch wedge impact to initiate cleavage. The conditions for arrest of statically initiated flaws in welded wide plates also are compared to predictions of the critical stress model.

#### Cleavage Initiation in Externally Notched, Axially Loaded Specimens

Hendrickson, Wood and Clark (39) report results of tensile tests of circumferentially notched specimens of the steel termed CW in Table 5. The root diameter was 0.3 in., the gross diameter 0.6 in., and the notch root radius 0.01 in. The stress field was considered to be defined by Eq. (C-6) of Appendix C for  $a/\rho = 15$ . The yield criterion for the CW steel is given in Table 7.

The fracture and yield stress curves corresponding to the critical stress model for cleavage are shown with the measured data points in Figs. 22a and 22b for temperatures of 194°K and 145°K respectively. The fracture stress curve contains a correction for the plastic zone effect on the total load carried by the specimen, i.e., reflects a reduction in load carried. The correction was made by assuming the elastic-plastic interface value of longitudinal stress to prevail throughout the plastic zone. Normally no such correction on average stress for the plastic zone effect is made herein because it gives a deceptive appearance of precision in an approximate analysis. However, the proportion of the area of a circumferentially notched specimen lying within a shallow plastic zone is so high that some correction seemed essential.

Two theoretical gross yield curves are shown. For a deeply circumferentially notched specimen, gross plastic deformation will take place in the region of the notch but the required nominal stress exceeds the uniaxial yield stress. Hendrickson, Wood and Clark assumed that the net section average yield stress would be 1.5 times the uniaxial yield stress; such a relation is given by the curve labeled PCN = 1.5. Drucker (50) suggests that a ratio of about 2.5 would be more appropriate; the curve labeled PCN = 2.5 corresponds to this ratio between net section stress for gross yield and the uniaxial yield stress. The gross yield condition would be better defined by lower yield stress criterion than the upper yield stress criterion employed here. However, the application of a lower yield stress criterion would require definition of the effective strain rate upon establishment of the yield mechanism. As discussed below, it was deemed better to use the upper yield stress criterion as the average stress rate remains quite well defined until the yield mechanism forms. This yield criterion probably provides an upper bound on the gross yield average stress as a function of pre-yield stress rate and temperature.

The data points fall in a very consistent path between the theoretical curves for critical fracture stresses of 160 and 200 ksi. The indicated value for critical fracture stress is of the order of 180 ksi. The more sophisticated elasto-plastic stress field solution used by Hendrickson, Wood and Clark gave a critical fracture stress of 210 ksi with a comparable scatter band.

Barton and Hall (45) tested flat tensile specimens with symmetrical external hyperbolic notches of  $a/\rho = 50$ . They used an as-rolled .18C semi-killed steel of Charpy V 15 ft-lb of 60°F. The test data for specimens of net section width of 1 in. and thicknesses ranging from 0.25 to 0.90 in. are shown in Fig. 23. A very slight tendency for fracture stress to increase with thickness was observed.

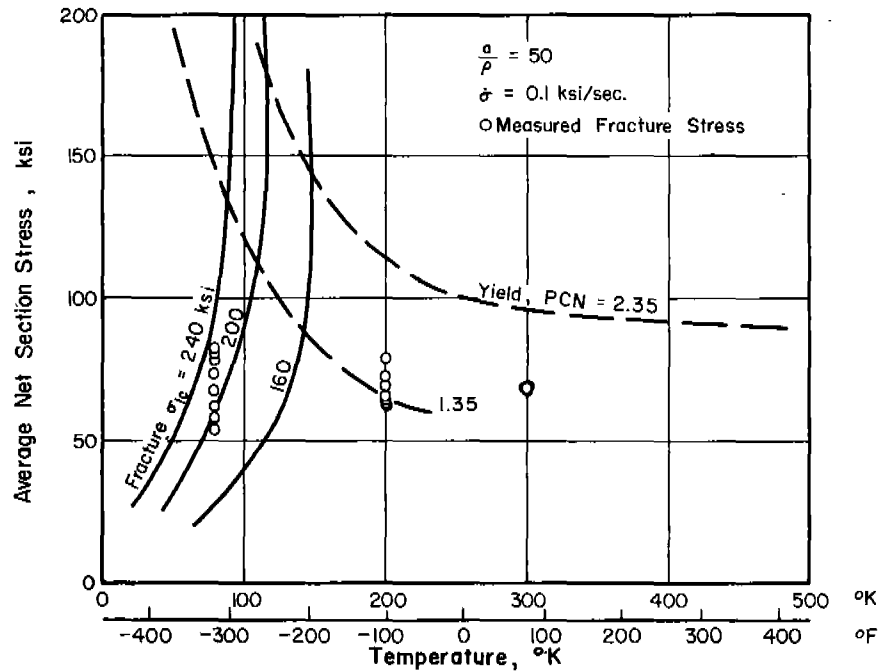


Fig. 23. Barton and Hall Deep Edge Notch Results.

In the application of the critical stress model the notch stress field of Eq. (C-4) of Appendix C was used. The yield criterion of the WHH steel of Table 7 with  $\tau_{ym}$  taken as 18.0 ksi appeared to fit the tensile test data and was used. A stress rate of 0.1 ksi/sec was considered to represent the "static" rate reported. Fracture stress curves for  $\sigma_{1c} = 160, 200,$  and  $240$  ksi are shown in Fig. 23. The steep rise of the fracture curve at the lowest test temperature explains the scatter in the data; the indicated critical fracture is of the order of 210 ksi. Barton and Hall obtained a value of about 250 ksi using an approximate elasto-plastic analysis of the stress field. The yield curves shown correspond to ratios of net section axial stress for plastic instability to uniaxial yield stress of 1.35 and 2.35. The former corresponds roughly to the stress for which the notch root plastic zones begin to grow diagonally toward the specimen axis (39). The latter ratio approaches that for plastic instability by plastic theory (50). The specimens tested at  $200^{\circ}\text{K}$  yielded significantly prior to fracture; apparently the ratio 1.35 corresponds better to the yield condition for these specimens -- a condition intermediate between plane stress and plane strain.

#### Cleavage Initiation in Notched Bend Specimens

The basic analysis procedure is considered applicable to specimens notched on one side with proportions of notch depth to net width similar to those of the Charpy V specimen.

Elastic Stress Field -- The stresses along the axis of a deep hyperbolic notch in pure bending are given by Eq. (C-5) of Appendix C. The solution is approximate in that the stress normal to the edge away from the notch is not zero. The stress solution satisfies the boundary conditions at the notch and is considered to be valid for the vicinity of the notch. It is applied here with no correction for finite depth or flank angle. Also, shear occurs in Izod and Charpy tests but, as discussed below, does not appear to influence the results significantly.

Yield Moment -- Green and Hundy (51) give a rigid plastic theory solution for a sharp 45° V-notched specimen in pure bending. The yield moment, which corresponds to gross yield for an elasto-plastic material, is given by

$$M_y = 0.363 Yta^2 \quad (43)$$

where

Y is the yield stress in uniaxial tension

a is the net section width

t is the specimen thickness

The von Mises yield criterion and plane strain deformation conditions were assumed. The maximum principal normal stress occurring in the specimen is given by

$$\sigma_{1m} = 2.52 Y \quad (44)$$

The gross yield moment and maximum principal normal stress can be related to the normal stress obtained by applying the flexure formula at the minimum cross section. The nominal flexural stress is given by

$$\sigma_n = \frac{6M}{ta^2} \quad (45)$$

The nominal flexural stress at gross yielding is

$$\sigma_{ny} = \frac{6M_y}{ta^2} = 2.18 Y \quad (46)$$

and the maximum principal normal stress is given in terms of the nominal flexural stress at gross yield by

$$\sigma_{1m} = 1.16 \sigma_{ny} \quad (47)$$

Green and Hundy obtained good agreement between gross yield moment computed by Eq. (43) and the gross yield moment measured in slow bend Izod and Charpy tests. In later work Alexander and Komoly (52) show very slight theoretical differences between Izod and Charpy conditions and pure bending. Therefore, the above expressions are used here for pure bending, three-point beam loading (Charpy V) and cantilever beam loading (Izod).

It is interesting to compare the results of the first order approximation used for the elastic stress field and the above rigid plastic theory. For a notch of Charpy V proportions, i.e.,  $a/\rho = 32$ , non rate-sensitive metal with no upper yield point, and a Poisson's ratio of 0.3, the elastic stress field gives a plastic zone penetration of 2.1 root radii for a nominal stress of  $\sigma_n = 2.18 Y$ . The corresponding principal normal stress is  $\sigma_1 = 2.3 Y$ . The result is not greatly different from the rigid plastic solution.

The influence of rate on the gross yield moment for rate-sensitive metal is difficult to formulate. The yield stress in terms of octahedral shear is given by

$$\tau_y = \frac{\sqrt{2}}{3} Y = \frac{\sqrt{2}}{3} \frac{\sigma_{ny}}{2.18} = 0.216 \sigma_{ny} \quad (48)$$

With  $\tau_y$  defined as a function of rate and temperature the nominal gross yield stress and gross yield moment can be determined. Because  $\tau_y$  is a lower yield stress its magnitude depends upon the plastic strain rate at the time of formation of the yield mechanism and the temperature. Prior to the formation of the yield mechanism most of the deformation results from elastic strains spread over a considerable region of the specimen. Following formation of the yield mechanism, most of the deformation results from plastic strain highly localized in the slip bands of the mechanism. The deformation rate is nearly constant through yield for most types of notch bend tests so the plastic strain rate can be expected to be much higher than the elastic strain rate just prior to yield. The actual magnitude of the plastic strain rate is not known either as a function of the elastic range rate of increase in moment or the deformation rate of the specimen at yield.

Because any procedure arbitrarily selected to estimate the rate-temperature effect on the yield condition is open to question, two simple procedures are used which are likely to bound the actual condition. The upper bound, in terms of yield moment, is obtained by considering the coefficient of Eq. (48) to relate  $\tau$  and  $\sigma_n$  just prior to gross yield

$$\tau = 0.216 \sigma_n$$

and that the upper yield stress corresponding to the stress rate

$$\dot{\tau} = 0.216 \dot{\sigma}_n \quad (49)$$

is an upper bound on the lower yield stress  $\tau_y$  of Eq. (48) that actually controls the gross yield moment. Essentially these assumptions amount to assuming that the internal stress distribution does not change markedly as the yield condition is established. This bound is termed the "gross yield condition."

The lower bound, in terms of yield moment, is obtained by considering that gross inelastic deformation is imminent when the nominal flexural stress of Eq. (46) becomes an upper yield stress for plane stress conditions. One might expect a specimen of Charpy V proportions to yield under plane stress conditions but Green and Hundy and others show the contrary. The nominal flexural stress  $\sigma_n$  is only a measure of the stress in the specimen but its value as a uniaxial yield stress for the applied rate of increase in moment and temperature also should be a measure of the variation of the actual yield moment with these parameters. This bound is termed the "nominal yield condition."

#### Ductile-Brittle Transition for Cleavage Initiation

The critical stress model for cleavage can be used to predict brittle cleavage initiation in the manner demonstrated in Section 10. Figure 24 shows fracture and yield curves for Charpy V-notch proportions, nominal stress rates of 1 ksi/sec and  $10^6$  ksi/sec, the WN yield criterion of Table 7, and a critical fracture stress of 220 ksi. The nominal and gross yield conditions give quite different transition temperatures. The stress rate does not affect the nominal stress for a transition fracture for a particular yield condition. If one upper yield point criterion of the form given by Eq. (19) governs both specimen yield and spread of the plastic zone at the notch root, and the particle size criterion does not control the transition, a transition fracture initiates at the same

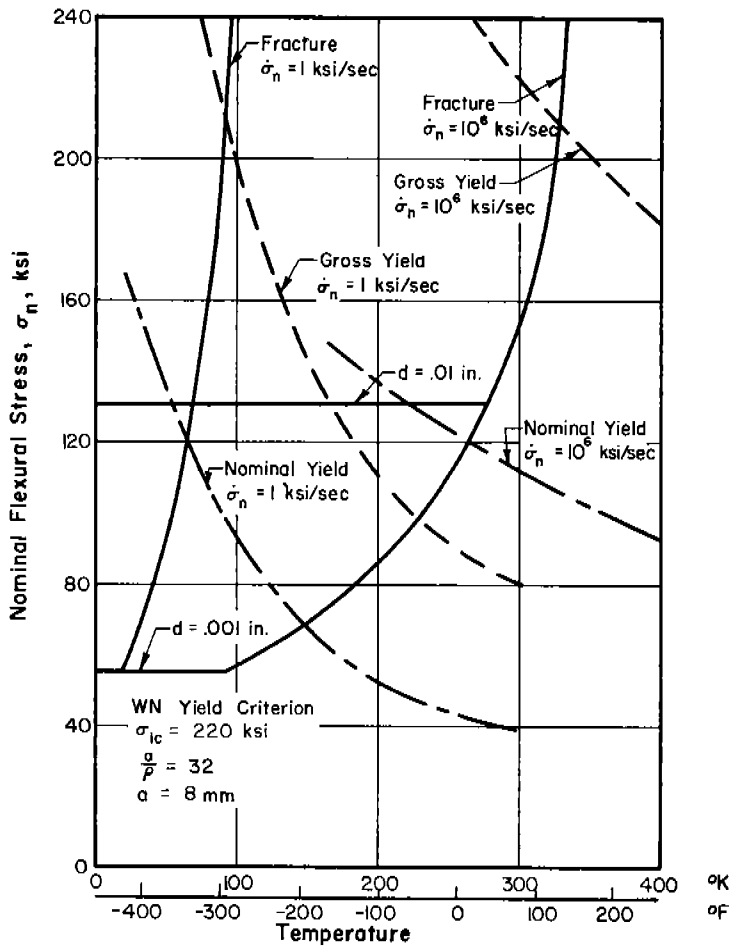


Fig. 24. Fracture and Yield Curves for Notch Bend Test.

plastic zone size for a particular notch geometry for any value of critical fracture stress and any set of yield criterion parameters. It is possible that, even though the yield condition is not well defined and the elastic stress field used here is a crude approximation, this constancy of initiation conditions will be observed. If so, the notched bend test transition temperature can provide an excellent measure of the critical fracture stress.

The ductile-brittle transition temperature defined above is not the same as an energy or appearance transition temperature for defined rate conditions. Referring to energy-temperature data shown in Fig. 26, for example, the ductile-brittle transition should correspond to the beginning of an increase in energy absorbed with increasing temperature. The energy required for a brittle initiation is probably negligible compared to the energy loss in impact so the slight increase in absorbed energy as the brittle cleavage stress increases to the transition value is unlikely to be observed. Thus the ductile-brittle initiation transition temperature should correspond to a temperature of  $255^{\circ}\text{K}$  in Fig. 26.

Instrumented Charpy tests would give a better measure of this transition temperature. As shown by Tardif and Marquis (53) this transition temperature would correspond to that at which the plateau in the force-time curve disappears as shown in Fig. 25. Accurate measurement of the peak moment would permit direct computation of the critical fracture stress by the rigid plastic theory using Eq. (47)

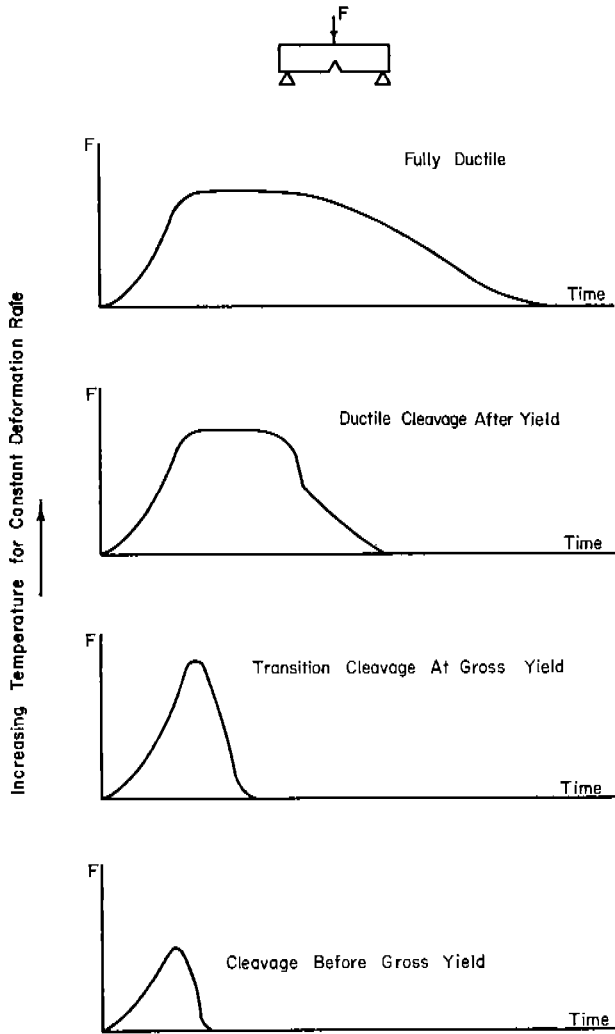


Fig. 25. Instrumented Notch Bend Test.

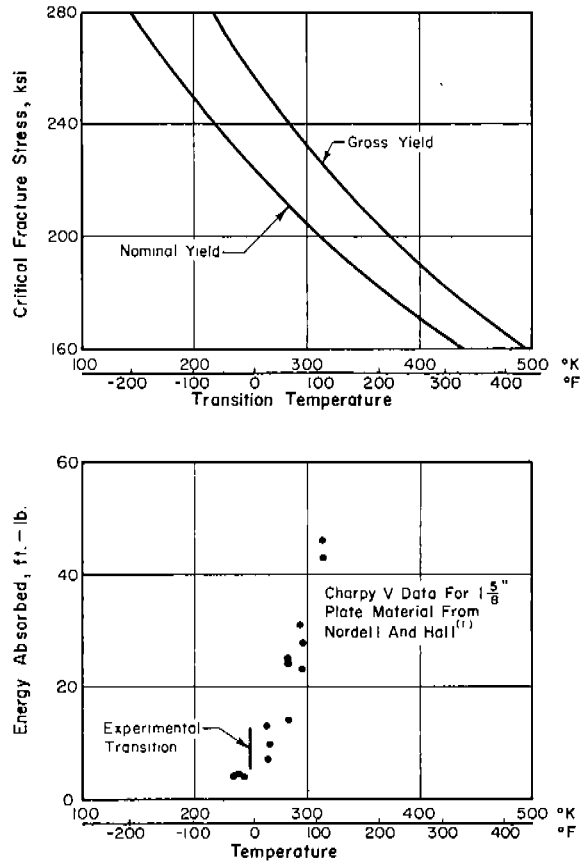


Fig. 26. Charpy Ductile-Brittle Transition and Energy Data for WN Steel.

$$\sigma_{lc} = \sigma_{lm} = 1.16 \sigma_{nyt} \quad (50)$$

where  $\sigma_{nyt}$  is the nominal stress obtained as cleavage initiation corresponds to the initiation of gross yielding. This would provide an excellent method for studying the influence of thermal and deformation cycling on the critical fracture stress. However, both the accuracy of measurement of  $\sigma_n$  in the instrument Charpy test and the reliability of Eq. (50) must be investigated.

Charpy V and Izod Impact Tests -- Charpy V and Izod specimens have the same notch geometry. The use of the nominal flexural stress and its rate of change as parameters and the neglect of shear effects, permits a given analysis to apply to both tests. At the same rate of nominal stress increase, the two tests give the same theoretical transition temperature for a particular steel. Instrumented Charpy V tests reported by Tardif and Marquis (53) show

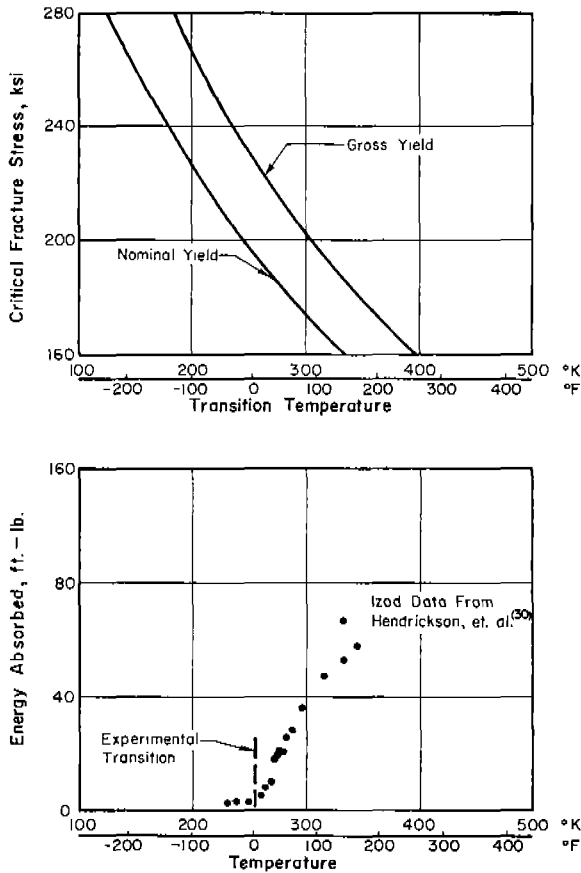


Fig. 27. IZOD Ductile-Brittle Transition and Energy Data for CW Steel.

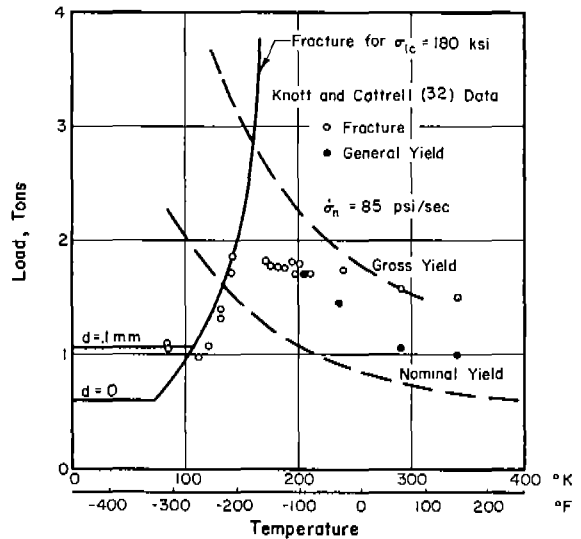


Fig. 28. Data and Theoretical Curves for Slow Bend Test.

$\dot{\sigma}_n$  to be on the order of  $10^6$  ksi/sec. Hendrickson, Wood and Clark (30) computed a similar value for the Izod test. Here a nominal stress rate of  $10^6$  ksi/sec will be used for the rate for both Izod and Charpy impact tests. More study of the yield criterion at rates of this order is needed; none of the data cited in Part II extend to this high a rate. Additional measurements of the nominal stress rate for the various impact tests also are required to better define the stress rate as a function of test conditions.

Charpy and Izod impact test ductile-brittle transition temperatures are shown in Figs. 26 and 27 as a function of critical fracture stress for the WN and CW steels described in Part II. The curves of critical fracture stress versus transition temperature were obtained by determining the transition temperature for a particular critical fracture stress from the intersection of yield and fracture curves of the type shown in Fig. 24 for  $\dot{\sigma}_n = 10^6$  ksi/sec. Impact test results for the steels were reported by Hendrickson, Wood and Clark (30) and Nordell and Hall (1); also shown is the experimental transition taken as the temperature at which absorbed energy appears to rise sharply.

The critical fracture stress corresponding to the experimentally observed initiation transition in the Izod tests of the CW steel appears to be on the order of 210 ksi. This does not correspond exactly to the value of critical fracture stress of 180 ksi obtained from results of tests on circumferentially notched specimens of the CW steel. The WN steel appears to have a higher critical fracture stress.

Slow Notch Bend Results obtained by Knott and Cottrell (32) are shown in Fig. 28. The yield criterion for this high nitrogen, basic Bessemer, rimming steel with grain diameter of .1 mm was obtained from limited upper yield point data for a single stress rate of .085 ksi/sec. Somewhat more extensive data for the lower yield point variation with rate and temperature were used to select the yield criterion parameters  $\tau_0$  and K. The upper yield criterion parameters are given in Table 7.

The notch bend specimens were of proportions comparable to a Charpy V specimen with  $a/\rho = 34$  and root radius  $\rho = .25$  mm. They were loaded in four-point bending at a nominal stress rate of 2.24 ksi/sec.\* The critical stress model was applied as described above. The brittle fractures are well described by the fracture stress curve cut off at a minimum extent of plastic zone corresponding to the grain diameter; a similar cut-off would be given by a critical shear for twinning. Fractures at temperatures in excess of 195°K were observed to occur after gross yielding. As expected, the nominal and gross yield conditions bound the measured load for gross yielding. Knott and Cottrell obtained a close fit to the measured gross yield load by estimating the effective strain rate and using the corresponding tensile coupon lower yield stress. The critical fracture stress of 180 ksi corresponds exactly to the value Knott and Cottrell obtained from Eq. (50) when fracture and gross yielding occurred simultaneously.

#### NDT Test

The drop weight test for nil ductility transition temperature uses a rectangular flexural specimen with a notched deposit of brittle weld metal added to promote fracture initiation. The specimens are supported as a simple beam and loaded by a drop weight inducing a tensile stress field around the notch. The test is described in detail in ASTM Standard E208-63T. The NDT or nil ductility temperature is the highest temperature at which the specimen fractures without gross plastic deformation.

An analysis of the NDT test was carried out along the lines of the above analysis for Charpy type specimens. The first fundamental flexural mode was used to define the nominal stress rate induced in the specimens according to elementary beam theory. The results of the analysis predicted an NDT temperature far higher than those actually observed, but did show a pronounced dependence of NDT temperature on critical fracture stress.

The lack of quantitative success in the application of the critical fracture stress model to the NDT test is clearly attributable to the oversimplification of the stress field and stress state in a beam subjected to impact loading. Work on shock wave propagation in beams by Leonard and Budiansky (54) shows that shearing stresses are amplified far more than flexural stresses. Such shear amplification is consistent with observed NDT temperatures lower than those computed using elementary beam theory to define the basic stress field.

A shock wave propagation analysis considering real material properties is not yet available for NDT test conditions. If it were available, the critical

---

\* The stress rates for the tensile coupon tests and notched bend tests were supplied by J. F. Knott in a personal communication.

stress model could be evaluated in the light of NDT test results. Empirical measurements of the flexural and shearing stress-time history in unnotched NDT specimens also would provide a basis for application of the critical stress model.

#### Wide Plate Studies of Cleavage Initiation

In the development of the critical stress model as applied to cleavage initiation in Section 10, it appears that very low temperatures or very high rates of stressing are required for pre-yield cleavage initiation of notched wide plate specimens when the material is in the virgin condition. This prediction of the model is confirmed by laboratory experience; no investigator has observed initiation of cleavage prior to yield in low-carbon steel plain plates under static loading conditions at temperatures above  $-100^{\circ}\text{F}$ . Mylonas and his co-workers (38) showed that low-stress brittle behavior can be obtained if the material is severely deformed prior to loading; Nordell and Hall (1), Wells (55), and others, have obtained low-stress brittle initiation in welded plates that had not been subjected to overall plastic deformation or wedge impact type methods of cleavage initiation.

The data on low-stress initiation of cleavage fracture reported by Nordell and Hall are studied here in the light of the critical stress model for cleavage to determine which parameters of the critical stress model must be affected by welding thermal and deformation cycling to lead to the observed difference between plain plate and welded plate behavior. The parameters considered include the critical fracture stress, the yield criterion parameters, and the residual stress field in the vicinity of the notch root, as well as the effective notch acuity.

Nordell and Hall tested 3/4-in., 1-in., and 1-5/8-in. plates of A212-B (firebox quality) steel. The chemical analyses for the steels were quite similar, as were the results of standard tensile coupon tests and the conditions for cleavage initiation. Only the results for the 1-5/8-in.-thick plates are considered in detail herein. The chemical analysis of the 1-5/8-in. plate is given in Table 1, and the yield criterion for this steel, termed WN, is evaluated in Table 7. The ferrite grain size of the 1-5/8-in. material was determined to be ASTM 5 from the sample used for the tensile testing reported in Section 5 of this report. Grain size measurements reported by Hall, Joshi and Munse (3) for these steels showed ASTM ferrite grain sizes ranging from 2 to 4 for the 1-5/8-in. material.

The 1-5/8-in. test plates were 2 ft wide. The plates contained a longitudinal butt weld (weld axis parallel to the direction of applied tension). The welds were notched as shown in Fig. 12; the weld was cut through after welding. Residual stresses at the location of the notch edge at the quarter thickness were measured in an unnotched plate and were found to be approximately 60 ksi tension parallel to the weld axis and 30 ksi tension in the direction of the plate width.

The plates were tested at constant temperature and an applied stress rate of 4 ksi/min. The initiation of cleavage at the sawed notch is termed primary fracture; many of the fractures initiated at low stress arrested and subsequently reinitiated upon increase of load. These second initiations from arrested cracks are termed secondary fractures. Figure 29 shows the average net section stress at fracture for as-welded and  $400^{\circ}\text{F}$  preheated 1-5/8-in.-thick specimens as a function of test temperature. These data also are representative of the primary fracture stress-temperature relation observed for the 3/4-in. and

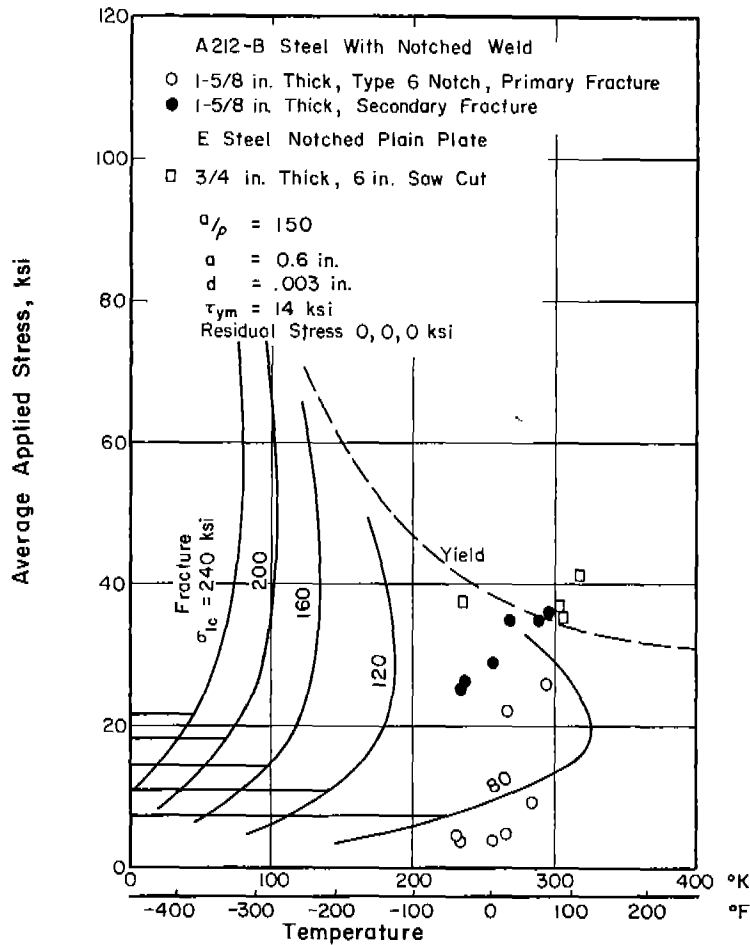


Fig. 29. Wide Plate Fracture Stress and Moderate Notch Theoretical Curves.

1-in.-thick as-welded and preheated specimens. The initiation of the primary fractures is discussed below in light of the critical stress model for cleavage. Conditions for the arrest of the primary fractures are considered later. The secondary fractures that appear to have reinitiated at stresses lower than that required for gross yielding of the specimen initiated from cracks between 7 and 13 in. long in a 24-in.-wide plate.

To emphasize the severe embrittlement resulting from a stress raiser in the vicinity of a weld, data points for 3/4-in.-thick, 2-ft-wide rimmed E steel plates tested by Wilson, Hechtman and Bruckner (56) also are shown in Fig. 29. These plates contained a central notch of 6-in. length formed by a jeweler's saw cut, a more severe stress raiser than the Nordell and Hall specimens. However, all of the E steel plates underwent gross yielding prior to fracture. Although the plates tested at lower temperatures showed reduced energy absorption the stress required for cleavage initiation remained high.

If the V notch shown in Fig. 12 is considered as an elliptical notch of half length 0.53 in., corresponding to the half length of the V notch near the quarter thickness of the plate, and root radius .0035 in., corresponding to half the saw cut width, the geometry factor  $a/p$  is 150 for the elliptical notch stress field of Eq. (C-3) of Appendix C. The predicted nominal yield and nominal fracture stress curves corresponding to this notch geometry, a stress rate of 4 ksi/min., the WN yield criterion, minimum plastic zone size  $d = .003$  in., and various levels of critical fracture stress are shown in Fig. 29 as a function of temperature.

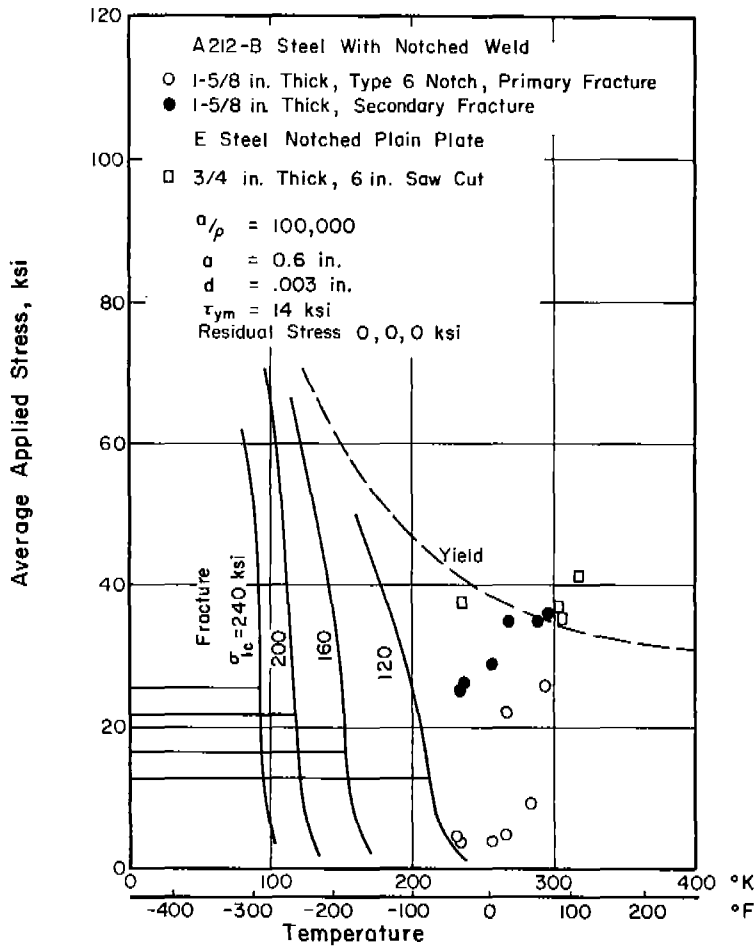


Fig. 30. Wide Plate Fracture Stress and Sharp Notch Theoretical Curves.

A very low level of critical fracture stress is required for correspondence to the observed brittle behavior. The possibility that sharp cracks existed at the end of the saw cut was considered by using an elliptical notch of  $a/p = 100,000$ , which has a root radius of 0.0000053 in. for a half length of 0.53 in. and corresponds well to an infinitely sharp flaw stress field for distance greater than 10 root radii from the notch root. As shown in Fig. 30, again very low values of critical fracture stress are required for brittle behavior at the temperatures of observed low-stress fracture.

Consideration of either a highly triaxial residual stress field or an increased rate-temperature independent component of the yield stress in the vicinity of the notch root would lead to predicted brittle behavior in the temperature range of observed brittle behavior; when applied in conjunction with sharp notch geometry the observed low fracture stress also would be predicted. However, it would appear that a residual stress field consistent with the increased rate-temperature independent component of the yield stress should be employed as discussed in Section 10. Figure 31 shows predicted nominal fracture and yield stress curves for the sharp notch geometry, a residual tensile stress field of 60 ksi in the direction of the crack opening stress, 30 ksi in the plate width direction and 0 ksi in the plate thickness direction, and a consistent  $\tau_{ym}$  in the vicinity of the notch root equal to 24 ksi. For this yield level residual stress field and a particular value of critical fracture stress, the temperature at which brittle behavior is predicted is lower but not much different from the no residual stress

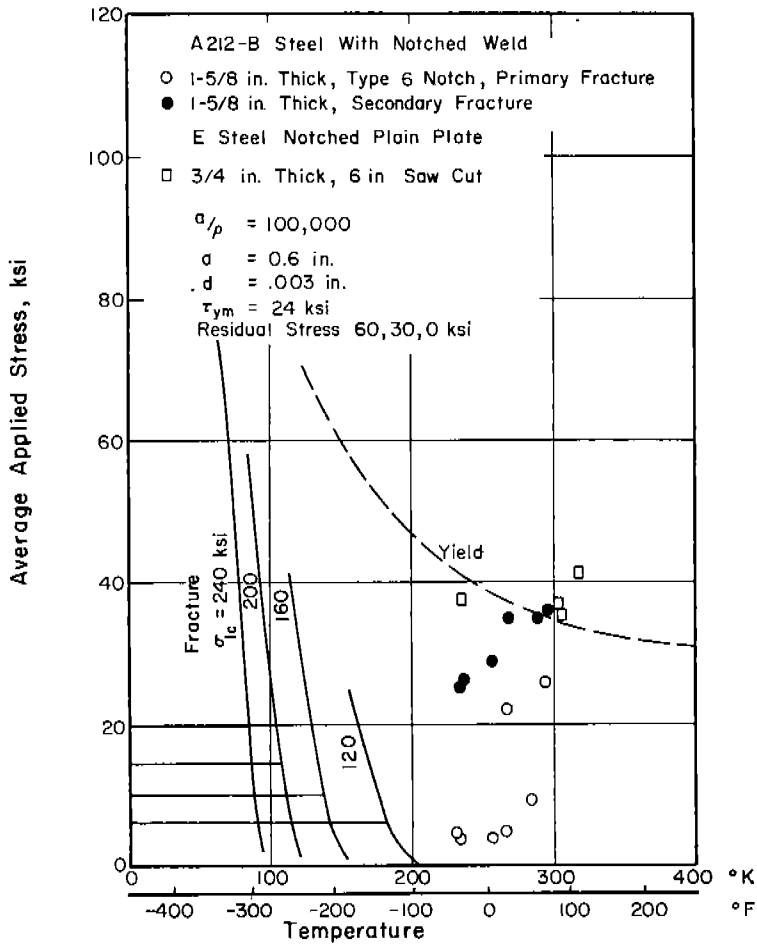


Fig. 31. Wide Plate Fracture Stress and Sharp Notch Theoretical Curves Including Residual Stress and Strain Hardening Effects.

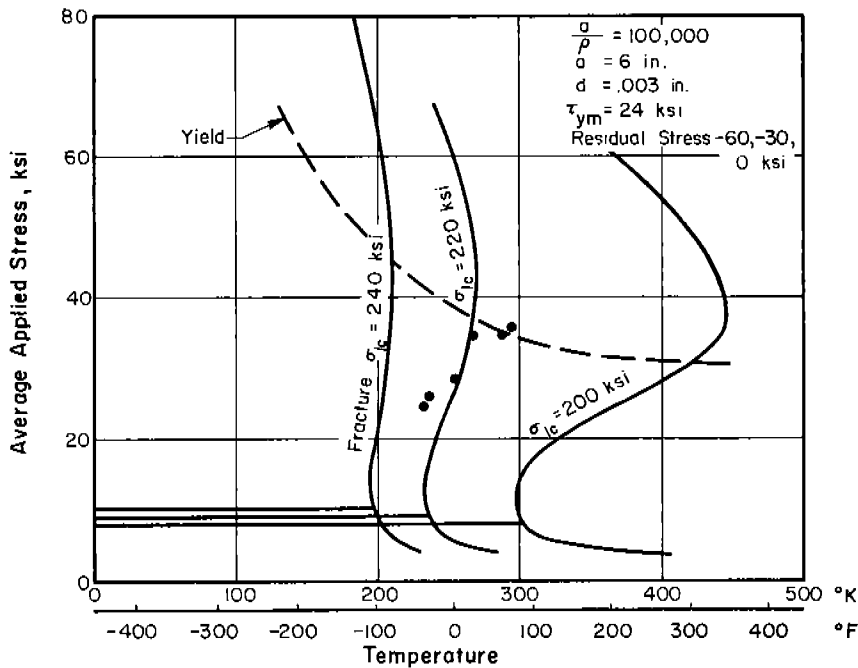


Fig. 32. Wide Plate Secondary Fracture Stress and Sharp Notch Theoretical Curves for Biaxial Compressive Residual Stress.

transition temperature for the same critical fracture stress and notch geometry. The only embrittling effect of the residual stress combined with local strain hardening is the lowering of the applied stress required for fracture in the temperature range of brittle behavior.

The appearance of markedly higher primary fracture stresses at temperatures above 265°K suggests that the effective notch acuity is not much greater than 1000. Such acuity provides fracture stress curves of the shape shown in Fig. 29 and predicts low-stress initiation at lower temperatures.

According to the critical stress model for cleavage initiation, the low-stress primary cleavage fracture initiation resulted from weld zone effects on the critical fracture stress and not from increased notch acuity due to cracking at the saw cut, residual stress, or strain hardening of the metal of the notch root. These latter effects would act to reduce the applied stress for fracture at a temperature below the ductile-brittle transition but do not appear accountable for raising the transition temperature to the high level observed in the tests.

The secondary fracture initiations may have followed extensive plastic deformation in the vicinity of the crack tip; if so, the essentially elastic approximation to the crack tip stress field used herein would be inapplicable to analysis of these fractures. If the sharp flaw analysis of Fig. 30, that considers no residual stress or strain hardening in vicinity of the crack tip, is applied, no pre-yield brittle behavior would be predicted at the test temperature for critical fracture stress of the order of 200 ksi. These curves, prepared for study of the primary fractures, would be changed only by lowering the plateau resulting from the minimum extent of plastic zone to correspond to the longer crack length.

It is interesting to note that a biaxial compressive residual stress field, such as might result from removing load from a cracked plate stressed in tension, could embrittle the flawed plate under subsequent tensile loading. Figure 32 shows the nominal fracture stress and yield stress curves for a residual stress field of 60 ksi compression parallel to the applied stress, 30 ksi compression in the width direction, and 0 in the thickness direction. This residual stress field is a yield stress field for  $\tau_{ym} = 24$  ksi. No Baushinger Effect on the flow stress for subsequent applied tension is considered. By comparison to Fig. 30, the plate is markedly embrittled. This behavior is predicted because the compressive biaxial residual stress field and the notch stress field from the applied stress sum to a nearly hydrostatic stress state. However, it is questionable whether the biaxial compressive residual stress field actually can be established; addition of compressive residual stress in the thickness direction equal to that in the width direction removes the embrittling effect.

Low stress brittle fractures of the type noted above in notched and welded plates have been obtained with both the V-type notch, such as the specimens noted above, as well as straight notches (such as those used by Wilson et al). The V notch has been found to give quite consistent results under given conditions, whereas the straight notch has not generally been shown to give quite as consistent results. No doubt there is considerable difference in the notch acuity and stress distribution associated with the two notch conditions and in part these may account for some of the differences noted in analysis by the model; the stress field expressions used with the model were developed for a straight notch.

Wide Plate Studies of Cleavage Propagation

In Section 10 it was shown that the critical stress model for cleavage applied to the propagation of a cleavage crack in a wide plate gives as the nominal stress required for propagation:

$$\sigma_{nf} = \sigma_{1c} \sqrt{\frac{2d}{a}} \quad (37)$$

where d is the minimum extent of plastic zone, "a" is the half crack length and  $\sigma_{1c}$  is the critical fracture stress. As discussed in Section 10 this necessary condition for continued cleavage fracture propagation ordinarily is sufficient; the yield criterion as evaluated in Table 7 suggests that plastic flow can blunt the crack only at very low propagation velocities when plane strain conditions apply.

Equation 37 can be corrected approximately for finite plate width using a correction factor given by Irwin (6)

$$\sigma_{nf} = \frac{\sigma_{1c} \sqrt{\frac{2d}{a}}}{\sqrt{\frac{W}{\pi a} \tan \frac{\pi a}{W}}} \quad (51)$$

for  $a/W = 0.25$ , or half the plate width cracked, the correction changes  $\sigma_{nf}$  by 13 percent.

Both Eq. (37) and Eq. (51) consider a condition of uniform gross section tensile stress  $\sigma_{nf}$  at infinity. The equation is, therefore, only approximately applicable to most test situations.

Nordell and Hall (1) data for the arrest of primary fractures is first considered. Three thicknesses of A212-B steel plates were tested; the basic plate width and the parameter d obtained from the reported grain size are tabulated below.

Thickness, in.	1-5/8	1	3/4
Width, in.	24	36	24
d, in.	.003	.002	.001

The effect of residual stress on the nominal stress required for propagation can be approximated using the  $K_r$  stress intensity factor for residual stress developed in Part I. The nominal stress equivalent provided by  $K_r$  is given for small  $a/W$  by

$$\sigma_{nfr} = \frac{K_r}{\sqrt{\pi a}} \quad (52)$$

or for large  $a/W$  by

$$\sigma_{nfr} = \frac{K_r}{\sqrt{\pi a} \sqrt{\frac{W}{\pi a} \tan \frac{\pi a}{W}}} \quad (53)$$

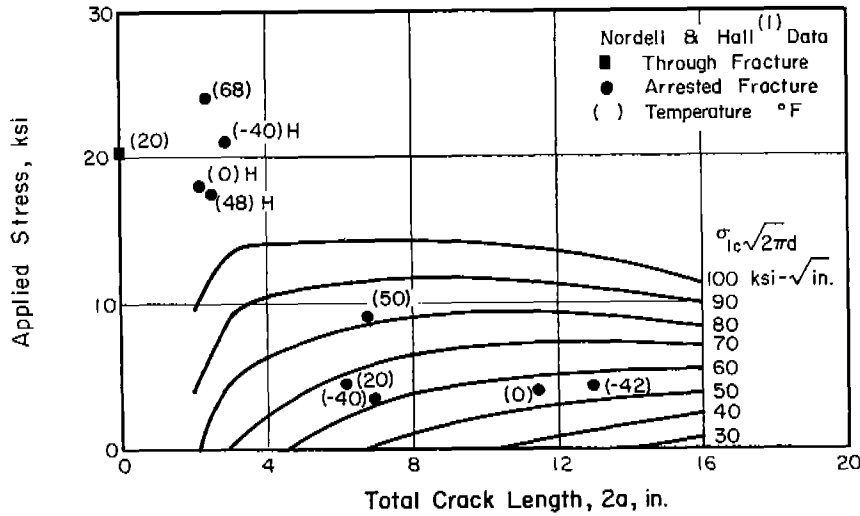


Fig. 33. Fracture Arrest in 2 ft Wide, 1-5/8 in. Plates.

If  $\sigma_{nf}$  of Eq. (51) is considered to consist of two components, part supplied by residual stress and the remainder by applied stress, the required applied stress for continued propagation,  $\sigma_{nfa}$ , is given by

$$\begin{aligned} \sigma_{nfa} &= \frac{\sigma_{1c}\sqrt{\frac{2d}{a}}}{\sqrt{\frac{W}{\pi a} \tan \frac{\pi a}{W}}} - \frac{K_r}{\sqrt{\pi a} \sqrt{\frac{W}{\pi a} \tan \frac{\pi a}{W}}} \\ &= \frac{1}{\sqrt{\pi a} \sqrt{\frac{W}{\pi a} \tan \frac{\pi a}{W}}} \left[ \sigma_{1c} \sqrt{2\pi d} - K_r \right] \end{aligned} \quad (54)$$

The material parameter  $\sigma_{1c}\sqrt{2\pi d}$  is equivalent to  $K_C$ . Figures 33, 34, and 35 show data points superimposed upon a plot of Eq. (54) for various values of  $\sigma_{1c}\sqrt{2\pi d}$ . The values of  $K_r$  as a function of "a" used to plot Eq. (54) were obtained from  $K_r$  curves described in Part I for the as-welded residual stress distributions. Data points are identified by an H for postheated specimens and an E for prestrained specimens; no identification of as-welded and preheated specimens are shown because the  $K_r$  curves for these conditions are quite similar. Temperature in °F is shown for each test.

Most of the arrested cracks follow the curve for a particular  $\sigma_{1c}\sqrt{2\pi d}$  quite closely. A few higher temperature specimens arrested at an applied stress level higher than that for through fracture at lower temperatures, and several higher stress fractures arrested at very short crack lengths. For the latter, it seems that the propagation velocity in the damaged material near the notch did not become high enough to initiate cleavage in the undamaged material. The tabulation below gives the apparent critical fracture stress corresponding to the  $\sigma_{1c}\sqrt{2\pi d}$  at arrest and the grain diameter

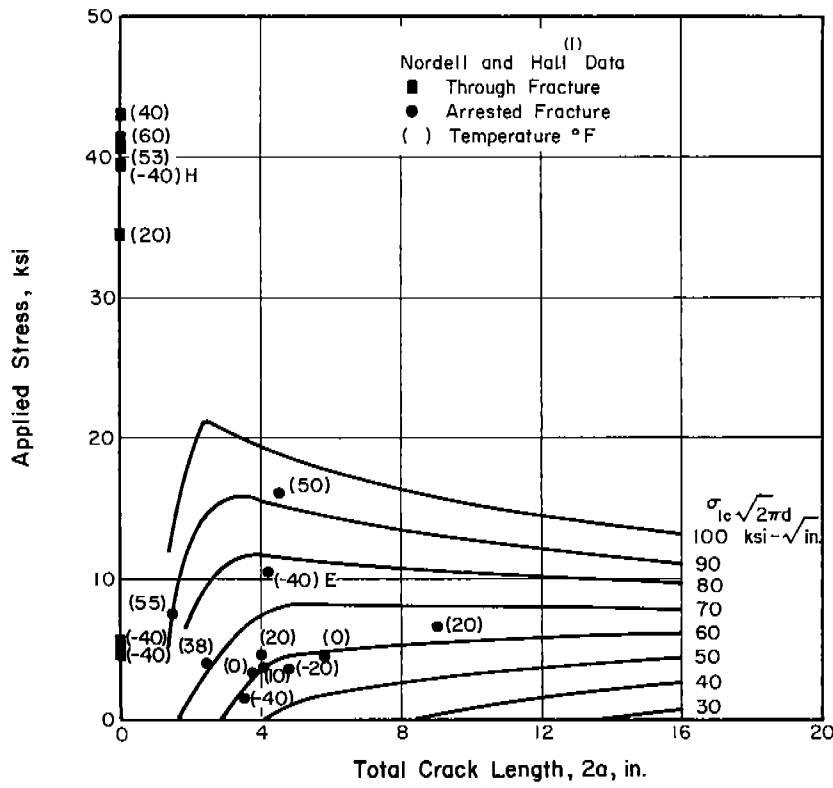


Fig. 34. Fracture Arrest in 3 ft Wide, 1 in. Plates.

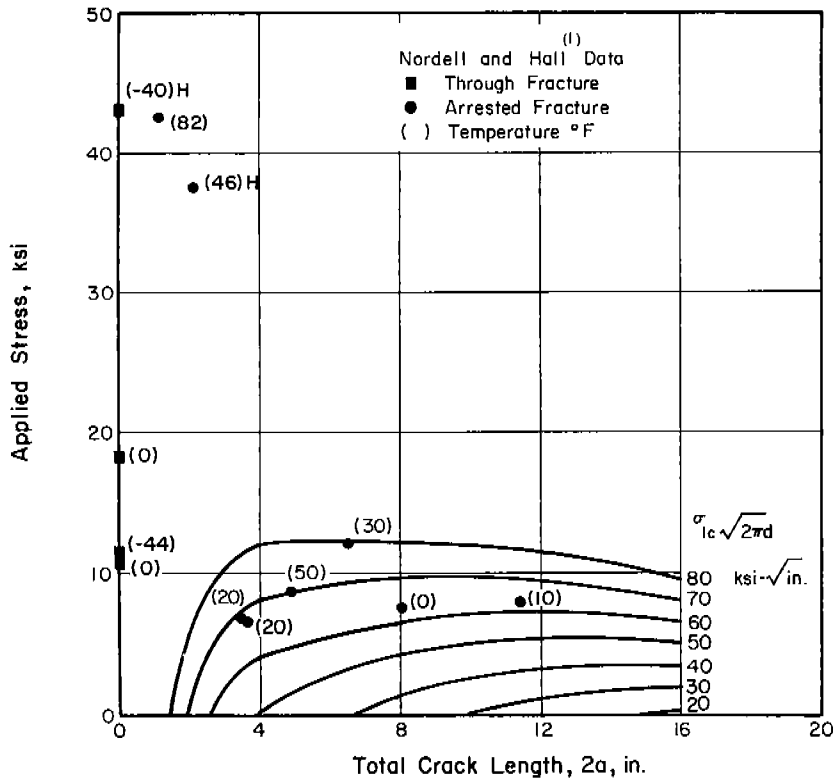


Fig. 35. Fracture Arrest in 2 ft Wide, 3/4 in. Plate.

Thickness, in.	1-5/8	1	3/4
d, in.	.003	.002	.001
$\sigma_{1c} \sqrt{2\pi d}$ , ksi- $\sqrt{\text{in.}}$	60	60	65
$\sigma_{1c}$ , ksi	438	534	822

The nearly constant value of  $\sigma_{1c} \sqrt{2\pi d}$  for these three steels of similar composition but different grain size suggests that  $\sigma_{1c}$  is proportional to  $d^{-1/2}$  rather than  $d^{-1}$  as hypothesized in Section 10. The range in grain diameter is not great enough to provide conclusive evidence. The values of  $\sigma_{1c}$  obtained when the minimum extent of plastic zone is taken equal to the grain diameter appear too high.

The minimum extent of plastic zone may be larger than one grain diameter. Also, consideration of dynamic effects on the fracture-driving force of residual stress, the finite plate length, and relaxation of both applied and residual stress with increasing crack length might bring the derived value of critical fracture stress more in line with values obtained in studies of cleavage initiation. However, the analysis is valuable in that the parameter  $K_{1c}$  or  $\sigma_{1c} \sqrt{2\pi d}$  very definitely correlates with the trend of the data.

The theoretical influence of the residual stress field on the stress required for cleavage propagation is shown in Fig. 36. The value of  $\sigma_{1c} \sqrt{2\pi d}$  corresponds to the 1-in.-thick, 3-ft-wide plates as does the curve showing residual stress effects. The importance of residual stress in propagation is evident.

Wells (55) has reported a study of static initiation and through or partial cleavage propagation for a number of steels. His results for steel P, semi-killed, C = .18, tested in the form of 3-ft-wide, 1-in.-thick plates containing longitudinal butt welds, show enough arrested fractures to provide a picture comparable to that obtained from the results of Nordell and Hall. Grain sizes reported for this steel range from ASTM 2 to 4; an average value  $d = .006$  in. is used in the analysis.

These data are analyzed in the manner described above for the Nordell and Hall results. The residual stress effect was accounted for by using the  $K_r$  versus "a" relation obtained for Nordell and Hall 3-ft-wide as-welded plates. As shown in Fig. 37 the arrest data falls in two bands with the apparent critical fracture stress values computed below

<u>Band</u>	<u>Higher Band</u>	<u>Lower Band</u>
d, in.	.006	.006
$\sigma_{1c} \sqrt{2\pi d}$ , ksi- $\sqrt{\text{in.}}$	75	55
$\sigma_{1c}$ , ksi	387	284

The difference might result from a change in d or  $\sigma_{1c}$  with temperature but the clear separation between bands argues against any continuous variations. It is more likely that some consistent difference in residual stress field or material separates the two bands.

Lazar and Hall (57) reported tests of 3/4-in.-thick 6-ft-wide plates tested in tension with fractures initiated by wedge impact at an edge notch. The results form a go or no-go picture with no-go tests showing submerged fractures as far as 2 in. beyond a 1-in. sawed notch. Tests were performed on a

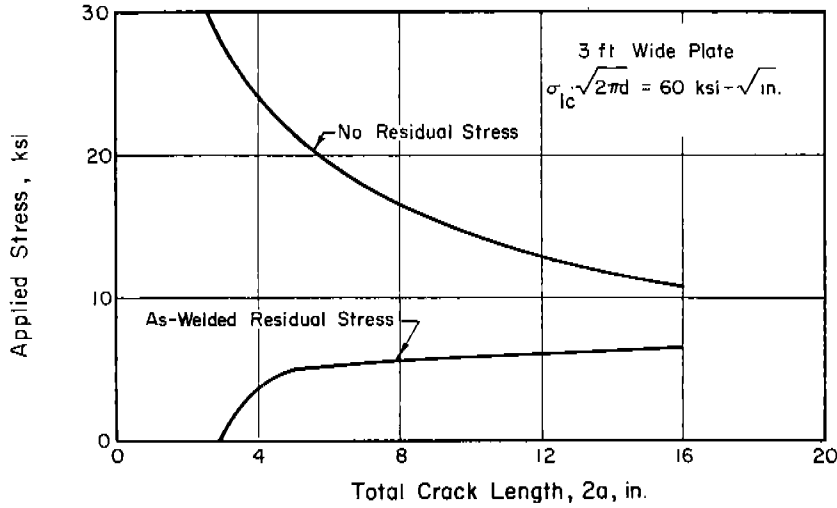


Fig. 36. Influence of Residual Stress Field on Applied Stress Required for Cleavage Propagation.

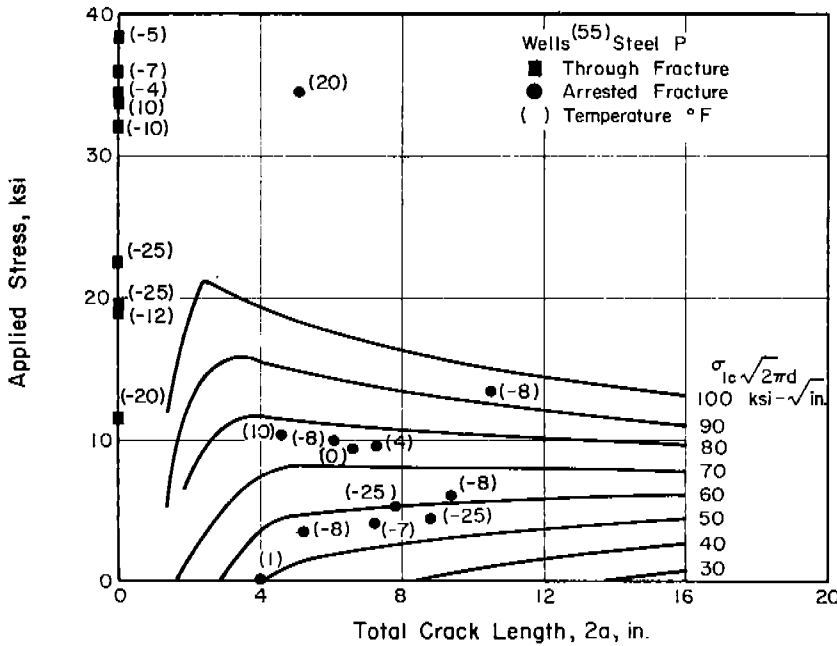


Fig. 37. Fracture Arrest in 3 ft Wide, 1 in. Plates.

rimmed steel of 40°F Charpy V 15 ft-lb, and a semi-killed steel of -10°F Charpy V 15 ft-lb. No grain size measurements were reported.

For analysis by the critical stress model for cleavage propagation a medium grain size is assumed; the particle size criterion is taken as  $d = .003 \text{ in.}$  The central sharp notch solution is considered to apply to the symmetrically edge notched test specimens. Because a submerged crack as long as 2 in. was observed in a no-go test it is assumed that, for wedge impact capable of initiating cleavage, the total driven crack length was 3 in. and in Eq. (37) "a" is taken as 3 in.

For the rimmed steel at the lower temperatures a gross section stress of 17.3 ksi was adequate for through fracture, the critical fracture stress, consistent with the above assumptions, could not exceed

$$\sigma_{1c} = \sigma_{nf} \sqrt{\frac{a}{2d}} = 17.3 \sqrt{\frac{3}{2(.003)}} = 388 \text{ ksi}$$

This value appears high for low-carbon steel; lower applied stress might have given through fracture.

For the semi-killed steel at lower temperatures, a gross section stress of 16.5 ksi was adequate for through fracture in one instance. Using the above assumptions for effective driven crack length and particle size criterion the critical fracture stress could not exceed

$$\sigma_{1c} = \sigma_{nf} \sqrt{\frac{a}{2d}} = 16.5 \sqrt{\frac{3}{2(.003)}} = 370 \text{ ksi}$$

Again, the value for  $\sigma_{1c}$  appears high for low-carbon steel. In one test initiation did not occur for the same temperature and gross stress. Apparently the wedge energy was barely adequate for initiation.

In summary, this test series did not cover a sufficiently wide range of applied stress to disclose the level of gross stress required for continued propagation of a cleavage crack initiated by wedge impact. The no-go situations logically are attributable to failure to initiate cleavage.

Videon, Hall and Barton (10) tested 6-ft-wide plates containing 18- or 20-in. welded slots above and below the crack initiating notch. Cleavage fractures were initiated by wedge impact in 3/4-in.-thick semi-killed steel plates with Charpy V 15 ft-lb of +10°F. Welded-up slots produced a residual tension field along the line between edge notches for a distance of about 20 in. from the plate edge. A number of fractures deviated markedly from the line between edge notches, apparently following the trace of maximum principal stress and arresting in the vicinity of far-side welded slots.

None of the zero applied stress fractures severed the plate; all but one tested at an average applied stress of 3 ksi resulted in through fracture. If the critical point for crack arrest is taken at about the end of the welded slot, where tensile residual stress faded out, an estimate of the critical fracture stress is possible. For a nominal applied stress of 3 ksi, medium grain material of  $d = 0.003$  in. and a crack length of 20 in., the level of critical fracture stress required for arrest is

$$\sigma_{1c} = \sigma_{nf} \sqrt{\frac{a}{2d}} = 3 \sqrt{\frac{20}{2(.003)}} = 173 \text{ ksi}$$

The influence of finite crack length was not considered in the above computation because of the neglect of more important factors such as stress redistribution with increasing crack length and the asymmetry of the flawed plate for a 20-in. crack length. However, the observed result -- that a stress of 3 ksi is adequate to provide continued propagation of a 20-in. flaw -- leads to a reasonable magnitude for the critical fracture stress.

Kihara, Yoshida and Oba (58) reported S.O.D. tests run on 1000 by 1000 by 25 mm specimens of three steels. The steels are described as: Brittle Semi-Killed Steel A with Charpy V 15 ft-lb of 35 C, Notch Tough Killed Steel B with Charpy V 15 ft-lb of -20°C, and Quenched and Tempered Welcon 2H Steel C with

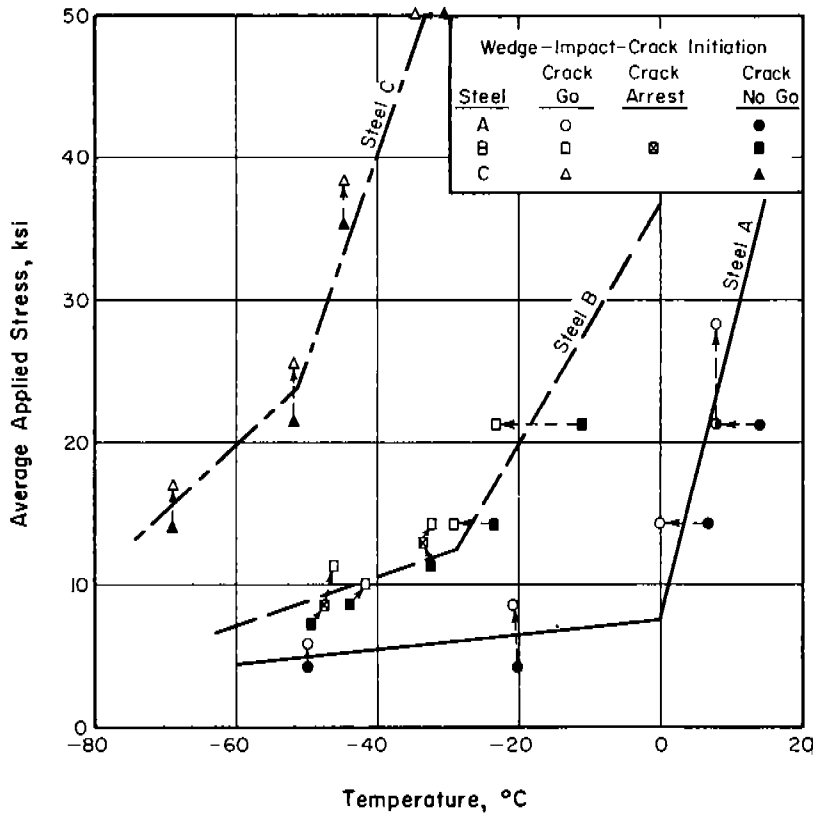


Fig. 38. Kihara, et al, (58)  
Fracture Propagation in Plain Plates.

Charpy V 15 ft-lb of  $-65^{\circ}\text{C}$ . Cleavage was initiated by wedge impact in a notch of 28 mm total depth. In many instances repeated impacts were required to initiate cleavage; the average applied stress usually was increased between attempts to initiate cleavage. No data was given on the depth of the driven crack produced by the initiation impact. Both plain and welded specimens were tested; major attention is given herein to the plain plate tests.

Nominal stress and temperature are shown in Fig. 38 for the last no-go impact and the impact producing cleavage for the plain plate specimens. No fracture was initiated in the heat affected zone or brittle zone of Steel A welded specimens at lower stress than that required to initiate cleavage in the plain plate specimens. This failure to achieve lower stress initiation in welded specimens may be attributed to the compressive residual stress in the crack opening direction at the crack starter notch. The increase with increasing temperature of stress required for initiation of a go fracture in the plain plates may be attributed to requirements for cleavage initiation rather than propagation. Arrested cracks, showing that conditions for continued propagation were not met, appeared only in tests of Steel B.

The material properties appearing in the critical stress model for cleavage propagation are tabulated below. It is questionable whether the model applies to the austenitic Steel C. The critical fracture stress is shown as computed by Eq. (37) using the initial notch depth for "a".

Steel	ASTM Grain Size	Particle Size Criterion d mm	Lowest Through Fracture Stress ksi	$\sigma_{lc}$ ksi
A	7	.0359	5.7	113
B	9	.0180	10.0	280
C	5	.0718	17.1	240

The crack length of 28 mm original notch depth would be a minimum since the depth of drive-crack produced by the initiation impact is unknown. A longer crack length would lead to higher critical fracture stress; logically the increase would be greatest for brittle Steel A which should have the greatest depth of driven crack.

Steel B showed arrested cracks as tabulated below. The level of critical fracture stress required for arrest at this length by Eq. (37) is also shown. These values are unreasonably high; it would appear that the applied stress is much relaxed by crack extension.

Arrested Cracks in Steel B

Nominal Stress ksi	Crack Length mm	$\sigma_{lc}$ ksi
8.5	200	633
12.8	200	954

Part IV

SUMMARY

12. Summary and Conclusions

The studies conducted as a part of this program were concerned with mild steels. However, the basic mechanisms involved in the cleavage fracture of mild steels are likely to control the brittle behavior of other body centered cubic iron alloys that show a rate-temperature dependence of their resistance to inelastic deformation of absolute magnitude similar to that for mild steels. Therefore the results of this program may be of value in the evaluation of the fracture toughness of a number of the higher strength steels.

The application of linear elastic fracture mechanics to the determination of the fracture toughness of mild steel in Part I shows that a meaningful measure of the fracture toughness as a material parameter can be obtained from conditions at fracture arrest. The contribution of an extensive residual stress field to the crack-driving force is evaluated and shown to aid significantly in the growth of a crack to such length that it may continue to propagate under low applied stress. A toughening with increasing temperature is observed and is attributed to an increase in the amount of shear lip and curvature of the crack front.

Many earlier efforts to apply linear elastic fracture mechanics to ductile steels in order to evaluate fracture toughness as a material parameter have proved disappointing. In this study well defined values of critical stress intensity factor are obtained for an ASTM A-212B and an ABS Class C steel. These steels were tested over a range of thicknesses and temperatures using welded wide plate specimens of different widths that had notches formed both before and after welding with the welds both intact and severed. A variety of treatments were applied including preheat, postheat, mechanical stress relief, and as-welded specimens. The success of the analysis may be attributed to the very small plastic zone accompanying a propagating crack at low stress. Stress rates ahead of a propagating crack are so high that little yielding occurs and the assumptions inherent in the linear elastic fracture mechanics analysis are met.

A linear elastic fracture mechanics analysis based on transient strain measurements in the vicinity of a propagating crack is applied to fractures propagating in 6-ft-wide semi-killed mild steel plates. The critical stress intensity factor for this steel appears to be markedly smaller than that for the steels cited above. It is not clear how much of this difference is a difference in material properties and how much results from differing computational procedures.

The magnitude of the resistance of steel to inelastic deformation is known to influence the tendency to brittle fracture. The effects of time and temperature on the upper yield stress of mild steel can be represented quantitatively by yield criteria that consider the yield stress to be made up of rate-temperature dependent and independent components as noted in Part II. The rate-temperature dependent component can be represented by a rate-process expression. One form of this expression is given that is applicable to a general time variation of stress prior to yield providing that aging under stress before yield is insignificant. Another form is presented that is applicable only to roughly constant stress rate conditions immediately prior to yield. Both yield criteria are evaluated for a number of steels.

The effect of welding on the yield behavior of metal from the thermally affected zone adjacent to the weld is determined experimentally for an ASTM A-212B steel. The thermal and deformation cycling associated with welding appear to influence only the rate-temperature independent component of the yield stress. The absolute change in the yield stress resulting from a given change in stress rate and temperature is the same for base metal and metal from the thermally affected zone. The studies of a number of investigators tend to confirm this indication that thermal and deformation history as well as grain size influence only the rate-temperature dependent component of the yield stress. If so, the effects of deformation and thermal history on the yield behavior of a particular steel, and their associated influence on the tendency toward brittle behavior, can be evaluated by ordinary static tensile testing at known stress rate and temperature if the rate-temperature dependent component of the yield stress is known.

Available experimental evidence suggests that cleavage fracture occurs in mild steel when a critical level of principal normal stress, termed the critical fracture stress, is attained locally in plastically deformed metal. In Part III a mechanism for cleavage fracture is explored which associates the critical fracture stress with the stress required to make a microcrack (formed as a result of plastic deformation) grow as a cleavage crack.

An approximate critical fracture stress model is developed that uses the peak principal normal stress at the boundary of the plastic zone as a measure of the critical fracture stress. The boundary of the plastic zone is located approximately by using the yield criterion described above in conjunction with the theoretical elastic stress distribution around a flaw or crack. The effects of rate of application of nominal applied stress or crack propagation velocity, temperature, notch acuity, residual stress, and local strain hardening can be accounted for by the model. The model based on the elastic stress distribution must become progressively less accurate as the size of the plastic zone relative to notch proportions increases, and it is inapplicable to post general yield ductile cleavage fracture. The basic concept of critical fracture stress can be applied to ductile cleavage fracture if a measure of the maximum principal normal stress acting in the metal is available.

The critical stress model gives an excellent qualitative representation of the influence of parameters known to influence brittle behavior. It provides a good quantitative representation of the influence of stress rate and temperature on brittle cleavage initiation in notched unwelded specimens. Available data are not adequate to define the model's effectiveness in accounting for notch acuity. Application of the model to cleavage initiation in notched welded wide plates suggests that the extremely brittle behavior observed with these specimens can be accounted for only by a reduction of the critical fracture stress in the region of cleavage initiation. Such reduction might be caused by the formation of unusually large microcracks in material that undergoes thermal and deformation cycling during welding, or by other damaging mechanisms.

Applied to cleavage propagation the critical stress model defines a stress dependent, crack length independent, upper limit velocity of propagation that is derived from the requirement that the maximum principal normal stress be directed so as to produce propagation in the direction of the extended crack axis. This upper limit velocity always is smaller than the Rayleigh surface wave velocity. A crack length dependent minimum stress for cleavage propagation also is defined as a function of the minimum size of plastic zone at the crack

tip -- here assumed to be one grain diameter. The formulation for this minimum stress for propagation as a function of critical fracture stress and minimum size of plastic zone is equivalent to the linear elastic fracture mechanics expression for critical applied stress in terms of the critical stress intensity factor.

The model discloses very little temperature effect on the conditions for cleavage propagation. Stress rates are so high near the tip of a propagating crack that the model indicates the plastic zone is difficult to extend beyond its minimum dimensions. However, the analysis is based on a straight fracture front and plane strain conditions. Temperature effects are more significant for plane stress; increased shear lip with increased temperature would modify the stress field at the crack tip and lead to increased resistance to propagation that is not accounted for by the present model.

The critical stress propagation model correlates well with available data on cleavage propagation and arrest. However, the value of critical fracture stress derived when the minimum extent of plastic zone is taken at one grain diameter is higher by a factor of about two than the critical fracture stress obtained from studies of cleavage initiation in similar metals. The one grain diameter minimum extent of plastic zone corresponds well with the results of cleavage initiation studies. Apparently some differences exist in the mechanisms of plastic flow and cleavage under initiation and propagation conditions or else the essentially static procedure used to account for the crack driving effect of residual stress overestimates the effect under propagation conditions.

The critical stress model provides a useful means for the study of parameters affecting the tendency to low-stress brittle cleavage fracture. The results of this study suggest that service initiation of cleavage fracture in fabricated steel structures results from damaged material -- having a far lower critical fracture stress than is normal for the material -- in the vicinity of stress raisers or flaws. Welded structures appear particularly susceptible to cleavage because high residual stresses permit growth of the cleavage fracture, initiated in damaged metal, to such length that it can propagate through sound material at low applied stress.

### 13. Applications and Further Studies

The successful use of linear elastic fracture mechanics to evaluate the toughness of mild steels from conditions for the arrest of propagating cleavage cracks suggests that  $K_C$  obtained in this manner can be used to select steel that will be fracture safe under given conditions of operating stress, temperature, and residual stress magnitude and distribution. The method of analysis gives no insight into the possibility of fracture initiation but will show whether a propagating crack can be expected to arrest at an acceptable length. It will be necessary to develop an economical test procedure for the evaluation of fracture

toughness at arrest that permits ready and reliable computation of the toughness. Most present-day crack arrest tests appear deficient in this latter requirement. The procedure used here for analysis of the crack-driving effect of residual stress gave consistent results but it should be verified by comparison of the fracture toughness determined in the same manner in plain and welded plates of the same steel.

The yield criterion form presented and applied herein compares well with experimental results at slow and moderate rates of stress. It has not, however, been directly verified at stress rates of the order encountered in impact materials tests and in the vicinity of propagating cracks. Such studies are needed for reliable general application of the critical stress model to cleavage fracture analysis. The rate-temperature dependent component of the yield stress appears to be little affected for a particular steel by changes in the grain size and thermal and deformation cycling. If the rate-temperature dependent component of the yield stress is evaluated for a number of steels covering the practical ranges of composition and structure, it may become possible to relate the formulation of the yield criterion to the manufacturer's description of the steel.

The effects of grain size and thermal and deformation cycling on the rate-temperature independent component of the yield stress have been fairly thoroughly explored and reported in the literature. However, correlation studies are needed to determine quantitatively the influence of welding operations and treatments intended to reduce the embrittling effects of welding on the yield behavior of the metal. Additional studies of the post-yield flow characteristics of steel as a function of strain rate, temperature, and time-temperature-deformation history would be valuable in extending the applicability of fracture analysis.

If the critical fracture stress model is to be used for applied fracture resistance analysis and material selection a direct and economical means for measuring the critical fracture stress is needed. The notched bend test appears well suited to this requirement. The available rigid plastic analysis permits direct computation of the critical fracture stress from the applied moment when the fracture and yield curves meet. Slow notch bend tests permit measurement of the critical fracture stress at low temperatures. Reliably instrumented impact notch bend tests are required for measurement of the critical fracture stress at the temperatures of greatest interest. An investigation of these means for evaluating the critical fracture stress, including appropriate correlation studies using other specimen geometries possibly might open the way to practical application of the critical stress model.

#### ACKNOWLEDGMENT

This program was conducted in the Structural Research Laboratory of the Department of Civil Engineering, University of Illinois, under sponsorship of the Ship Structure Committee through the Bureau of Ships, Department of the Navy, Contract NObS 86688. The writers wish to acknowledge the assistance provided by Mr. A. R. Lytle and Mr. R. W. Rumke of the National Academy of Sciences--National Research Council in the administration of this program, as well as that of the members of the Project SR-163 Advisory Committee, Dr. D. K. Felbeck, Chairman, under cognizance of the Ship Hull Research Committee of the National Academy of Sciences--National Research Council.

The writers gratefully acknowledge the assistance of others who have contributed to the success of the program, particularly Professor F. W. Barton, Professor V. J. McDonald, Mr. F. F. Videon, and Mr. M. W. Emerson.

REFERENCES

1. Nordell, W. J. and W. J. Hall, "Two-Stage Fracturing in Welded Mild Steel Plates," Welding Journal, 44:3, Res. Suppl., p. 124-s, 1965.
2. Hall, W. J., W. J. Nordell and W. H. Munse, "Studies of Welding Procedures," Welding Journal, 41:11, Res. Suppl., p. 505-s, 1962.
3. Hall, W. J., J. R. Joshi and W. H. Munse, "Studies of Welding Procedures-- Part II," Welding Journal, 44:4, Res. Suppl., p. 182-s, 1965
4. Irwin, G. R., "Fracture Dynamics," Trans. American Society of Metals, 40A, p. 147, 1948.
5. Orowan, E., "Fundamentals of Brittle Behavior in Metals," Fatigue and Fracture of Metals (A Symposium held at MIT in 1950), ed. W. M. Murray, Tech. Press of MIT and John Wiley and Sons, Inc., New York, p. 139, 1952.
6. Irwin, G. R., "Fracture Mechanics," Structural Mechanics (Proc. of the First Symposium on Naval Structural Mechanics), ed. J. N. Goodier and N. J. Hoff, Pergamon Press, New York, p. 557, 1960.
7. Irwin, G. R., "Structural Aspects of Brittle Fracture," AGARD 17th S & M Panel Meeting, Sept. 1963.
8. ASTM Special Committee on Fracture Testing of High-Strength Metallic Materials, "Fracture Testing of High-Strength Materials," ASTM Bulletin, No. 243, p. 29, Jan. 1960 and No. 244, p. 18, Feb. 1960; "The Slow Growth and Rapid Propagation of Cracks," Materials Research and Standards, 1:5, p. 389, 1961; "Fracture Testing of High-Strength Sheet Materials," Materials Research and Standards, 1:11, p. 877, 1961; "Screening Test for High-Strength Alloys Using Sharply Notched Cylindrical Specimens," Materials Research and Standards, 2:3, p. 196, 1962; "Progress in Measuring Fracture Toughness and Using Fracture Mechanics," Materials Research and Standards, 4:3, p. 107, 1964.
9. Wells, A. A., "The Brittle Fracture Strengths of Welded Steel Plates," Trans. Royal Inst. of Naval Architects, 98, p. 296, 1956.
10. Videon, F. F., F. W. Barton and W. J. Hall, "Brittle Fracture Propagation Studies," Ship Structure Committee Report SSC-148, 1963.
11. Barton, F. W. and W. J. Hall, "Brittle-Fracture Tests of Six-Foot Wide Prestressed Steel Plates," Welding Journal, 39:9, Res. Suppl., p. 379-s, 1960.
12. Wells, A. A., "Notched Bar Tests, Fracture Mechanics and the Brittle Strengths of Welded Structures," 1964 Houdremont lecture to the Int. Inst. of Welding.
13. Irwin, G. R., "Crack-Toughness Testing of Strain-Rate Sensitive Materials," ASME Paper 63-WA-217, 1963.
14. Hahn, G. T. and A. R. Rosenfield, "Local Yielding and Extension of a Crack Under Plane Stress," Ship Structure Committee Report No. SSC-165, 1964.

15. Rosenthal, D. and J. T. Norton, "A Method of Measuring Triaxial Residual Stress in Plates," Welding Journal, 24:5, Res. Suppl., p. 295-s, 1945.
16. Westergaard, H. M., "Bearing Pressures and Cracks," Journal of Applied Mechanics, 6, p. A-49, 1939.
17. Irwin, G. R., "Analysis of Stresses and Strains Near the End of a Crack Traversing a Plate," Journal of Applied Mechanics, 24:3, p. 361, Sept. 1957.
18. Irwin, G. R., "Analytical Aspects of Crack Stress Field Problems," University of Illinois, Dept. of Theoretical and Applied Mech., Report No. 213, March 1962.
19. Private communication of selected data from the Low-Cycle Fatigue Program, conducted by the Dept. of Civil Engineering, University of Illinois, Ship Structure Committee Subproject No. SR-149.
20. Eftis, J. and J. M. Krafft, "A Comparison of the Initiation With the Rapid Propagation of a Crack in a Mild Steel Plate," ASME Paper No. 64-Met-16.
21. Kanazawa, T., H. Oba and S. Machida, "Effect of Welding Residual Stress on Brittle Fracture Propagation," University of Tokyo, Tech. Report SR-6105, 1961.
22. Wright, R. N., W. J. Hall and H. S. Hamada, "The Behavior of Structural Steel Under Slow and Rapid Reversal of Loading," Proc. ASTM, 64, p. 612, 1964.
23. Conrad, H., "Yielding and Flow of the B.C.C. Metals at Low Temperatures," The Relation Between the Structure and Mechanical Properties of Metals, National Physical Laboratory Symposium No. 15, Her Majesty's Stationery Office, London, p. 475, 1963.
24. Sleswyk, A. W. and J. N. Helle, "Ductile Cleavage Fracture, Yielding, and Twinning in  $\alpha$ -Iron," Acta Metallurgica, 11:2, p. 187, 1963.
25. Campbell, J. D. and J. DUBY, "Delayed Yield and Other Dynamic Loading Phenomena in a Medium Carbon Steel," Properties of Materials at High Rates of Strain, Inst. of Mech. Engrs., London, p. 214, 1957.
26. Yokobori, T., "The Cottrell-Bilby Theory of Yielding of Iron," Physical Review, 88, p. 1423, 1952.
27. Wood, D. S. and D. S. Clark, "The Influence of Temperature Upon the Time Delay for Yielding in Annealed Mild Steel," Trans. ASM, 43, p. 571, 1951.
28. Johnson, J. E., D. S. Wood and D. S. Clark, "Delayed Yielding in Annealed Low-Carbon Steel Under Compression Impact," Proc. ASTM, 53, p. 75, 1953.
29. Hendrickson, J. A. and D. S. Wood, "The Effect of Stress Application and Temperature on the Upper Yield Stress of Mild Steel," Trans. ASM, 50, p. 458, 1958.
30. Hendrickson, J. A., D. S. Wood and D. S. Clark, "Prediction of Transition Temperature in a Notched Bar Impact Test," Trans. ASM, 51, p. 629, 1959.
31. Krafft, J. M. and A. M. Sullivan, "Effect of Grain Size and Carbon Content on the Yield Delay-Time of Mild Steel," Trans. ASM, 51, p. 643, 1959.

32. Knott, J. F. and A. H. Cottrell, "Notch Brittleness in Mild Steel," Journ. Iron and Steel Inst. 201:3, p. 249, 1963.
33. Bennett, P. E., "Low Temperature Yielding Behavior of the Body-Centered Cubic Transition Metals," Ph.D. Thesis, University of Illinois, Urbana, 1963.
34. Heslop, J. and N. J. Petch, "The Stress to Move a Free Dislocation in Alpha-Iron," Philosophical Magazine, Series 8, 1, p. 866, 1956.
35. Petch, N. J., "The Ductile-Cleavage Transition in Alpha-Iron," Fracture, ed. B. L. Averbach, et al, John Wiley and Sons, Inc., New York, p. 54, 1959.
36. Hutchison, M. M., "High Upper Yield Points in Mild Steel," Journ. Iron and Steel Inst., 186, p. 431, 1957.
37. Ludwik, P., Elemente der Technologischen Mechanik, Springer, Berlin, 1909.
38. Mylonas, C., "Exhaustion of Ductility and Brittle Fracture of E-Steel Caused by Prestrain and Aging," Ship Structure Committee, SSC-162, July 1964.
39. Hendrickson, J. A., D. S. Wood and D. S. Clark, "The Initiation of Brittle Fracture in Mild Steel," Trans. ASM, 50, p. 656, 1958.
40. Orowan, E., "Energy Criteria of Fracture," Mechanics of Brittle Fracture, Ship Structure Committee Report SSC-69, p. 201, 1954.
41. Hahn, G. T., B. L. Averbach, W. S. Owen and M. Cohen, "Initiation of Cleavage Microcracks in Polycrystalline Iron and Steel," Fracture, ed. B. L. Averbach, et al, John Wiley and Sons, Inc., New York, p. 91, 1959.
42. McMahon, C. J., "Micromechanisms of Cleavage Fracture in Polycrystalline Iron," Ship Structure Committee Report SSC-161, 1964.
43. Friedel, J., "Propagation of Cracks and Work Hardening," Fracture, ed. B. L. Averbach, et al, John Wiley and Sons, Inc., New York, p. 498, 1959.
44. Cottrell, A. H., "Theory of Brittle Fracture in Steel and Similar Metals," Trans. AIME, 212, p. 192, 1958.
45. Barton, F. W. and W. J. Hail, "A Study of Brittle Fracture Initiation in Mild Steel," Ship Structure Committee Report SSC-147, 1963.
46. Drucker, D. C., "A Continuum Approach to the Fracture of Metals," Fracture of Solids, ed. D. C. Drucker and J. J. Gilman, Metallurgical Societies Conferences Vol. 20, Interscience Publishers, New York-London, 1963.
47. Yoffe, E. H., "The Moving Griffith Crack," Philosophical Magazine, 42, p. 739, 1951.
48. Neuber, H., Theory of Notch Stresses, United States Atomic Energy Commission Translation AEC-tr-4547, 1961.
49. Frankland, J. H., "Triaxial Tension at the Head of a Rapidly Running Crack in a Plate," Trans. ASME, Journal of Applied Mechanics, 81, p. 570, 1959.
50. Drucker, D. C., "An Evaluation of Current Knowledge of the Mechanics of Brittle Fracture," Mechanics of Brittle Fracture, Ship Structure Committee Report SSC-69, p. 5, 1954.

51. Green, A. P. and B. B. Hundy, "Initial Plastic Yielding in Notch Bend Tests," Journal of the Mechanics and Physics of Solids, 4, p. 128, 1956.
52. Alexander, J. M. and T. J. Komoly, "On the Yielding of a Rigid Plastic Bar with an Izod Notch," Journal of the Mechanics and Physics of Solids, 10, p. 265, 1962.
53. Tardif, H. P. and H. Marquis, "Impact Testing with an Instrumented Machine," Metal Progress, 85:2, p. 79, 1964.
54. Leonard, R. W. and B. Budiansky, "On Traveling Waves in Beams," National Advisory Committee for Aeronautics, Report 1173, 1954.
55. Wells, A. A., "Brittle Fracture Strength of Welded Steel Plates--tests on five further steels," British Welding Journal, 8, p. 259, 1961.
56. Wilson, W. M., R. A. Hechtman and W. H. Bruckner, "Cleavage Fractures of Ship Plates," University of Illinois Engineering Experiment Station Bulletin No. 388, 1951.
57. Lazar, R. and W. J. Hall, "Studies of Brittle Fracture Propagation in Six-Foot Wide Structural Steel Plates," Ship Structure Committee Report No. SSC-112, 1959.
58. Kihara, H., Y. Yoshida and H. Oba, "Initiation and Propagation of Brittle Fracture in Welded Steel Plate," Int. Inst. of Welding Doc. No. X-217-59, 1959.

Appendix A

RESIDUAL STRESS MEASUREMENTS

1. General Remarks

The distribution of residual stress in the longitudinal direction (parallel to weld axis) and in the transverse direction (perpendicular to weld axis) was measured using the Rosenthal-Norton relaxation technique (15) in longitudinally butt welded specimens of the type noted in Fig. 2. In general, the procedure involved sawing small rectangular blocks from the welded plate on which strain gages were bonded back-to-back to the plate surface. These blocks then were sawed in half at mid-thickness and layers of material were removed from the block in successive steps progressing outward toward the surface on which the strain gage was bonded. Strain gage readings were taken after removal of the block from the plate and at particular increments of thickness until the block had been reduced to a thickness of about 5 percent of the original plate thickness. The residual stresses were calculated using these measurements.

The material was an ASTM A212-B firebox quality steel, the properties of which are noted in Table 1. The residual stress was measured in the following 2-ft-wide by 3-ft-long welded plate specimens; the data are shown in the figures denoted to the right of the listing.

<u>Specimen</u>	<u>Fig. No.</u>
As-Welded, 1 in. thick	A1
Preheated, 1 in. thick	A4
Postheated, 1 in. thick	A5
Mechanically Stress Relieved, 1 in. thick	A5
As-Welded, 1-5/8 in. thick	A4

In addition, for the study of primary crack arrest, the longitudinal residual stress distributions were estimated, as described later, for the following 2-ft-wide and 3-ft-wide by 3-ft-long welded plate specimens. The residual stress distribution assumed to exist for each specimen is given in the cited figure.

<u>Specimen</u>	<u>Fig. No.</u>
As-Welded, 3 ft wide by 1 in. thick	A7*
Preheated, 3 ft wide by 1 in. thick	A7*
Mechanically Stress Relieved, 3 ft wide by 1 in. thick	A5
As-Welded, 2 ft wide by 3/4 in. thick	A1

---

\* Figure A7 illustrates the technique used for estimating the residual stresses in the 3 ft wide as-welded and preheated plates.

<u>Specimen</u>	<u>Fig. No.</u>
Preheated, 2 ft wide by 1-5/8 in. thick	A4
Postheated, 2 ft wide by 1-5/8 in. thick	A5

## 2. Comments on Data

A summary of the residual stress measurements for a 1-in.-thick 2-ft-wide as-welded specimen is presented in Figs. A1, A2, and A3. The values of the longitudinal stress, as presented in Fig. A1, are averages of the stress distribution through the thickness of the specimen as shown in Figs. A2 and A3. As shown by the distribution of the longitudinal residual stress through the weld, Fig. A2, the magnitude of the stress at a particular point may differ appreciably from the averages given in Fig. A1. However, the residual stress distribution across the thickness at locations outside the region of the weld was approximately uniform through the plate thickness as shown by the stress distributions in Fig. A3 for locations about 1, 2, and 10 in. from the centerline of the weld.

The average longitudinal residual stress decreased rapidly from a value of 65 ksi at the centerline of the weld to a value of approximately 10 ksi at a distance 1 in. from the weld as may be noted in Fig. A1. From a point 2 in. from the weld, the stress decreased almost linearly across the width of the plate reaching a compressive stress of approximately 15 ksi at the edge of the plate. The equilibrium condition which requires that the total tensile and compressive forces in the longitudinal direction be equal was satisfied by passing a curve through all the data points and then adjusting it only slightly to balance the tensile and compressive areas. The adjusting of the curve was done primarily in the region of the large stress gradient near the weld as there was more likelihood of the stress being in error in this region as a result of measuring the stress over a finite area. Actually only a very small adjustment was necessary, and the final curve as shown in Fig. A1 was representative of the test data.

Also of interest is the large variation in transverse residual stress shown in Fig. A2. It will be noted that the peak tensile stress value for both the longitudinal and transverse stress occurred at about quarter thickness of the plate, or at the location where the precracking occurred during sawing of the Type 6 notches in the 1-5/8-in.-thick plate material. As Fig. A4 shows, the average residual stress distributions in the 1-5/8-in.-thick as-welded specimen and the 1-in.-thick preheated specimen were similar, and were not greatly different in shape from that in the 1-in. as-welded specimen (Fig. A1) except for a "broadening" of the tensile zone. The stress distribution as a function of thickness was quite similar to that shown in Figs. A2 and A3.

Similar residual stress data for a mechanically stress relieved specimen (0.6 percent prestrain) and a postheated specimen are shown in Fig. A5. The average transverse stress is not shown, and in both cases is nearly of zero magnitude. The treatments markedly leveled out the stress distribution through the thickness as shown in Fig. A6.

The distribution of longitudinal residual stress in 3-ft-wide preheated and as-welded specimens was estimated by assuming that the longitudinal stress distributions near the weld were the same as for 2-ft-wide preheated and as-welded specimens respectively. An estimate of the longitudinal stress distribu-

tion in the compressive zone was aided by surface strain measurements obtained from Berry gage (6-in. gage length) readings taken before and after welding for a 3-ft-wide preheated specimen. In all cases the gross stress distributions were balanced in terms of net force. The derived stress distributions are shown in Fig. A7.

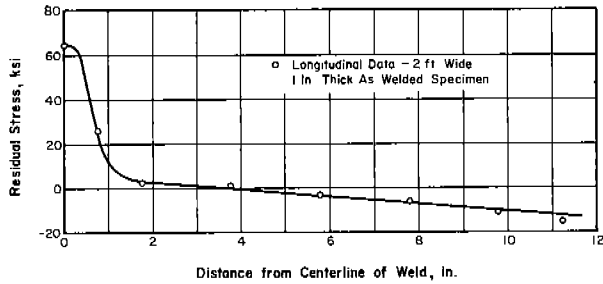


Fig. A-1. Distribution of Residual Stress in a 2 ft wide, 1 in. thick, As-Welded Specimen.

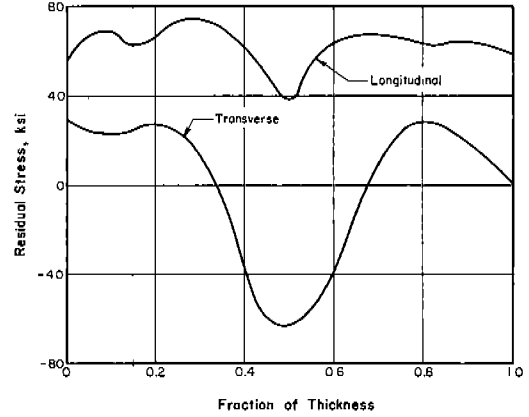


Fig. A-2. Distribution of Longitudinal and Transverse Residual Stress Through the Thickness of Weld-- 2 ft wide, 1 in. thick, As-Welded Specimen.

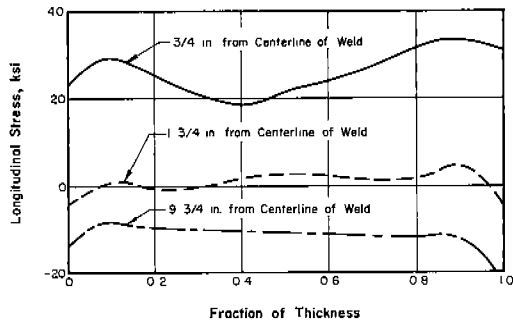


Fig. A-3. Distribution of Longitudinal Residual Stress Through Plate Thickness-- 2 ft wide, 1 in. thick, As-Welded Specimen.

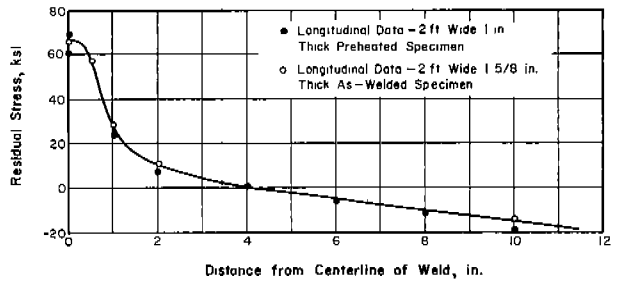


Fig. A-4. Distribution of Residual Stress in a 2 ft wide, 1 in. thick, Preheated Specimen and 2 ft wide, 1-5/8 in. thick, As-Welded Specimen.

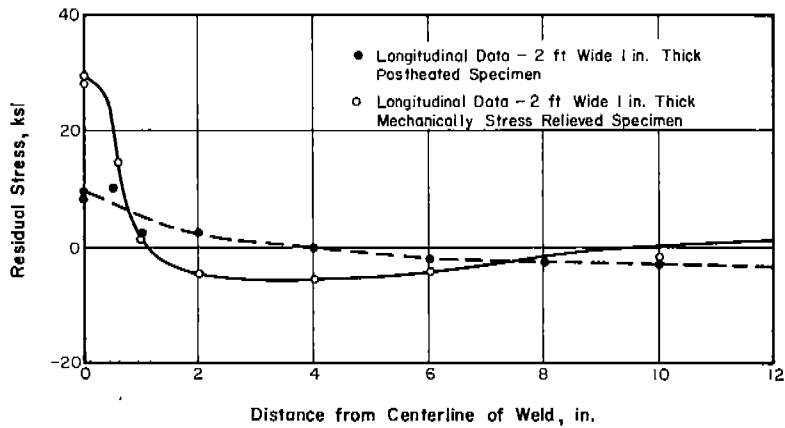


Fig. A-5. Distribution of Residual Stress in a 2 ft wide, 1 in. thick, Postheated and Mechanically Stress Relieved Specimens.

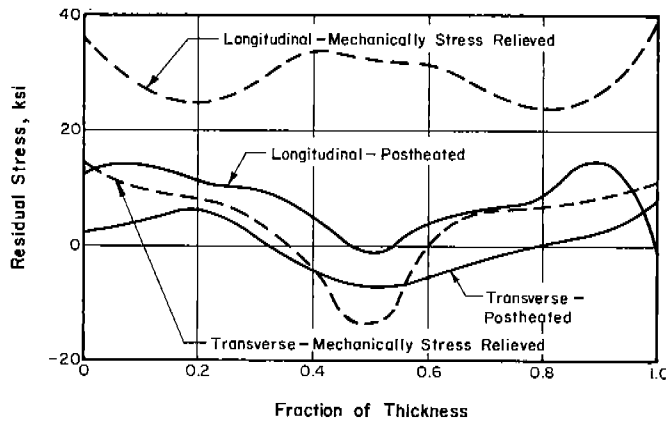


Fig. A-6. Distribution of Longitudinal and Transverse Residual Stress Through the Thickness of Weld-- 2 ft wide, 1 in. thick, Postheated and Mechanically Stress Relieved Specimens.

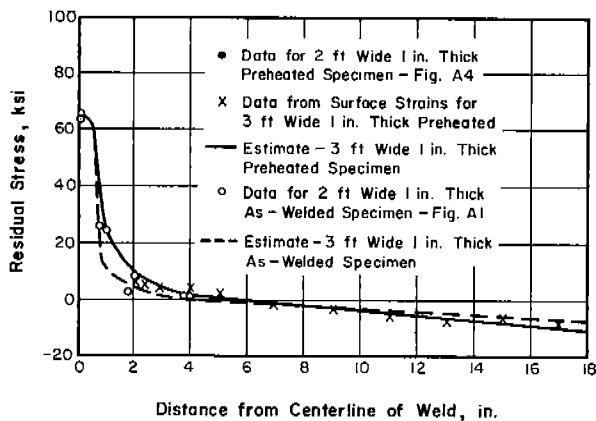


Fig. A-7. Estimated Distribution of Longitudinal Residual Stress in a 3 ft wide, 1 in. thick, As-Welded and Preheated Specimen.

Appendix B

LINEAR ELASTIC FRACTURE ANALYSIS EXPRESSIONS  
AND SAMPLE COMPUTATIONS

1. Linear Elastic Fracture Analysis

For the stress field in the vicinity of a crack tip, Westergaard (16) assumed the stresses to have the form:

$$\begin{aligned}\sigma_x &= \operatorname{Re} Z - y \operatorname{Im} Z' \\ \sigma_y &= \operatorname{Re} Z + y \operatorname{Im} Z' \\ \tau_{xy} &= -y \operatorname{Re} Z'\end{aligned}\tag{B-1}$$

where  $dZ/dz = Z'$  and  $z = x + iy$ .

Using the Westergaard procedure Irwin (17) found the stress function

$$Z(z) = \frac{2\sigma a}{\pi(z^2 - b^2)} \left[ \frac{1 - (b/a)^2}{1 - (a/z)^2} \right]^{1/2}\tag{B-2}$$

to represent the problem of a central crack extending from  $x = -a$  to  $x = a$  in an infinite plate with a pair of opposing forces located at  $x = \pm b$ ; Eq. (B-2) may be used in the solution of problems in which the magnitude of  $\sigma_y$  in the absence of a crack is the function of  $x$  (18). For the problem of a central crack in a welded plate, by letting  $\sigma(z)$  represent the  $y$ -direction stress on the  $x$ -axis for the welded plate without a crack, the effect of the crack may be taken into account by using the stress function

$$Z(z) = \frac{2a}{\pi \sqrt{1 - (a/z)^2}} \int_0^a \frac{\sigma(b) \sqrt{1 - (b/a)^2}}{(z^2 - b^2)} db\tag{B-3}$$

where  $\sigma(b) = \sigma(z)$  between  $x = -a$  and  $x = 0$ .

The stress  $\sigma(x)$  is assumed to be symmetrical about the  $y$ -axis. By Eqs. (B-1) and (B-3) the value of  $\sigma_y$  on  $y = 0$  is

$$\sigma_y = \sigma(x) + \frac{2a}{\pi \sqrt{1 - (a/x)^2}} \int_0^a \frac{\sigma(b) \sqrt{1 - (b/a)^2}}{(x^2 - b^2)} db\tag{B-4}$$

By letting  $x = a + r$  and combining Eqs. (4) of text and (B-4) the value of  $K$  can be obtained by letting  $r$  go to zero. Thus,

$$K = \lim_{r \rightarrow 0} \sqrt{2\pi r} \left[ \sigma(x) + \frac{2a(a+r)}{\pi \sqrt{(a+r)^2 - a^2}} \int_0^a \frac{\sigma(b) \sqrt{1 - (b/a)^2}}{(a+r)^2 - b^2} db \right]\tag{B-5}$$

which yields

$$K = \sqrt{\frac{a}{\pi}} \int_0^a \frac{\sigma(b)}{\sqrt{a^2-b^2}} db \quad (B-6)$$

when  $\sigma(b)$  is known  $K$  can be determined by integration. In the case of the longitudinal stress distribution in the welded plates an exact formulation for  $\sigma(x)$  is not readily obtained. However, the stress distribution can be expressed as a multiple step function such that

$$\sigma(x) = \sigma(x_i) \text{ for } x_{i-1} < x < x_i, \quad i=1,2,3,\dots,n$$

where  $x_0 = 0$  and  $x_n = a$ . Eq. (B-6) then may be rewritten as follows:

$$K = 2\sqrt{\frac{a}{\pi}} \sum_{i=1}^n \int_{x_{i-1}}^{x_i} \frac{\sigma(x_i)}{\sqrt{a^2-x^2}} dx \quad (B-7)$$

Since  $\sigma(x_i)$  is constant between  $x_{i-1}$  and  $x_i$ , Eq. (B-7) may be integrated. Thus,

$$K = 2\sqrt{\frac{a}{\pi}} \sum_{i=1}^n \sigma(x_i) \left[ \sin^{-1} \frac{x_i}{a} - \sin^{-1} \frac{x_{i-1}}{a} \right] \quad (B-8)$$

For the case of a uniform stress  $\sigma$  between  $x = -a$  and  $x = a$ , Eq. (B-8) yields the solution for a crack in a uniform stress field,

$$K = \sigma \sqrt{\pi a} \quad (B-9)$$

As noted earlier, the solution for  $K$  given in Eq. (B-8) is for the case of an infinite plate. The welded plates under study, however, were either 2 or 3 ft wide, therefore, to obtain an estimate of the effect of plate width on the  $K$ -values an approximation for the solution of a plate of finite width was considered. The stress function

$$Z(z) = \frac{\sigma \sin \frac{\pi a}{W}}{W \sin \frac{\pi(z-b)}{W} \sin \frac{\pi z}{W}} \left[ \frac{1 - \left( \sin \frac{\pi b}{W} / \sin \frac{\pi a}{W} \right)^2}{1 - \left( \sin \frac{\pi a}{W} / \sin \frac{\pi z}{W} \right)^2} \right]^{1/2} \quad (B-10)$$

was suggested by Kanazawa, Oba and Machida (21) as providing an approximation for the case of a crack in a plate of width  $W$ . Equation (B-10) represents the stress system in an infinite plate with crack of length  $2a$  spaced at a distance  $W$  center-to-center with a pair of opposing forces acting at  $x = b$  with the origin located at the center of the crack. The solution is approximate because  $\sigma_x$  is not zero along  $x = \pm W/2$  (or the plate edges). By the same procedure used to obtain Eq. (B-8) the solution for  $K$  may be derived from the stress function given in Eq. (B-10). The result is

$$K = \frac{2}{\pi} \sqrt{W \tan \frac{\pi a}{W}} \sum_{i=1}^n \sigma(x_i) \left[ \sin^{-1} \left( \frac{\sin \frac{\pi x_i}{W}}{\sin \frac{\pi a}{W}} \right) - \sin^{-1} \left( \frac{\sin \frac{\pi x_{i-1}}{W}}{\sin \frac{\pi a}{W}} \right) \right] \quad (B-11)$$

For  $W$  large in comparison to  $a$ , Eq. (B-11) yields Eq. (B-8). For the case of a uniform pressure between  $x = -a$  and  $x = a$ , Eq. (B-11) yields

$$K = \sigma \sqrt{W \tan \frac{\pi a}{W}}$$

To compare the two solutions, Eqs. (B-8) and (B-11), the  $K$ -values were computed using the residual stress distribution for a 2-ft-wide 1-in.-thick as-welded plate shown in Fig. A1. The comparison indicated that for the present study Eq. (B-8) provides an adequate solution as most of the arrested cracks were 2 to 7 in. in length and the difference between the two solutions was not appreciable even at a crack length of 10 in. For crack lengths less than 6 in., the values of  $K$  were computed using the residual stress distribution marked (A) in Fig. 4 (text), whereas for crack lengths greater than 6 in. the stress distribution marked (B) was used.

## 2. Example of Calculations of the Stress Intensity Factor for Notched and Welded Plates

The equations used for the computations, as discussed in the text, of  $K_r$ ,  $K_a$ , and  $K_c$  are (5), (6), and (10) respectively. The following sample computations are made on a 2-ft-wide 1-in.-thick as-welded plate (Specimen 2-22):

Data (See Table 2):

Crack Length ( $2a$ ) = 3.5 in.

Primary Fracture Stress ( $\sigma$ ) = 4.2 ksi

Residual Stress Stepwise Distribution (Fig. 4)

$\sigma(x_1) = 65$ ksi	$x_1 = 0.30$ in.
$\sigma(x_2) = 64$ ksi	$x_2 = 0.50$ in.
$\sigma(x_3) = 48$ ksi	$x_3 = 0.70$ in.
$\sigma(x_4) = 30$ ksi	$x_4 = 0.85$ in.
$\sigma(x_5) = 15$ ksi	$x_5 = 1.00$ in.
$\sigma(x_6) = 10$ ksi	$x_6 = 1.30$ in.
$\sigma(x_7) = 6$ ksi	$x_7 = 1.60$ in.
$\sigma(x_8) = 4$ ksi	$x_8 = 1.75$ in.

Computation of  $K_r$ , Eq. (5):

$$\begin{aligned}
 K_r &= 2\sqrt{\frac{1.75}{\pi}} \left[ 65 \left( \sin^{-1} \left( \frac{0.30}{1.75} \right) \right) + 64 \left( \sin^{-1} \left( \frac{0.50}{1.75} \right) - \sin^{-1} \left( \frac{0.30}{1.75} \right) \right) \right. \\
 &\quad + 48 \left( \sin^{-1} \left( \frac{0.70}{1.75} \right) - \sin^{-1} \left( \frac{0.50}{1.75} \right) \right) + 30 \left( \sin^{-1} \left( \frac{0.85}{1.75} \right) - \sin^{-1} \left( \frac{0.70}{1.75} \right) \right) \\
 &\quad + 15 \left( \sin^{-1} \left( \frac{1.00}{1.75} \right) - \sin^{-1} \left( \frac{0.85}{1.75} \right) \right) + 10 \left( \sin^{-1} \left( \frac{1.30}{1.75} \right) - \sin^{-1} \left( \frac{1.00}{1.75} \right) \right) \\
 &\quad \left. + 6 \left( \sin^{-1} \left( \frac{1.60}{1.75} \right) - \sin^{-1} \left( \frac{1.30}{1.75} \right) \right) + 4 \left( \sin^{-1} \left( \frac{1.75}{1.75} \right) - \sin^{-1} \left( \frac{1.60}{1.75} \right) \right) \right] \\
 &= 52 \text{ ksi } \sqrt{\text{in.}}
 \end{aligned}$$

$K_r$  was computed for various crack lengths. A plot of these values, for a 2-ft-wide by 1-in.-thick as-welded specimen, is shown in Fig. 4.

Computation of  $K_a$ , Eq. (6):

$$K_a = 4.2 \sqrt{\pi(1.75)} = 10 \text{ ksi } \sqrt{\text{in.}}$$

Computation of  $K_c$ , Eq. (10):

$$K_c = K_r + K_a = 52 + 10 = 62 \text{ ksi } \sqrt{\text{in.}}$$

This value is plotted in Fig. 7 at the temperature of +20°F appropriate to the test conditions.

### 3. Example of Calculations of the Stress Intensity Factor From Stress Field of a Propagating Crack

Equation (10) is used for computing the stress intensity factor. The following sample computations are made on Test No. 46 (6 ft wide by 3/4 in.) for Rosette No. 14 (See Table 4):

Data:

Perpendicular distance from  
gage centerline to crack = 0.38 in.

$$\epsilon_y = +0.61 \times 10^{-3} \text{ in./in.}$$

$$\epsilon_x = +0.30 \times 10^{-3} \text{ in./in.}$$

$$\text{use } \nu = \frac{1}{3}$$

Compute K:

$$K = \frac{\sqrt{2\pi r} E (\epsilon_y + \nu \epsilon_x)}{(1 - \nu^2) \cos \frac{\theta}{2} (1 + \sin \frac{\theta}{2} \sin \frac{3\theta}{2})}$$

$$\text{at } \theta = 60^\circ, \quad r = \frac{0.38 \text{ in.}}{\sin 60^\circ} = 0.44 \text{ in.}$$

$$K = \frac{\sqrt{2\pi(0.44)} (30 \times 10^3) (0.61 + (\frac{1}{3}) 0.30) (10^{-3})}{(1 - \frac{1}{9}) \cos 30^\circ (1 + \sin 30^\circ \sin 90^\circ)}$$

$$\underline{\underline{K = 30 \text{ ksi } \sqrt{\text{in.}}}}$$

Appendix C

NOTCH STRESS DISTRIBUTIONS

1. Introduction

This appendix summarizes the elastic stress field solutions used in the study of the critical stress model for fracture initiation. The stresses are given along the axis of the notch. The geometry of the notch is defined and the definition of nominal stress for the notch is given.

2. The Sharp Flaw Under Tension

The elastic stress field for a sharp flaw of zero root radius is taken from Yoffe (47). The solution was derived for a slit of length  $2a$  in an infinite plate for plane strain conditions, with a uniform tensile stress  $\sigma_n$  acting perpendicular to the slit at infinity.

For the stationary crack the stress field is given by

$$\begin{aligned}\sigma_{\ell} &= \frac{\sigma_n}{\sqrt{2k}} \\ \sigma_t &= \frac{\sigma_n}{\sqrt{2k}} (1 - \sqrt{2k}) \\ \tau_{\ell t} &= 0\end{aligned}\tag{C-1}$$

The parameter  $k$  defines the distance from the edge of the slit as shown in Fig. C-1. The stress field of Eq. (C-1) corresponds to the Westergaard (16) solution for crack length small compared to plate width. Terms of the order of  $k$  were neglected in the derivation so the equation is inaccurate for  $k \geq 0.1$ .

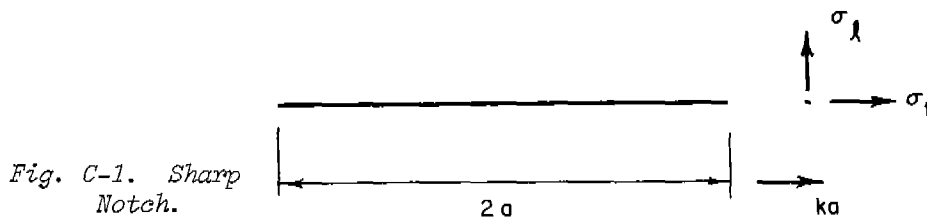


Fig. C-1. Sharp Notch.

For the crack moving at velocity  $c$

$$\begin{aligned}\sigma_{\ell} &= \frac{\sigma_n}{\sqrt{2k}} \\ \sigma_t &= \frac{\sigma_n}{\sqrt{2k}} (1 - \sqrt{2k}) H \\ \tau_{\ell t} &= 0\end{aligned}\tag{C-2}$$

where

$$H = \frac{\frac{\lambda+2\mu}{\gamma} - \lambda\gamma - \frac{4\mu\beta}{1+\beta^2}}{\frac{\lambda}{\gamma} - (\lambda+2\mu)\gamma + \frac{4\mu\beta}{1+\beta^2}}$$

$$\mu = \frac{E}{2(1+\nu)}$$

$$\lambda = \frac{\nu E}{(1+\nu)(1-2\nu)}$$

$$\gamma^2 = 1 - \left(\frac{c}{c_1}\right)^2$$

$$\beta^2 = 1 - \left(\frac{c}{c_2}\right)^2$$

$$c_1^2 = \frac{\lambda + 2\mu}{\rho}$$

$$c_2^2 = \frac{\mu}{\rho}$$

E = Young's modulus

$\nu$  = Poisson's ratio

$\rho$  = Mass density

The  $\sigma_l$  stresses are the same for moving and stationary flaws. The  $\sigma_t$  stress increases with increasing crack velocity and comes to exceed  $\sigma_l$ . The stress  $\sigma_t$  becomes infinite at the Rayleigh surface wave velocity

$$c_3 = \alpha c_2$$

$$\nu \quad 1/4 \quad 1/3 \quad 1/2$$

$$\alpha \quad 0.9194 \quad 0.9325 \quad 0.9553$$

### 3. Elastic Stress Field for Finite Radius Notches

The following stress field solutions from Neuber (48) are used for flaws of finite root radius.

Central Elliptical Notch Under Tension -- The solution applies to an elliptical notch of length 2a in a plate of infinite extent under a uniform

tensile stress  $\sigma_n$  acting at infinity perpendicular to the major axis of the ellipse.

$$\sigma_{\ell} = \sigma_n \left\{ 1 + \frac{\cosh u_o}{2 \sinh^2 u} \left[ e^{u_o} (e^{2u_o} - 3) \left( 1 + \frac{1}{2} \coth u \right) e^{-2u} + \cosh u_o \coth u \right] \right\}$$

$$\sigma_t = \frac{\sigma_n}{2 \sinh^2 u} \left[ 2Be^{-2u} + 2Ce^{-u} \sinh u - \cosh 2u - 1 + (\coth u) \left( \sinh 2u + \frac{A}{2} + Be^{-2u} \right) \right] \quad (C-3)$$

$$\tau_{\ell t} = 0$$

where

$$A = -(1 + \cosh 2u_o)$$

$$B = \frac{1}{2} e^{2u_o} + \frac{3}{4} - \frac{1}{4} e^{4u_o}$$

$$C = 1 + e^{2u_o}$$

$$\sinh u_o = \frac{1}{\sqrt{\frac{a}{\rho} - 1}}$$

$$\cosh u = (1+k) \cosh u_o$$

The notch proportions and stress directions are shown in Fig. C-2.

The Deep Edge Notch in Tension -- The notch has a theoretical hyperbolic profile and a root radius of  $\rho$ . The stresses along the notch axis are given in terms of the average stress on the minimum section  $\sigma_n = P/2ab$  where  $b$  is the thickness of the deeply notched bar

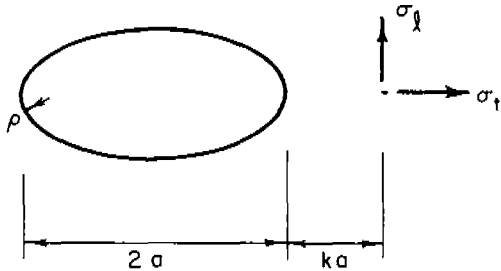


Fig. C-2. Elliptical Notch.

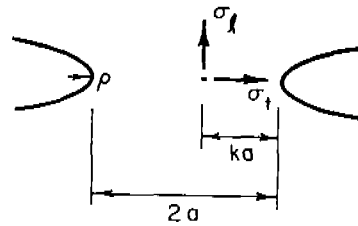


Fig. C-3. Deep Edge Notch.

$$\begin{aligned}\sigma_l &= \sigma_n \frac{A}{\cos v} \left[ 1 + \frac{\cos^2 v_o}{\cos^2 v} \right] \\ \sigma_t &= \sigma_n \frac{A}{\cos^3 v} \left[ \cos^2 v - \cos^2 v_o \right] \\ \tau_{lt} &= 0\end{aligned}\tag{C-4}$$

where

$$\begin{aligned}A &= \frac{\sin v_o}{v_o + \sin v_o \cos v_o} \\ \cos v_o &= \frac{1}{\sqrt{\frac{a}{\rho} + 1}} \\ \sin v &= (1-k) \sin v_o\end{aligned}$$

The notch proportions and stress directions are shown in Fig. C-3.

Deep One-Side Edge Notch in Flexure -- The solution for this case satisfies the boundary conditions at the notch but shows a compressive  $\sigma_t$  at the straight free edge away from the notch. The equations below give stresses along the notch axis in terms of a nominal flexural stress  $\sigma_n = 6M/a^2b$ , where  $b$  is the thickness of the notched bar.

$$\begin{aligned}\sigma_l &= \sigma_n \left\{ \frac{A' \sin 2v}{\cos^2 v} \left[ -4 + \frac{\cos 2v - \cos 2v_o}{\cos^2 v} \right] + \right. \\ &\quad \left. + \frac{A}{\cos v} \left[ 1 + \frac{\cos^2 v_o}{\cos^2 v} \right] \right\} \\ \sigma_t &= \sigma_n \left\{ \frac{A' \sin 2v}{\cos^4 v} \left[ \cos 2v_o - \cos 2v \right] + \right. \\ &\quad \left. + \frac{A}{\cos^3 v} \left[ \cos^2 v - \cos^2 v_o \right] \right\} \\ \tau_{lt} &= 0\end{aligned}\tag{C-5}$$

where

$$\frac{A'}{A} = \frac{v_o + \sin v_o \cos v_o}{4 \sin^2 v_o}$$

$$A = \frac{1}{6} \left[ \frac{1}{1 + \frac{A'}{A} \left( \frac{2v_0 \cos 2v_0 - \sin 2v_0}{\sin^2 v_0} \right)} \right]$$

$$\cos v_0 = \frac{1}{\sqrt{\frac{a}{\rho} + 1}}$$

$$\sin v = (1-k) \sin v_0$$

Notch proportions and stress directions are shown in Fig. C-4.

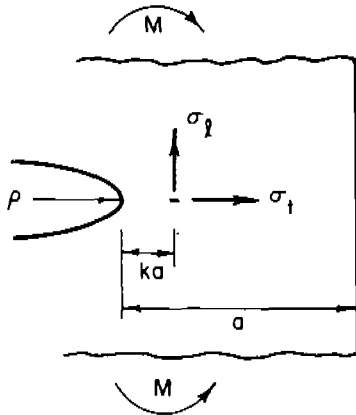


Fig. C-4. Deep One-Sided Edge Notch in Flexure.

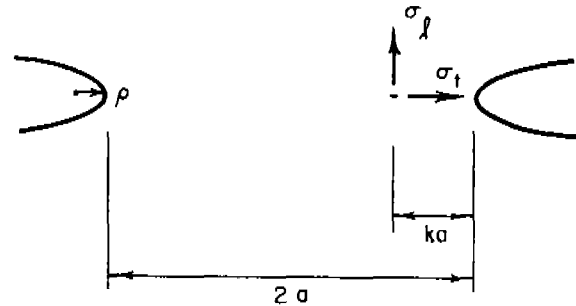


Fig. C-5. Deep Circumferential Notch.

Deep Circumferential Notch in Tension -- The longitudinal,  $\sigma_l$ , radial,  $\sigma_r$ , and hoop,  $\sigma_t$ , stresses at the minimum section for a deep hyperbolic circumferential notch are given below. The nominal stress  $\sigma_n$  is the average net section stress,  $\sigma_n = P/\pi a^2$ .

$$\begin{aligned} \sigma_l &= \sigma_n \left\{ \frac{1}{\cos v} \left[ B - 2(1-\nu)C \right] + \frac{1}{\cos^3 v} \left[ B - A \right] \right\} \\ \sigma_r &= \sigma_n \left\{ \frac{1}{\cos v} \left[ -\frac{A}{1 + \cos v} - 2\nu C \right] + \frac{1}{\cos^3 v} \left[ A - B \right] \right\} \\ \sigma_t &= \sigma_n \left\{ \frac{1}{\cos v} \left[ \frac{A}{1 + \cos v} - 2\nu C - B \right] \right\} \end{aligned} \quad (C-6)$$

where

$\nu$  = Poisson's ratio

$$C = -\frac{1}{2} \left[ \frac{1 + \cos v_o}{1 + 2\nu \cos v_o + \cos^2 v_o} \right]$$

$$A = (1 - 2\nu)(1 + \cos v_o)C$$

$$B = A - C \cos^2 v_o$$

$$\cos v_o = \frac{1}{\sqrt{\frac{a}{\rho} + 1}}$$

$$\sin v = (1 - k) \sin v_o$$

The notch proportions and stress directions are shown in Fig. C-5.

NONE

Security Classification

DOCUMENT CONTROL DATA - R&D		
<i>(Security classification of title, body of abstract and indexing annotation must be entered when the overall report is classified)</i>		
1. ORIGINATING ACTIVITY (Corporate author) Ship Structure Committee		2a. REPORT SECURITY CLASSIFICATION UNCLASSIFIED
		2b. GROUP
3. REPORT TITLE Studies of Some Brittle Fracture Concepts		
4. DESCRIPTIVE NOTES (Type of report and inclusive dates) Final Report		
5. AUTHOR(S) (Last name, first name, initial) R. N. Wright, W. J. Hall, S. W. Terry, W. J. Nordell and G. R. Erhard		
6. REPORT DATE September 1965	7a. TOTAL NO. OF PAGES 86	7b. NO. OF REFS 58
8a. CONTRACT OR GRANT NO. BuShips NObs-86688	9a. ORIGINATOR'S REPORT NUMBER(S) SSC-170	
b. PROJECT NO.	9b. OTHER REPORT NO(S) (Any other numbers that may be assigned this report)	
c.		
d.		
10. AVAILABILITY/LIMITATION NOTICES All distribution of this report is controlled. Qualified DDC users shall request through Ship Structure Committee, U.S.Coast Guard Headquarters, Wash., D.C.		
11. SUPPLEMENTARY NOTES	12. SPONSORING MILITARY ACTIVITY Bureau of Ships, Dept. of the Navy Washington, D. C.	
13. ABSTRACT Interpretive studies based on available information on the low-stress brittle fracture behavior of mild steel are made to suggest additional guides for the evaluation of the fracture resistance of fabricated steel structures. An experimental investigation was conducted to investigate the influence of welding on the yield behavior of metal from the thermally affected zone in the vicinity of a weld. The study suggests that low-stress cleavage initiation at service temperatures can be associated with a marked local reduction of critical fracture stress, that residual stresses can be responsible for the propagation through sound metal of fractures initiated in damaged material, and that the critical fracture stress and fracture mechanics approaches are equivalent when applied to cleavage propagation and arrest.		

DD FORM 1473  
1 JAN 64

NONE

Security Classification

NONE

Security Classification

14. KEY WORDS	LINK A		LINK B		LINK C	
	ROLE	WT	ROLE	WT	ROLE	WT

INSTRUCTIONS

1. **ORIGINATING ACTIVITY:** Enter the name and address of the contractor, subcontractor, grantee, Department of Defense activity or other organization (*corporate author*) issuing the report.
- 2a. **REPORT SECURITY CLASSIFICATION:** Enter the overall security classification of the report. Indicate whether "Restricted Data" is included. Marking is to be in accordance with appropriate security regulations.
- 2b. **GROUP:** Automatic downgrading is specified in DoD Directive 5200.10 and Armed Forces Industrial Manual. Enter the group number. Also, when applicable, show that optional markings have been used for Group 3 and Group 4 as authorized.
3. **REPORT TITLE:** Enter the complete report title in all capital letters. Titles in all cases should be unclassified. If a meaningful title cannot be selected without classification, show title classification in all capitals in parenthesis immediately following the title.
4. **DESCRIPTIVE NOTES:** If appropriate, enter the type of report, e.g., interim, progress, summary, annual, or final. Give the inclusive dates when a specific reporting period is covered.
5. **AUTHOR(S):** Enter the name(s) of author(s) as shown on or in the report. Enter last name, first name, middle initial. If military, show rank and branch of service. The name of the principal author is an absolute minimum requirement.
6. **REPORT DATE:** Enter the date of the report as day, month, year, or month, year. If more than one date appears on the report, use date of publication.
- 7a. **TOTAL NUMBER OF PAGES:** The total page count should follow normal pagination procedures, i.e., enter the number of pages containing information.
- 7b. **NUMBER OF REFERENCES:** Enter the total number of references cited in the report.
- 8a. **CONTRACT OR GRANT NUMBER:** If appropriate, enter the applicable number of the contract or grant under which the report was written.
- 8b, 8c, & 8d. **PROJECT NUMBER:** Enter the appropriate military department identification, such as project number, subproject number, system numbers, task number, etc.
- 9a. **ORIGINATOR'S REPORT NUMBER(S):** Enter the official report number by which the document will be identified and controlled by the originating activity. This number must be unique to this report.
- 9b. **OTHER REPORT NUMBER(S):** If the report has been assigned any other report numbers (*either by the originator or by the sponsor*), also enter this number(s).
10. **AVAILABILITY/LIMITATION NOTICES:** Enter any limitations on further dissemination of the report, other than those

imposed by security classification, using standard statements such as:

- (1) "Qualified requesters may obtain copies of this report from DDC."
- (2) "Foreign announcement and dissemination of this report by DDC is not authorized."
- (3) "U. S. Government agencies may obtain copies of this report directly from DDC. Other qualified DDC users shall request through \_\_\_\_\_."
- (4) "U. S. military agencies may obtain copies of this report directly from DDC. Other qualified users shall request through \_\_\_\_\_."
- (5) "All distribution of this report is controlled. Qualified DDC users shall request through \_\_\_\_\_."

If the report has been furnished to the Office of Technical Services, Department of Commerce, for sale to the public, indicate this fact and enter the price, if known.

11. **SUPPLEMENTARY NOTES:** Use for additional explanatory notes.

12. **SPONSORING MILITARY ACTIVITY:** Enter the name of the departmental project office or laboratory sponsoring (*paying for*) the research and development. Include address.

13. **ABSTRACT:** Enter an abstract giving a brief and factual summary of the document indicative of the report, even though it may also appear elsewhere in the body of the technical report. If additional space is required, a continuation sheet shall be attached.

It is highly desirable that the abstract of classified reports be unclassified. Each paragraph of the abstract shall end with an indication of the military security classification of the information in the paragraph, represented as (TS), (S), (C), or (U).

There is no limitation on the length of the abstract. However, the suggested length is from 150 to 225 words.

14. **KEY WORDS:** Key words are technically meaningful terms or short phrases that characterize a report and may be used as index entries for cataloging the report. Key words must be selected so that no security classification is required. Identifiers, such as equipment model designation, trade name, military project code name, geographic location, may be used as key words but will be followed by an indication of technical context. The assignment of links, roles, and weights is optional.

NATIONAL ACADEMY OF SCIENCES-NATIONAL RESEARCH COUNCIL  
DIVISION OF ENGINEERING AND INDUSTRIAL RESEARCH

The Ship Hull Research Committee undertakes research service activities in the general fields of materials, design, and fabrication, as relating to improved ship hull structure, when such activities are accepted by the Academy as part of its functions. The Committee recommends research objectives and projects; provides liaison and technical guidance to such studies; reviews project reports; and stimulates productive avenues of research.

SHIP HULL RESEARCH COMMITTEE

Chairman: RADM A. G. Mumma, USN (Ret.)  
Executive Vice President  
Worthington Corporation

<u>Members:</u> Prof. R. B. Couch, Chairman Dept. of Naval Architecture & Marine Engineering University of Michigan	Professor J. E. Goldberg Prof. of Civil Engineering Purdue University
Mr. Hollinshead de Luce Asst. to Vice President Bethlehem Steel Co.	Mr. James Goodrich Exec. Vice President Bath Iron Works
Dr. C. O. Dohrenwend Vice President & Provost Rensselaer Polytechnic Inst.	
Prof. J. Harvey Evans Prof. of Naval Architecture Mass. Institute of Technology	Mr. D. C. MacMillan President George G. Sharp, Inc.

Arthur R. Lytle  
Director

R. W. Rumke  
Executive Secretary

SR-163 PROJECT ADVISORY COMMITTEE  
"Fracture Concepts"

Professor D. K. Felbeck, Chairman Associate Professor of Mechanical Engineering University of Michigan	Mr. S. S. Manson Chief, Materials & Structures Research Division, NASA
Professor J. Harvey Evans Professor of Naval Architecture Massachusetts Institute of Technology	Mr. R. W. Vanderbeck Chief Research Engineer U. S. Steel Corporation
Mr. P. E. Lagasse Chef de Service au Centre National de Recherches Metallurgiques	Professor D. S. Wood Professor of Mechanical Engineering California Institute of Technology

## SHIP STRUCTURE COMMITTEE PUBLICATIONS

- SSC-159, Acquisition and Analysis of Acceleration Data by F. C. Bailey, D. J. Fritch and N. S. Wise. February 17, 1964
- SSC-160, Geometric Effects of Plate Thickness by R. D. Stout, C. R. Roper and D. A. Magee. February 7, 1964.
- SSC-161, Micromechanisms of Cleavage Fracture in Polycrystalline Iron by Charles J. McMahon, Jr. May 1964
- SSC-162, Exhaustion of Ductility and Brittle Fracture of E-Steel Caused by Prestrain and Aging by C. Mylonas. July 1964.
- SSC-163, Investigation of Bending Moments within the Midships Half Length of a Mariner Model in Extreme Waves by N. M. Maniar. June 1964.
- SSC-164, Results from Full-Scale Measurements of Midship Bending Stresses on Two C4-S-B5 Dry-Cargo Ships Operating in North Atlantic Service by D. J. Fritch, F. C. Bailey and N. S. Wise. September 1964.
- SSC-165, Local Yielding and Extension of a Crack Under Plane Stress by G. T. Hahn and A. R. Rosenfield. December 1964.
- SSC-166, Reversed-Bend Tests of ABS-C Steel with As-Rolled and Machined Surfaces by K. Satoh and C. Mylonas. April 1965.
- SSC-167, Restoration of Ductility of Hot or Cold Strained ABS-B Steel by Treatment at 700 to 1150 F by C. Mylonas and R. J. Beaulieu. April 1965.
- SSC-168, Rolling History in Relation to the Toughness of Ship Plate by B. M. Kapadia and W. A. Backofen. May 1965.
- SSC-169, Interpretative Report on Weld-Metal Toughness by K. Masubuchi, R. E. Monroe and D. C. Martin. July 1965.